Technische Universität München
TUM School of Life Sciences

Molecular Engineering of Nucleocytoplasmic Shuttling CRISPR/Cas13d for Next-Generation RNA Targeting

Christoph Gerhard Gruber

Vollständiger Abdruck der von der TUM School of Life Sciences der Technischen Universität München zur Erlangung des akademischen Grades eines

Doktors der Naturwissenschaften

genehmigten Dissertation.

Vorsitz: Prof. Dr. Aphrodite Kapurniotu

Prüfer*innen der Dissertation:

1. Prof. Dr. Wolfgang Wurst
2. Prof. Angelika Schnieke, Ph.D.

Die Dissertation wurde am 16.12.2022 bei der Technischen Universität München eingereicht und durch die TUM School of Life Sciences am 03.07.2023 angenommen.

Publications & Patents resulting from this study

Parts of this work were published in the following journal article:

Truong, DJ.J., Phlairaharn, T., Eßwein, B., **Gruber, C.** *et al.* Non-invasive and high-throughput interrogation of exon-specific isoform expression. *Nat Cell Biol* **23**, 652–663 (2021). https://doi.org/10.1038/s41556-021-00678-x

Another part of this work is in preparation to submission:

Gruber, C., Krautner, L. *et al.* Molecular Engineering of a nucleocytoplasmic shuttling Cas13d, *in preparation*

A patent application covering this work was filed and published:

Gruber, C., Giesert, F., Truong, D. J. J., Wurst, W. (2021). Application of CRISPR/Cas13 for therapy of RNA virus and/ or bacterium induced diseases. *WO2022136370A1.*

Another patent application was filed:

Gruber, C., Krautner, L., Giesert, F., Wurst, W. (2022). Viral load-depended CRISPR/Cas13 system. *EP22181376.9*

Data and figures of this work might be used in similar form in other publications.

Table of Contents

1 Abstract

RNA is one of the central molecules in biological processes as it codes for proteins, has regulatory functions, and serves as a structural element for many ribonucleoproteins. Because of these important properties, targeted manipulation of RNA can provide insight into its function and networks in which it is involved or opens the possibility of intervening in disease processes. Endogenous proteins have been used in the past to manipulate cellular RNAs in mammalian systems, such as RNase H or components of the RNA interference pathway. However, these approaches have often been shown to be error-prone or inefficient. Recently, a novel molecular tool based on the bacterial immune system CRISPR/Cas13d was described that enables the programmable degradation of RNAs in mammalian cells without the need for additional cellular factors. Here, a short crRNA complementary to the target RNA directs the Cas13d nuclease to the RNA of interest and triggers its degradation. However, this system has limitations. To date, it has only been possible to degrade nuclear RNAs. Furthermore, the Cas13d enzyme exhibits a nonspecific activity (so-called collateral activity), whose exact mechanism and consequences in mammalian cells have not been sufficiently described. In this study, I engineered a Cas13d variant that is active in the cytoplasm of a mammalian cell by manipulating the crRNA localization and elucidated that the collateral activity of the enzyme inhibits the translation of cellular proteins. I used this new enzyme variant in combination with the knowledge gained on the inhibition of translation to develop a novel therapeutic approach against cytoplasmic replicating RNA viruses. Hereby, I was able to block the replication of SARS-CoV-2 almost completely. Previously, it was unknown whether crRNA localization was the limiting factor for cytoplasmic activity of the system, and a random degradation pattern was previously assumed due to collateral activity. Therefore, the results of this study allow for the first time the targeting of RNA with subcellular precision by altering the localization of the Cas13d/crRNA complex. In addition, insights into Cas13d's influence on cellular protein translation open new possibilities for engineering specific Cas13d variants or harnessing target RNA-induced collateral effects. The progressive discovery of new biological mechanisms and their adaptation and optimization for biotechnological applications will continue to increase in the coming years. This will lead to a wave of novel molecular tools with broad applications in research and clinical settings. RNA-targeting tools, such as Cas13d studied here, will play a crucial role in this development.

2 Zusammenfassung

RNA ist eines der zentralen Moleküle in biologischen Prozessen, da sie für Proteine kodiert, regulatorische Aufgaben erfüllt und als Strukturelement für zahlreiche Ribonukleoproteine dient. Aufgrund dieser wichtigen Eigenschaften kann die zielgerichtete Manipulation von RNA zum Verständnis ihrer Funktion und der Netzwerke, in denen sie beteiligt ist, liefern, oder die Möglichkeit eröffnen, in fehlgeleitete Krankheitsprozesse einzugreifen. Um zelluläre RNAs in Säugersystemen zu manipulieren, wurden in der Vergangenheit endogene Proteine genutzt, wie RNase H oder Komponenten der RNA-Interferenz, wobei sich diese Ansätze oft als fehleranfällig oder ineffizient herausstellten. Kürzlich wurde ein neuartiges molekulares Werkzeug, basierend auf dem bakteriellen Immunsystem CRISPR/Cas13d, beschrieben, mit dem es möglich ist, RNA in Säugerzellen programmierbar zu degradieren, ohne das weitere zelluläre Faktoren notwendig sind. Hierbei leitet eine kurze crRNA, die komplementär zur Ziel-RNA ist, die Cas13d Nuklease an eine beliebige RNA und löst deren Degradation aus. Dieses System weißt aber einige Limitationen auf. So war es bisher nur möglich, nukleäre RNAs anzugreifen. Des Weiteren besitzt das Cas13d Enzyms eine unspezifische Aktivität (sog. Kollateralaktivität), dessen genaue Wirkweise und Konsequenzen in Säugerzellen nur unzureichend beschrieben war. In dieser Arbeit habe ich durch Manipulation der crRNA Lokalisation eine Cas13d Variante entwickelt, die im Zytoplasma der Zelle aktiv ist und konnte aufklären, dass die Kollateralaktivität des Enzyms die zelluläre Proteintranslation hemmt. Diese neue Enzymvariante, in Verbindung mit den gewonnenen Erkenntnissen zur Inhibition der Translation, habe ich genutzt, um einen therapeutischen Ansatz gegen zytoplasmatisch replizierende RNA-Viren zu entwickeln. Hiermit konnte ich die Replikation von SARS-CoV-2 nahezu vollständig blockieren. Bisher war nicht bekannt, dass die crRNA Lokalisation der limitierende Faktor für die zytoplasmatische Aktivität des Systems ist, ebenso wie bisher von einem zufälligen Degradationsmuster durch die Kollateralaktivität ausgegangen wurde. Die Ergebnisse dieser Arbeit ermöglichen es daher erstmals, RNA mit subzellulärer Präzision anzugreifen, indem die Lokalisation des Cas13d/crRNA Komplexes verändert wird. Zusätzlich eröffnen die gewonnen Erkenntnisse zu Cas13ds Einfluss auf die zelluläre Proteintranslation neue Möglichkeiten zur Entwicklung spezifischer Cas13d Varianten oder zur gezielten Nutzung des Ziel-RNA induzierten Kollateraleffekts. Die fortschreitende Entdeckung neuer biologischer Mechanismen und deren Adaption und Optimierung für biotechnologische Anwendungen wird in den kommenden Jahren weiter zunehmen. Dies wird zu einer Welle neuartiger molekularer Werkzeuge führen, die breiten Nutzen in Forschung und klinischer Anwendung finden werden. RNA angreifende Werkzeuge, wie das hier untersuchte Cas13d, werden in dieser Entwicklung eine entscheidende Rolle spielen.

3 Introduction

One of the central aims of biological research is to decipher how genes and gene regulatory networks determine the fate of cells, tissues, and ultimately, organisms. The manipulation of genes and expression patterns is an indispensable way to study these processes.

3.1 Genetic perturbations on the DNA and RNA level

Manipulation of genetic sequences is one of the most powerful technologies in fundamental research and biomedical applications, as it allows testing hypotheses in different model systems or potentially curing a disease by altering the genetic sequences of a gene. Genetic manipulations in mammalians can be performed on the DNA level by harnessing endogenous repair pathways, such as Homology directed repair (HDR) or Non-homologous end joining (NHEJ)[1]. Designer nucleases have been developed to trigger DNA repair at specific positions. Typically, these nucleases consist of a DNA-binding domain and a nuclease domain[2]. Modular designs were established based on zinc finger[3, 4], or transcription activator-like effector (TALE) DNA-binding domains[5, 6], fused to nicking enzymes such as FokI[7]. Recently, these technologies have been largely replaced by CRISPR/Cas9. CRISPR/Cas is a rudimentary immune defense system in prokaryotes, consisting of an effector protein and a short guide RNA (gRNA)[8]. CRISPR effector proteins, such as Cas9, bind to the gRNA, which is complementary to a target sequence of an invading phage. Recognition of the target sequence induces Cas9-mediated cleavage of the phage genome[9]. This system was repurposed for mammalian genome engineering by expressing Cas9 along with a gRNA, which is complementary to a genomic target sequence that should be edited. Cas9-induced cleavage of the genomic locus then triggers repair by endogenous DNA repair pathways, eventually resulting in a modified sequence[10, 11].

In addition to targeting DNA, genetic manipulations can also be performed at the RNA level. Other than the genome, the transcriptome is dynamic. Therefore, manipulations on the RNA level are transient. The transient nature of perturbations at the RNA level allows reversible induction of a phenotype by knocking down an RNA of interest, which is reversed after the knockdown tool disappears[12, 13]. Consequently, RNA perturbations allow modeling of dynamic changes in a biological system but do not induce consistent phenotypes across cell types, cell states, or even offspring. Other than DNA targeting, RNA targeting cannot cause a full knockout of a certain gene[14]. For some genes, several thousand RNA molecules are present inside a cell[15]; consequently, some molecules escape targeting. Depending on the biological question, this feature may be desired or problematic. Essential genes are especially important targets in this regard because a full

knockout would result in a lethal phenotype; however, the consequences of expression changes can be studied by targeting the mRNA of the gene[13].

DNA and RNA perturbation tools are widely applied in fundamental biological research and in the clinic to treat not only the symptoms but also the actual cause of a disease at the genetic level. Several incidents with DNA-based therapies in clinical studies, such as cancer cases induced by insertion mutagenesis, have led to greater caution with these technologies[16]. RNA targeting manipulations must be repeated periodically, which can be disadvantageous in settings where the delivery route of the tool is challenging, such as requiring brain surgeries. However, several RNA-based therapies are currently being tested in clinical studies or have been approved[17, 18]. The significant advantage of RNA-based treatments over DNA-based therapies is that the potential side effects of a drug are reversible; therefore, the safety profile of RNA-based medications is preferred[19]. It is widely accepted that drugs acting at the genetic level will open up new treatment options for incurable and orphan diseases. In particular, RNA-based drugs may contribute significantly to this development.

3.2 Tools for manipulating the RNA level of a gene

Since its discovery in 1998, RNA interference (RNAi) has been the most widely used method for manipulating the expression of certain genes[20]. RNA interference (RNAi) is an endogenous pathway that regulates cellular RNA pools. In the nucleus, miRNA genes are transcribed and processed by Dicer and Drosha. Processed miRNAs are integrated into the RISC complex to induce translational silencing or degradation of complementary target RNA[21, 22]. This process was harnessed to degrade target RNAs in a programmable manner by delivering synthetic, processed, or unprocessed miRNA-like RNAs such as siRNA or shRNAs[23-25]. To date, the efficiency and specificity of RNAi-based tools are challenging to predict and control, which is why the results of studies relying exclusively on RNAi can be problematic, and clinical trials based on these tools have in many cases not resulted in treatments for patients[26, 27].

Based on these early developments, antisense oligonucleotides (ASOs) have recently been used in basic research or clinical settings[28]. ASOs are short single DNA molecules that are complementary to a target RNA and, in many cases, chemically modified to increase stability and binding affinity toward their target RNA[29]. The resulting RNA-DNA Hybrids act by blocking splicing factors[30], manipulating protein translation[31], or recruiting endogenous RNase H, which recognizes and cleaves the RNA-DNA Hybrid[32]. ASOs are currently one of the most widely used therapeutic agents for manipulating the expression of specific genes. For example, the approved therapy for spinal muscular atrophy, Spinranza, is based on an

ASO that affects the splicing of the SMN2 gene such that it rescues the effect of a defective SMN1 gene[33].

In addition to these established tools, other technologies have been developed to specifically degrade target RNAs. Similar to TALENs at the DNA level, RNA-binding Pumilio family (PUF) domains were fused to a PIN RNase domain to induce cleavage of the bound target RNA[34, 35]. In addition, chemical options have been explored to recruit endogenous RNases to specific target RNAs. To date, these technologies have not been widely adopted because of their low efficiencies.

The tools described so far reduce the RNA level of an already expressed gene. In addition, other technologies have been developed not only to degrade a target RNA but also to alter it in multiple ways. The expression levels of genes can be directly manipulated using artificial transcriptional activators and inhibitors. These proteins were developed by fusing a DNA-binding domain with a transcriptional effector domain. For instance, an inactive version of Cas9 fused to the tripartite activator complex VPR can be directed to the promoter region of a particular gene to induce its activation[36, 37]. Other enzymes are capable of mutating certain positions in a target RNA. ADAR is an RNA-specific deaminase that recognizes mismatches in dsRNA regions and subsequently deaminates cytosine to inosine, which is then read as guanine by the ribosome[38]. This activity was used to repair point mutations at the RNA level or to express proteins in a cell-type-specific manner[39, 40]. Other technologies recruit translational repressors to mRNAs or map RNA binding proteins by bringing labeling enzymes in proximity[41, 42]. The most recent tool for manipulating RNA in various ways is based on the RNA-guided RNase CRISPR/Cas13[43-45].

3.3 The prokaryotic RNA defense system CRISPR/Cas13

CRISPR/Cas is one of prokaryotes' most important phage defense systems. Upon infection of a prokaryotic cell, the adaption phase is initiated, in which multiple proteins of the CRISPR operon recognize invading phage DNA and integrate pieces of DNA into the genome[46, 47]. These so-called spacer sequences are subsequently transcribed, processed, and bound by effector proteins of the CRISPR defense system. Upon reinfection with the same phage, the effector protein is guided toward the complementary target sequence of the invading phage and cleaves phage DNA[48, 49].

Initially, DNA-targeting effectors, such as CRISPR/Cas9 or CRISPR/Cas12a, were discovered [9, 50]. Later, different types of CRISPR systems were described, ranging from CRISPR-guided transposases to CRISPR-induced proteases[51-53]. Within this considerable diversity of defense systems, the Class 2, type VI CRISPR system is of particular interest. It encodes the single effector protein Cas13 (previously named C2c2), which was predicted to be an RNA-

targeting enzyme because of its highly conserved HEPN nuclease domain[54, 55]. Nine Subtypes of the Cas13 system were described (a-i). All subtypes have in common that they are RNA-guided RNases[45, 55-59]. Interestingly, whether Cas13 protects the bacterial cell against DNA or RNA phages is still not fully understood. Initial bioinformatic analysis suggested that DNA phage transcripts are Cas13s target and therefore build a second line of defense against these phages, along with DNA targeting systems[58]. Recently, several Cas1-Cas2 spacer integrases fused to reverse transcriptase have been discovered and even been harnessed for biotechnological applications[60-63]. It was suggested that these systems work together with Cas13 to acquire spacers from and subsequently defend against RNA phages, therefore questioning the previously claimed defense against DNA phages[64].

The effector protein Cas13 is, with less than 1,000 amino acids, smaller than DNA targeting Cas9 and does not require a tracrRNA[9, 55, 57, 58]. Additionally, it can process one or multiple CRISPR RNAs (crRNA) from a large transcript by using an additional RNase activity of the protein[65, 66]. All Cas13 subtypes and orthologs harbor a split HEPN RNase domain on the protein surface. Upon recognition of the target RNA, the protein undergoes a molecular rearrangement, which brings the HEPN halves in proximity and activates the RNase activity of the protein. This activation leads not only to cleavage of the target RNA but also to RNA cleavage in the vicinity of the activated protein[45, 55, 58, 65]. This bystander cleavage, called trans-RNA or collateral RNA cleavage, was first discovered in Cas13 systems and has recently been expanded to a wide variety of other CRISPR systems, suggesting a fundamental role in anti-phage defense[67-69].

3.4 Collateral RNA cleavage by CRISPR/Cas13

Collateral RNA cleavage was first described for Cas13a and depends on the presence of three elements: nuclease-competent Cas13 protein, target RNA, and complementary crRNA. Upon recognition of the target RNA, the binary Cas13/crRNA complex is activated and cleaves RNA randomly[55]. The biological reason for Cas13s collateral RNA cleavage is not fully understood, but it is thought to induce cellular dormancy by degrading not only phage but also host RNA. This dormancy state might slow down phage replication since cellular resources are not available to express phage proteins and replicate the phage genome. It has also been suggested that such a mechanism reduces the risk of escaper mutations because a single active crRNA is sufficient to block phage replication[70]. Additionally, from a population perspective, the infected cell might have an altruistic role in protecting other surrounding cells from getting infected by activating Cas13[55]. Transcriptomic analysis of the natural host of Cas13a upon activation suggests a random cleavage pattern without preferences for specific sequences or motifs[70]. Of note is that the library preparation method in this study selected for mRNA, which does not exclude

the possibility that other RNAs inside the cell are not targeted as well by Cas13s collateral activity.

Cas13 is a programmable, RNA-guided RNase. Therefore, the system has rapidly been adapted for multiple RNA targeting applications in different hosts, such as plants[71], yeast[72], zebrafish[73], and mammalians[74]. Strikingly, the initially described collateral RNA cleavage in bacterial hosts was absent in all these eukaryotic applications. Many studies compared Cas13 targeting with conventional RNA interference and found Cas13 to be more specific, which contradicts its mechanism in prokaryotes[43, 45, 57].

Recent reports show some degree of collateral activity also in eukaryotic hosts, but the exact nature of this activity and the reason for the contradictory results are still not understood[75-77].

3.5 Adaptation of the prokaryotic CRISPR/Cas13d system for knockdown of mammalian RNA

Besides the uncertainty around non-specific collateral RNA cleavage by Cas13, multiple groups have used Cas13 for targeted knockdown of different genes in mammalians. To date, most RNA knockdown applications were limited to cell lines, but also the reduction of toxic repeat RNAs in patient-derived cells and cellular reprogramming by knocking down PTBP1 in an *in vivo* mouse model was reported[75, 78]. Other approaches used Cas13 enzymes to knock down circular RNAs or to screen for essential RNAs[79, 80]. In addition, different Cas13 subtypes were used as an antiviral system to inhibit the replication of human RNA viruses (such as Influenza A and SARS-CoV-2)[81-85].

In addition to RNA knockdown, an inactive Cas13 variant was generated by mutating the catalytic residues of the HEPN domain to alanine. This inactive enzyme variant was then fused to different proteins, such as GFP for imaging purposes[86], ADAR2 for RNA editing[44, 87], methyltransferase for m^{6}A modifying RNA[88], APEX for mapping RNA-binding proteins[41], and splicing factors to enhance or repress RNA splicing[89].

For all these applications in a heterologous mammalian host, the original prokaryotic system had to be adapted. The effector enzyme was codon optimized, cloned into a mammalian expression vector, and fused to a nuclear localization signal. Additionally, the crRNA was expressed from the Polymerase III-driven human U6 promoter, which transcribes short RNAs without 5'Cap and 3'polyA in the cell's nucleus[43-45].

3.6 Shuttling proteins connect cellular compartments

In this work, an enzyme variant was generated which relies on nucleocytoplasmic shuttling of Cas13d. Cellular compartments are required in a substantially larger eukaryotic cell compared to most prokaryotic cells to sustain a sufficiently high local concentration of proteins in a compartment. Eukaryotic compartments need to communicate for certain tasks. Therefore, different cellular transport systems exist, such as unidirectional translocons[90], mitochondrial translocases[91], or bidirectional nuclear pores[92]. For bidirectional transport, proteins are required to travel in both directions, depending on the cellular state. Therefore, shuttling systems are an elegant way to cope with the compartmentalization of eukaryotic cells. Such shuttling systems are widely used in nature to transport different cargos from the cytosol to the nucleus or vice versa[93]. One example is the nuclear import/export mechanism itself which relies on importin and exportin. Both of these proteins shuttle between the nucleus and cytosol and sort proteins and RanGTP during this process[94, 95]. Other examples of a shuttling protein are nucleolin, which harbors several nuclear localization signals (NLS) and nuclear export signals (NES), causing its nuclear import/export[93], and the nucleoprotein from Influenza A[96], which is involved in viral RNA export from the nucleus.

Even though shuttling systems are widely used in nature, they are rarely used as molecular tools. One example of such an application are optogenetic systems, which dimerize upon light exposure while one dimerization partner is a shuttling protein[97]; however, RNA transport with shuttling enzymes, as developed here, has not been described so far.

3.7 28S ribosomal RNA and dependency of ribosomal integrity on protein translation

Characterizing Cas13s collateral activity in its native host suggested that the cleavage pattern is entirely random without having a consensus sequence or preferred RNA species[55]. This study here, observed a strong preference for the human 28S ribosomal RNA (rRNA).

Human ribosomes are composed of a large 60S subunit, consisting of proteins, 28S, 5.8S, and 5S rRNA, and the small 40S subunit, consisting of proteins and 18S rRNA. Ribosomal proteins are transcribed, translated, and then imported into the nucleus. Ribosomal RNA is transcribed by RNA polymerase I/III (pol I/III) at multiple genomic loci. Transcribed pre-rRNA is processed via several enzymatic steps to 28S rRNA, which is then assembled in the pre-60S ribosome in the nucleus along with ribosomal proteins. Subsequently, the pre-60S ribosome is exported to the cytosol, where the mature 60S large subunit can form. Upon mRNA recognition, the 60S and 40S ribosomal subunits form the translationally active 80S ribosome[98, 99].

Several biological systems, such as the highly potent toxins Sarcin and Ricin, interfere with 28S rRNA to inhibit cellular protein translation. Sarcin is a ribonuclease from *Aspergillus giganteus* that cleaves 28S rRNA at the Sarcin-Ricin loop at approximately 4330 nt[100, 101]. Similarly, ricinus from *Ricinus communis* hydrolyzes the glycosidic bond of Adenin 4324 nt[102]. Both events strongly inhibit cellular protein translation. In addition, RNase L, an endogenous protein involved in viral defense, has been reported to cleave various cellular RNAs, thus blocking the translation of viral proteins[103].

3.8 The 28S rRNA ES15L loop

I observed an unexpected impact of Cas13d activation on the 28S ribosomal ES15L loop in this study. The ES15L element is continuously extruded during evolutionary development from yeast to fruit flies to humans. In yeast, the segment is 20 nt long; in humans 180 nt[104]. Interestingly, this loop extrusion in humans causes new contacts between ES15L and the ribosomal proteins L6 and L30. Neither for the ES15L loop, nor L6 and L30, a precise function is known[105]. Therefore, it can be assumed that all three contribute to the overall function of the ribosome in translating proteins, and any change in the sequence interferes with ribosomal integrity. Surprisingly, ES15L is not solved in structures of the human ribosome, indicating high flexibility in this region, and the areas around ES15L are highly conserved between mammals but not ES15L itself[104].

Some species exhibit a so-called 'hidden break' in their rRNA. At this position, the rRNA is cleaved into two parts, but neither the reason nor the mechanism for this cleavage is known. In other species, an intron was found in this position, which is spliced in some tissues, avoiding the breaking of rRNA, whereas it is not spliced in other tissues, thus leading to a cleaved rRNA[106, 107]. However, no such splicing of rRNA has been described in humans. Interestingly, the Cas13d cleavage site in human 28S rRNA I found here is precisely located at this position.

3.9 Differences between mammalian and prokaryotic defense systems

Cas13 is part of the prokaryotic immune defense system against phage infections[55]. Antiviral defense in prokaryotes is mainly based on recognizing primary genetic information, as is the case for restriction enzymes or the CRISPR/Cas system[49, 108]. Phages and viruses are parasitic genetic information, therefore, a system that directly targets this core feature of viruses is applicable to a wide range or even all viruses. One potential disadvantage is that mutations in the crRNA targeting region could abolish the antiviral effect, even if the mutation is a sense mutation and does not alter the characteristics of the proteins[109].

In contrast, the mammalian defense system recognizes the protein tertiary structure of invading pathogens. Antibodies and B and T cell receptors mature from random recombination events[110, 111]. This characteristic of the mammalian defense system provides greater flexibility because multiple pathogen-targeting affinity molecules are generated; thus, a single point mutation does not necessarily abort the defense. However, the eukaryotic defense system is less programmable than its prokaryotic counterparts.

From a biological perspective, the eukaryotic immune defense system provides greater flexibility to adapt to the host–pathogen arm race. From a technical perspective, the prokaryotic approach is more predictable and easier to program. Therefore, Repurposing the prokaryotic immune defense system can be a valuable approach for developing targeted antivirals[83, 84].

3.10 RNA viruses and derived RNA replicons

Here, I targeted an RNA virus and an RNA virus-derived replicon RNA. RNA viruses consist of an RNA genome that is replicated by the replicase complex. Additionally, they encode different proteins to package the viral genome in viral particles to transfer genetic information to other cells or new hosts[112, 113]. Besides these basic characteristics, RNA viruses can differ significantly, ranging from filamentous morphology for Ebolavirus to spherical morphology for influenza A[114, 115]. Also, the hazard potential of RNA viruses differ greatly, ranging from relatively harmless viruses, such as most rhinoviruses, to some of the deadliest viruses, such as Marburgvirus[116, 117]. RNA viruses make up a large number of potentially human pathogenic viruses and therefore represent a significant threat to humanity.

Replicons are virus-derived, minimal, replication-incompetent mostly RNA viruses that only contain replicase proteins and regulatory elements for replication. These minimal sequences can be extended to genes of interest that should co-replicate with the replicon RNA[118, 119]. Reporter-expressing replicons can be a valuable tool for drug screening because they mimic viral biology without being able to propagate and therefore provide a beneficial safety profile[120]. Replicons can also be used to increase or extend the expression of proteins of interest. For example, mRNA-based vaccines can be expressed using RNA replicons to increase their efficiency[121].

One of the most widely used RNA replicon is derived from the Venezuelan equine encephalitis (VEE) virus. The replicon consists of four nonstructural proteins (nsp) that build the replicase complex. Furthermore, regulatory elements of the viral 5’ and 3’ untranslated regions (UTR) are present in the RNA of the replicon to be recognized by the

replicase and a 26S subgenomic promoter, which drives the expression of the RNA of interest[122, 123]. Several mutants and other improvements of the system have been established, namely, one of them to express E3L from the subgenomic promoter. E3L is a Vaccina virus-derived protein that is a potent inhibitor of the cellular interferon response and therefore enhances the replicon expression[123, 124].

3.11 Therapeutic approaches to treat diseases caused by RNA viruses

Since RNA viruses are one of the major health threats to society, multiple therapeutic approaches have been developed in the past century to target them. Other than antibiotics, the development of broad-spectrum antivirals has not been successful so far. Broad-spectrum antibiotics, such as penicillin, target one conserved characteristic common to a group of bacteria[125]. The vast diversity of RNA viruses does not allow isolation of such a common feature. Instead, individual therapies have been developed for certain viruses.

Typically, antiviral therapies rely on small molecule-dependent inhibition of critical enzymes. One example of such a drug is Oseltamivir, which inhibits Influenza neuraminidase activity, thereby blocking viral entry into cells[126]. In addition to small molecules, monoclonal antibodies are commonly used to prevent viral infection. In most cases, these antibodies block viral receptor-binding proteins, thereby preventing cellular uptake. Bebtelovimab is such an antibody that is used to treat COVID-19 infections by binding to the SARS-CoV-2 Spike protein[127]. These therapeutic approaches require laborious and time-consuming screening processes to find a molecule or antibody which is on the one hand, efficient but on the other, does not have side effects. In addition to drugs that can help patients during acute infection, protective vaccines against some RNA viruses are available. Many vaccines have greatly contributed to containing or even eradicating diseases such as poliovirus or measles[128, 129]. Vaccine development requires rigorous clinical testing because millions or even billions of healthy humans are subjected to medical intervention without being infected. Even extremely rare side effects of vaccines can lead to a relatively high number of people being affected by side effects.

Because of these limitations of current therapies and preventive measures against RNA viruses, novel therapeutic concepts are urgently needed. One such approach are Cas13-based antivirals. The programmable nature of Cas13 enables to adapt the system to multiple viral strains and therefore opens the opportunity to create a broad-spectrum antiviral. Recently, Cas13a, b and d were used to treat influenza A and SARS-CoV-2 infections, but the efficiencies remained moderate[81-83, 85]. Improper localization of the crRNA/Cas13 complex was raised as one potential explanation for that[85].

4 Aim of the thesis

Genetic perturbations are powerful tools in modern molecular biology. Beyond targeting the DNA level, targeting the RNA level of a gene provides various opportunities. In addition to established RNAi methods, recently developed RNA targeting using CRISPR/Cas13d holds great promise in this regard.

This thesis aimed to engineer a novel CRISPR/Cas13d system with improved properties to develop next-generation programmable RNA targeting tool for fundamental research and clinical applications:

- **Molecular engineering** of the subcellular localization of CRISPR/Cas13d. Current Cas13d is limited to the targeting of nuclear RNAs. Therefore, the cause of this limitation should be identified, and targeting of RNAs in the cytoplasm should be enabled.
- **Biological characterization** of the cellular consequences of target RNA-dependent collateral RNA cleavage. The elusive collateral activity of Cas13d should be analyzed and described mechanistically.
- **Antiviral application** of the developed Cas13d system. The characterized and optimized Cas13d should be harnessed as a broad-spectrum programmable antiviral system.

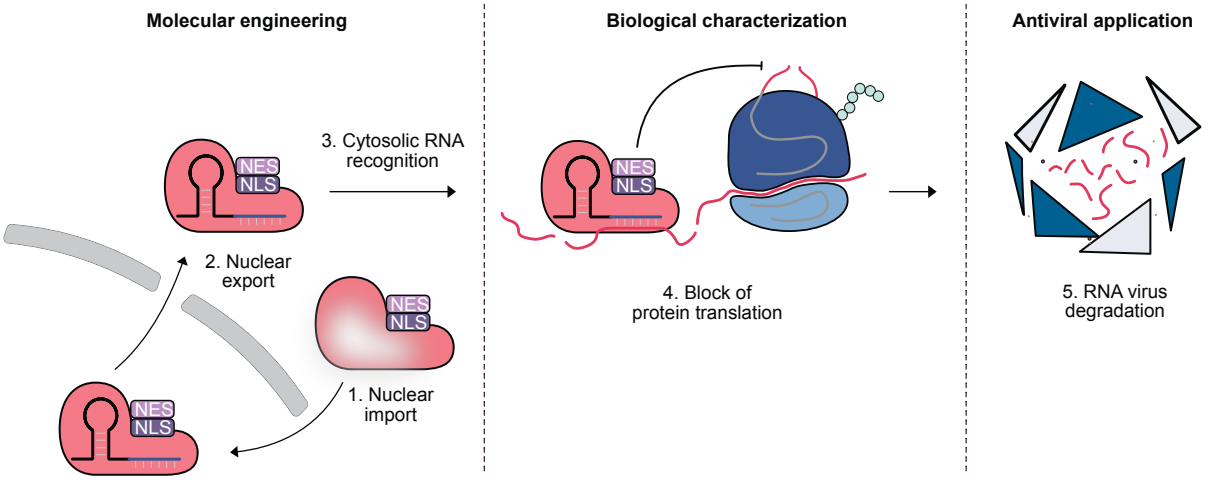

5 Results

Recent studies harnessed different subtypes and orthologs of the Cas13 family for targeted RNA knockdown in heterologous systems. Most of these studies compared different Cas13 systems and concluded that Cas13 from *Ruminococcus flavefaciens strain XPD3002* (RfxCas13d, subsequently named Cas13d) is the most efficient[45, 59]. Therefore, I focused my work on this particular ortholog.

5.1 Improved RNA targeting with CRISPR/Cas13d in mammalian cells

Since the first CRISPR/Cas systems were expressed in heterologous mammalian hosts in 2012, very similar expression constructs were used. The effector proteins (e.g., Cas9 and Cas12a) were codon-optimized for mammals and expressed under the control of an RNA polymerase II (pol II) promoter, such as CAG or CMV. Because most of these proteins are relatively large, exceeding the cut-off of 60 kDa for free nucleocytoplasmic diffusion, additional localization signals were added to the proteins. DNA targeting systems, such as Cas9, were fused to a nuclear localization sequence to transport the protein to the nucleus, where it could act on genomic DNA. In addition, a guide RNA needs to be expressed for a functional CRISPR system. This short RNA binds to the protein component and guides the ribonucleoprotein (RNP) complex to its target sequence. Since the gRNA should not be modified and needs to be expressed in the nucleus, it is expressed by an RNA polymerase III (pol III) promoter, such as the human U6 promoter[10, 50].

This basic design principle was not changed for Cas13d, which is an RNA-targeting CRISPR system (Fig. 1a)[45].

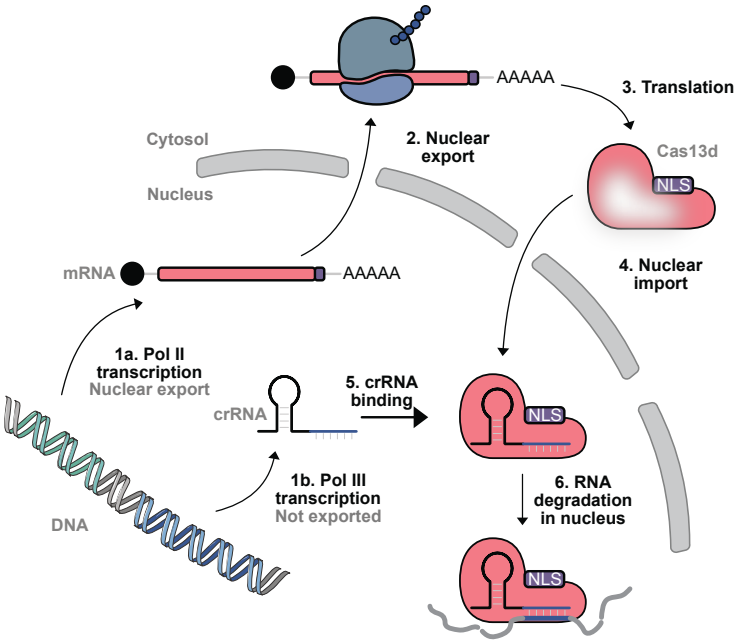

Fig. 1 | RNA targeting by CRISPR/Cas13d in mammalian cells. Cas13d mRNA is transcribed from a polymerase II-driven promoter (1a), capped, polyadenylated, and exported into the cytosol (2). Here, the mRNAs are translated into the Cas13d protein (3), which is fused to a nuclear localization sequence, causing its import into the nucleus (4). Cas13d crRNA is transcribed from a polymerase III-driven promoter (1b) and is subsequently bound by the imported Cas13d protein (5). The binary complex searches for a complementary target RNA. Upon target RNA recognition, Cas13d undergoes a structural rearrangement, leading to target RNA degradation (6).

I first wanted to solve previously contradictory information for an optimal Cas13d expression system in mammalian cells. Direct measurement of RNA knockdown efficiency is challenging for a medium number of conditions since it requires multiple steps (RNA isolation, reverse transcription, and cDNA amplification), most of which are not screening-compatible. To still be able to compare different Cas13d constructs in a medium-throughput manner, I set up a luciferase-based assay, assuming that luciferase mRNA levels are closely related to actually measured luciferase protein levels. The luciferase assay could be performed in a one-step manner in 96-well plates, allowing the efficient comparison of multiple conditions. I added a mouse ornithine decarboxylase-derived degron sequence to further couple RNA and protein levels. This degron is widely used because of its ability to reduce the nanoluciferase half-life from several days to few hours[130]. This means that changes in RNA levels by Cas13d targeting induced the same changes in protein levels within a short time window. Therefore, it can be assumed that the measured luciferase activity is a good proxy for luciferase mRNA levels in cells. To compare different Cas13d expression constructs, I transfected Cas13d variants along with a nanoluciferase encoding plasmid and crRNAs targeting nanoluciferase mRNA and subsequently measured nanoluciferase activity.

Initially, Cas13d was found to have an optimal crRNA length of 22 nt. Recent studies came to different conclusions, claiming an optimal crRNA length of 26-30 nt[45, 74, 79]. Because of

these opposing results, I reanalyzed the length of the crRNA, leading to an optimal length of 26 nt (Fig. 2a).

Different Cas13d orthologs contain a highly conserved AAAC motif 3' of their crRNA, which might be important for the proper function of the enzyme[58]. I hypothesized that this sequence might pair to some extent with the 6x U terminator sequence of the human U6 promoter, from which crRNAs are expressed. Therefore, I added upstream of the U6 terminator sequence either a tRNA motif which endogenous RNase P/Z processes[131], or a ribozyme that is autocatalytically cleaved along with the remaining 6xU terminator sequence[132]. Cleaving of this motif led to an improved knockdown efficiency (Fig. 2b).

I confirmed these two aspects for two independent crRNAs, suggesting that an improved crRNA for Cas13d RNA targeting consists of a 26 nt spacer length and a tRNA or ribozyme motif added to the 3'part.

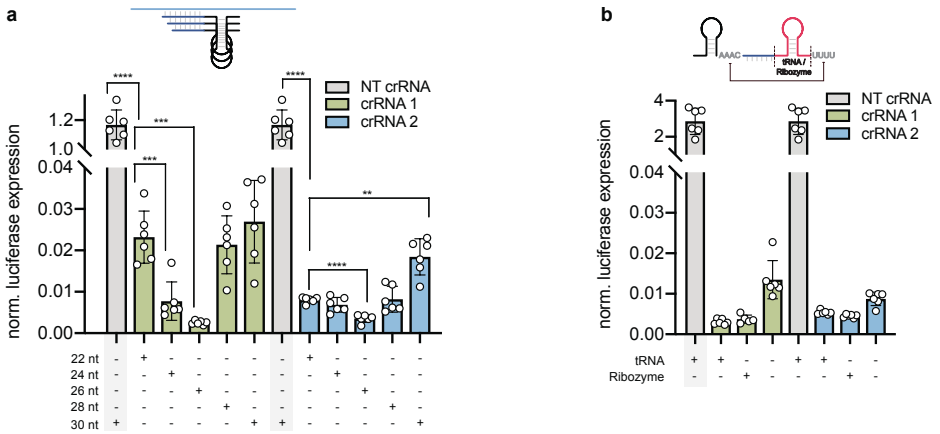

Fig. 2 | Improvement of Cas13d crRNAs. a, Characterization of optimal crRNA length by knocking down a co-transfected nanoluciferase reporter plasmid. **b,** Improvement of crRNA folding by adding a tRNA or ribozyme, 3' of the crRNA. Analysis of knockdown efficiency against a co-transfected nanoluciferase. Analysis in **a** and **b**: Shown as mean +/- s.d. for n=6 independent biological replicates.

Coincidentally, I analyzed the sequence of a crRNA after expression in mammalian cells. I transfected cells with a crRNA expression plasmid, isolated RNA from transfected cells, and sent them for library preparation and Next-Generation Sequencing. Surprisingly, when analyzing the reads obtained for these expressed crRNAs, I found a mutation at position 25 from U to C in 75.6% of the crRNAs (Fig. 3a, b). The cause of this mutation remains unclear. Interestingly, when I introduced this mutation into a plasmid, it almost completely abolished the knockdown efficiency.

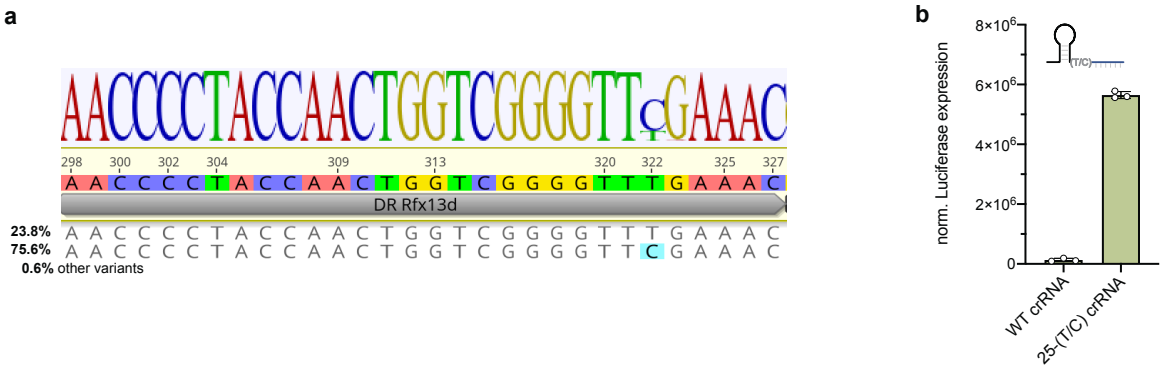

Fig. 3 | T/C Transition in expressed crRNAs. a, RNA-seq analysis of Cas13d crRNAs extracted from transfected cells. The consensus sequence of 80,000 reads shows a T/C mutation at position 25. **b,** Knockdown efficiency of T/C-mutated crRNA by luminescence measurement of co-transfected firefly luciferase, shown as mean +/- s.d. for n=3 independent biological replicates.

5.2 Manipulation of Cas13ds crRNA localization

Other than prokaryotic cells, eukaryotic cells are compartmentalized, leading to the question of the ideal Cas13d localization in the cytoplasm or the nucleus for improved knockdown efficiency. To investigate this question, I cloned a Cas13d variant fused to three nuclear localization signals derived from the SV40 virus[133], c-Myc[134], and a synthetic signal sequence into a CAG promoter expression plasmid. Additionally, I cloned a Cas13d variant fused to the HIV nuclear export signal[135]. Both variants were fused to a FLAG epitope tag to enable staining for their respective subcellular localization. I transfected the NLS, or NES-tagged Cas13d protein, and confirmed their proper localization via immunostaining by referring to nuclear and membrane staining (Fig. 4).

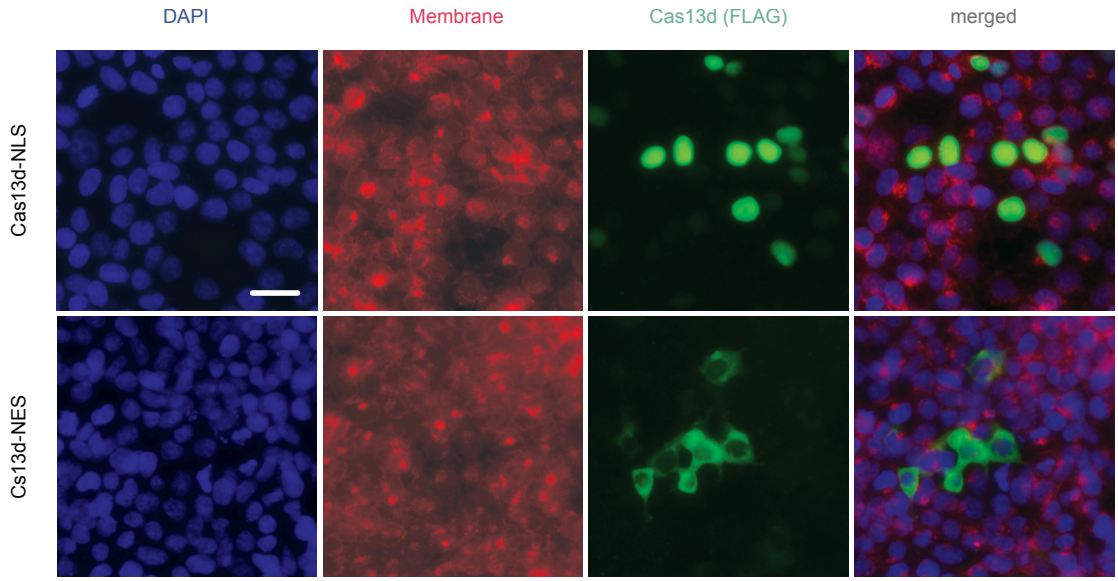

Fig. 4 | Characterization of Cas13d protein localization. Immunofluorescence staining and imaging of NLS- or NES-fused Cas13d subcellular localization, scale bar corresponds to 15 µm.

After confirming the expected localization for both variants, I tested their knockdown efficiencies. Therefore, I transfected cells with Cas13d constructs and two crRNAs targeting TFRC. I analyzed the knockdown efficiency by staining for TFRC protein on the cell surface and subsequent quantification by flow cytometry. Consistent with previous reports[45], the nuclear-localized Cas13d protein was more potent in knocking down endogenous TFRC than NES-Cas13d (Fig. 5a).

Given that mRNA is transcribed in the nucleus and, within minutes, transported to the cytoplasm, where it remains, with a half-life of 10 h[136], I was surprised that Ca13d is more efficient in destroying nuclear RNAs. Thus, the time window in which Cas13d can target the nuclear pre-mRNA is relatively short. To elucidate whether other aspects beyond the ability of Cas13d to find its target sequence might contribute to this localization preference, I analyzed not only protein localization but also crRNA localization by RNA fluorescence in situ hybridization (FISH). CRISPR crRNAs are short RNAs transcribed from a pol III-driven promoter. Polymerase III-driven transcripts are neither capped nor polyadenylated or spliced; therefore, they are expected to remain in the nucleus without being exported to the cytosol, which I confirmed for a Cas13d crRNA (Fig. 5b). As expected, staining with the same method for polymerase II expressed, capped, spliced, and polyadenylated GAPDH mRNA confirmed its cytosolic localization.

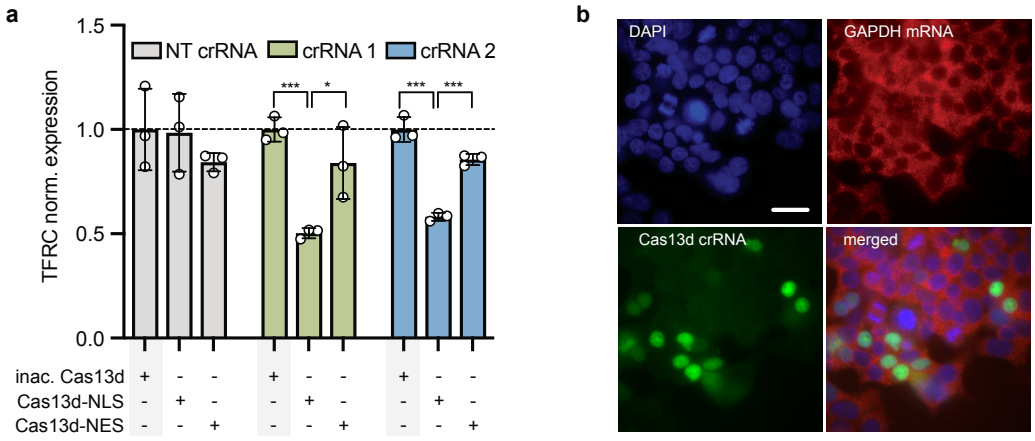

Fig. 5 | Nuclear preference of Cas13d is caused by crRNA localization. a, Flow cytometry analysis of TFRC knockdown efficiencies for nuclear and cytosolic Cas13d. Statistical analysis: Unpaired Student's t-test with *$P < 0.05$; **$P < 0.01$; ***$P < 0.001$; ****$P < 0.0001$, shown as mean +/- s.d. for n=3 independent biological replicates. **b,** Subcellular localization of pol II expressed GAPDH mRNA and pol III expressed Cas13d crRNA by RNA FISH staining, scale bar corresponds to 15 µm.

For DNA-targeting CRISPR systems, such as Cas9, the nuclear localization of the gRNA is advantageous because the target DNA is also present in the nucleus. However, for RNA targeting CRISPR systems, this does not necessarily apply as well since cytosolic mRNAs are often targeted. To date, it has not been analyzed whether these systems are more potent if not only the protein but also the crRNA is exported to the cytosol, where the majority of mRNA is located.

To test whether Cas13d knockdown efficiency could be improved by transporting the protein/crRNA complex to the cytosol, I developed two crRNA export strategies: I expressed a crRNA from a polymerase II promoter, leading to capping and polyadenylation, and therefore transport of crRNA to the cytosol. As a second strategy, I added an Adenovirus-derived RNA motif (minihelix) to the crRNA[137], which is recognized by exportin-5 and exported to the cytosol (Fig. 6a). To find an optimal insertion position for the motif, I tested the knockdown efficiency of crRNA versions with extensions at different positions (5', 3' or in the crRNA loop region of the crRNA) in the previously developed nanoluciferase reporter assay. All insertions were well tolerated, with a slight preference for 5'insertions (Fig. 6b).

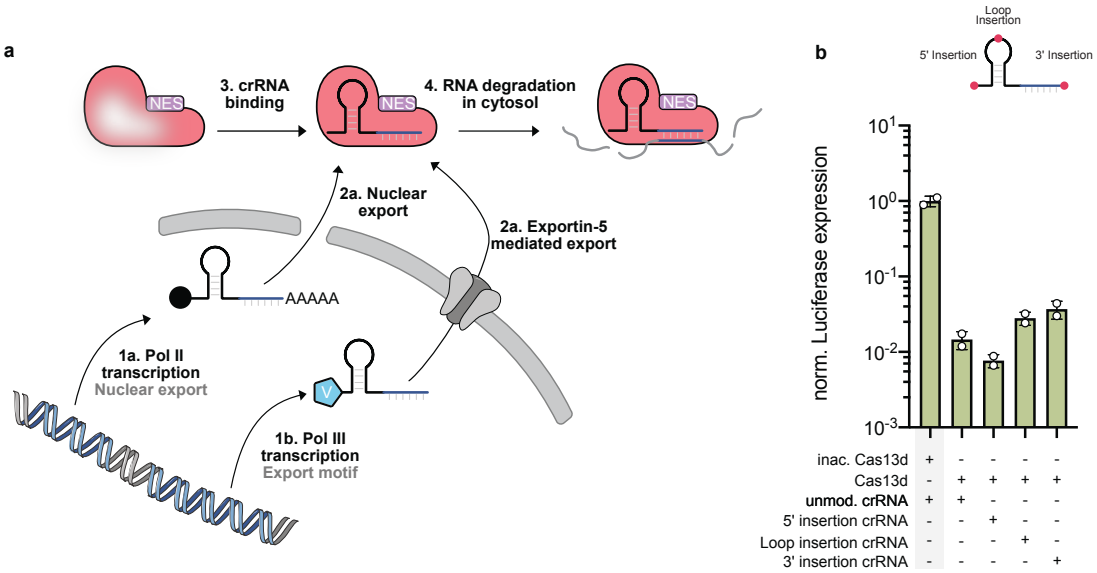

Fig. 6 | Engineering of crRNA export from the nucleus. a, Pol II expressed crRNAs are capped and polyadenylated (1a) and therefore exported to the cytosol (2a), where they are bound by cytosolic Cas13d protein (3) and induce RNA degradation (4). Alternatively, crRNAs are modified with an RNA export motif and expressed from a pol III promoter (1b). The motif leads to exportin-5 mediated crRNA export to the cytosol (2a), cytosolic protein binding (3), and subsequent RNA degradation (4) **b,** Knockdown efficiency against a luciferase reporter RNA for crRNAs with 5', 3' or loop insertions (n=2 independent biological replicates).

Therefore, I inserted the export motif here and analyzed the resulting crRNA localization using RNA FISH. Pol II-driven crRNAs were exported to the cytosol. However, crRNAs fused with the minihelix motif did not show clear nuclear export (Fig. 7a). Subsequent measurements of the knockdown efficiency of the new crRNA variants revealed that the knockdown efficiency for pol II-expressed crRNA was indeed preferred for the NES-tagged enzyme rather than the NLS variant. However, both versions were less efficient than regular NLS Cas13d with pol III-driven crRNA. This result suggests that cap and polyA modifications of crRNAs interfere with their function. The knockdown efficiency of minihelix-modified crRNA was comparable to that of unmodified crRNA and did not show a clear preference for NLS or NES-fused Cas13d (Fig. 7b). Taking the minihelix-crRNA localization into account, which was mainly nuclear, this result was expected. Technically,

improper crRNA export leads to a normal crRNA and therefore, no change in knockdown efficiency.

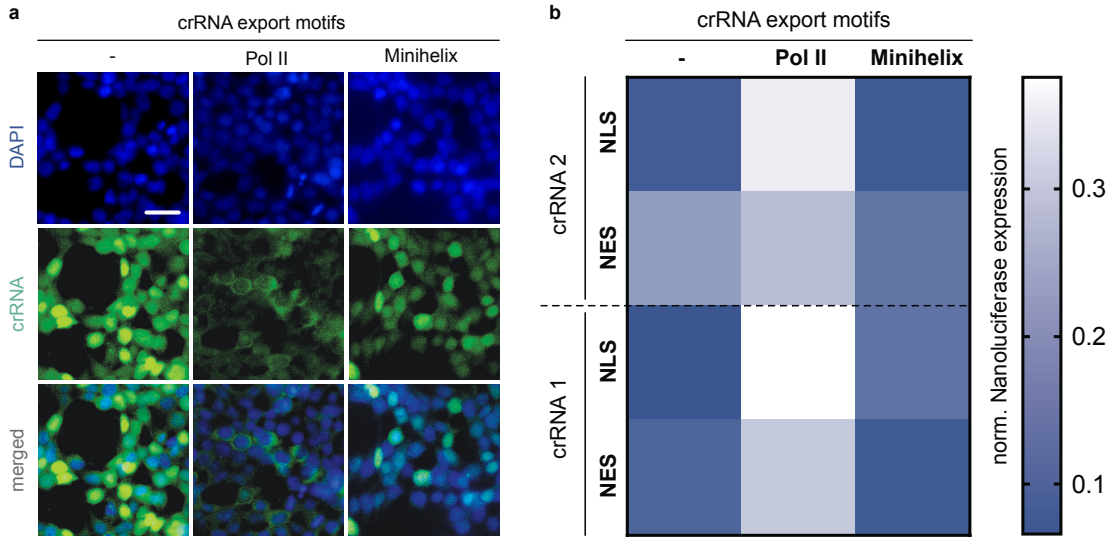

Fig. 7 | Characterization of exported crRNAs. a, RNA FISH staining to test for subcellular localization of pol II expressed and minihelix modified crRNA, scale bar corresponds to 20 µm. **b,** Knockdown efficiency against nanoluciferase of pol II expressed or minihelix modified crRNAs in combination with either nuclear or cytosolic localized Cas13d protein (n=6 independent biological replicates).

5.3 Engineering of a Cas13d shuttling enzyme

Inspired by the ability of pol II-driven crRNAs to work more efficiently with an NES Cas13d compared to the NLS variant, I further explored possibilities of transferring crRNAs to the cytosol. In nature, several examples are described where cargos are transferred from the nucleus to the cytosol by being transported by shuttling enzymes, harboring, NLS, and additionally an NES motif. Protein import and export from or to the nucleus occur in a folded state. Since the binding interface is not unfolded during nuclear trafficking, shuttling proteins can transport different cargos, such as proteins, or co-factors, across the nuclear membrane[58, 59]. I explored the possibility that shuttling Cas13d could transport nuclear-expressed crRNAs to the cytosol. Therefore, I fused Cas13d to both, NLS and NES signals, and analyzed the localization of pol III-driven crRNAs when co-expressed with such a double-tagged enzyme (Fig. 8).

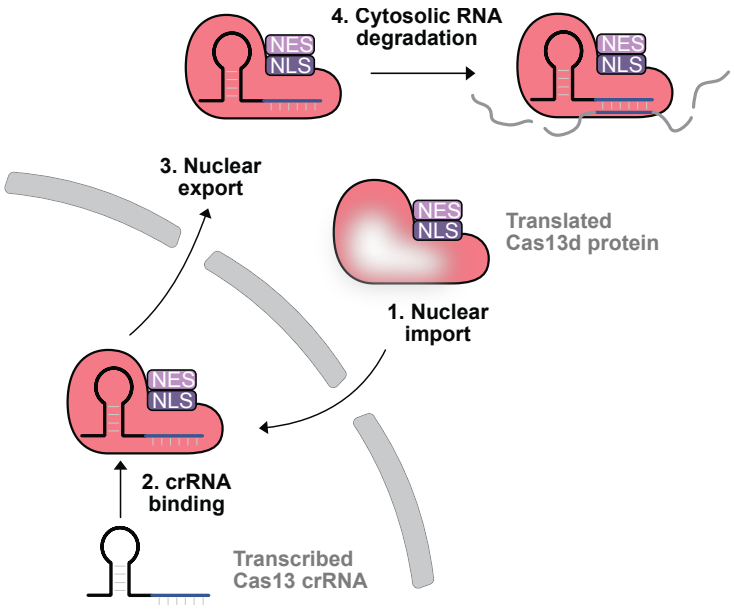

Fig. 8 | crRNA export by shuttling Cas13d. Expressed Cas13d, fused to an NLS and NES signal, is imported into the nucleus (1). Here, Cas13d binds to pol III transcribed crRNA (2) and the RNP complex is exported to the cytosol again (3), where it finds and degrades a complementary target RNA (4).

I first tested whether crRNA was transported into the cytosol when co-expressed with such a shuttling Cas13d enzyme. RNA FISH staining revealed that the crRNA was exported to the cytosol in most cells, presumably by binding to the nuclear Cas13d protein and being exported along with the protein (Fig. 9a). Calculation of cytosolic/nuclear crRNA staining intensity suggests that there are two distinct populations in the shuttling Cas13d sample. One major population with substantial crRNA transfer and one minor population with relatively weak crRNA export (Fig. 9b). This suggests that additional factors, such as cell cycle state, contribute to the efficiency of shuttling Cas13d-mediated crRNA export.

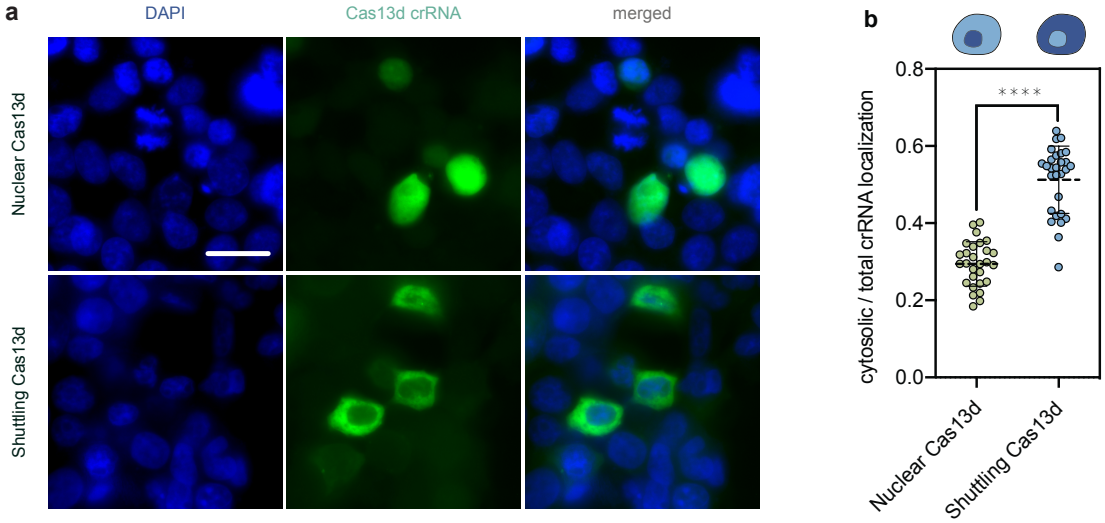

Fig. 9 | Analysis of crRNA export by shuttling Cas13d. a, RNA FISH staining for pol III expressed crRNAs in combination with either nuclear or shuttling Cas13d, scale bar corresponds to 10 µm. **b,** Quantification of cytosolic/total crRNA staining intensity for nuclear and shuttling Cas13d. Statistical analysis: Unpaired Student's t-test with $*P < 0.05$; $**P < 0.01$; $***P < 0.001$; $****P < 0.0001$, shown as mean +/- s.d. for n=30 cells.

These initial experiments confirmed that shuttling Cas13d can bind to nuclear-expressed crRNA and transfer it to the cytosol. To further explore an optimal configuration of shuttling Cas13d-mediated nuclear export of crRNAs, I fused different combinations of NLS and NES signals to Cas13d (Fig. 10).

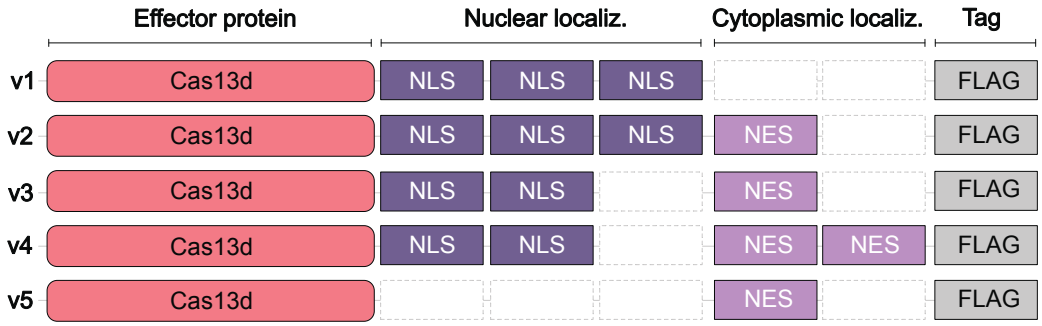

Fig. 10 | Development of different shuttling Cas13d variants. v1-v5 represents increasing amounts of nuclear export signals and decreasing nuclear localization sequences, fused to Cas13d to promote nuclear crRNA export and cytosolic RNA knockdown.

First, I analyzed changes in subcellular localization for these different fusion variants. Decreasing NLS signals, along with increasing NES signals, should lead to continuous transfer of the Cas13d protein to the cytosol. As expected, variants harboring a gradual decrease in NLS signals, along with an increase in NES signals, led to an increase in staining intensity for these protein variants in the cytosol and a decrease in intensity in the nucleus (Fig. 11a). In contrast to the previous staining for crRNA localization, quantification of protein localization revealed a relatively homogeneous distribution across multiple cells within the sample (Fig. 11b).

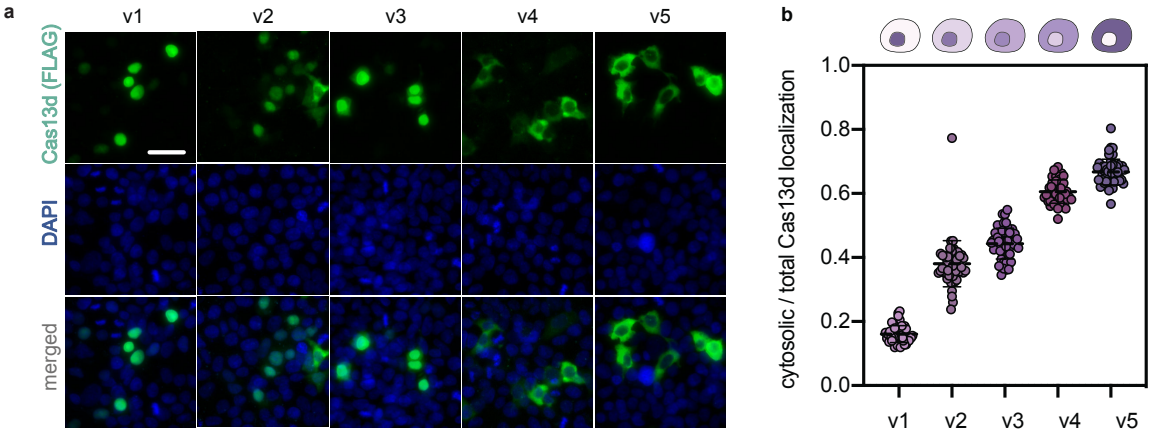

Fig. 11 | Characterization of Cas13d localization for different combinations of NLS and NES. a, Immunostaining for Cas13d protein variants v1-v5 and imaging of their respective subcellular localization, scale bar corresponds to 20 µm. **b,** Quantification of cytosolic / total Cas13d protein staining intensity for different variants v1-v5 (n=30 cells).

Initially, I hypothesized that relocation of the Cas13d/crRNA complex to the cytosol might enhance its knockdown efficiency against cytosolic mRNA targets. Based on the successful transfer of crRNA by shuttling Cas13d to the cytosol, I next tested whether this improves the knockdown efficiency and which NLS/NES combination is optimal. Therefore, I tested the knockdown efficiency of differentially localized protein variants in my previously established nanoluciferase reporter assay and confirmed that shuttling Cas13d improved the knockdown efficiency compared to published NLS-Cas13d from 85% to almost 99%. Furthermore, I found an optimal combination of shuttling Cas13d, consisting of two NLS and one NES signal (Fig. 12). Subsequently, this version is called shuttling Cas13d (Cas13d-SL). This combination of import and export signals most likely optimally balances the import of Cas13d protein to the nucleus to pick up the crRNA and sufficient export to the cytosol to cleave the target RNA located here.

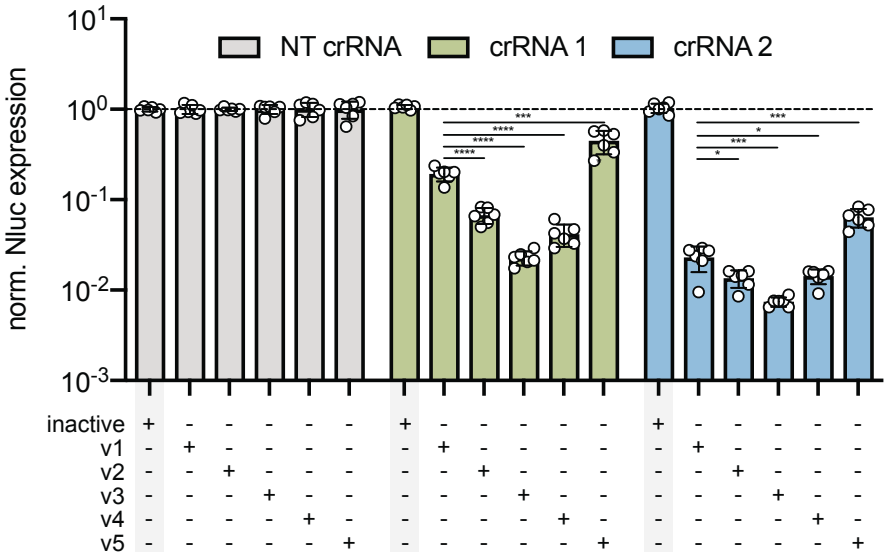

Fig. 12 | Analysis of knockdown efficiencies of shuttling Cas13d variants. Quantification of nanoluciferase knockdown of v1-v5. Statistical analysis: Unpaired Student's t-test with $*P < 0.05$; $**P < 0.01$; $***P < 0.001$; $****P < 0.0001$, shown as mean +/- s.d. for n=6 independent biological replicates.

Coincidently, I observed a gradual decrease in the stability of Cas13d protein variants v1-v5 with increasing cytosolic localization for a pol III-driven crRNA (Fig. 13a), and vice versa, an increase in protein stability for a pol II-driven crRNA (Fig. 13b). For Cas9, the protein was previously described to be stabilized by the scaffold function of the gRNA[9]. Cas13d seems to be stabilized by the crRNA as well since nuclear Cas13d is most stable in the presence of a nuclear crRNA and cytosolic Cas13d is most stable in the presence of a cytosolic crRNA.

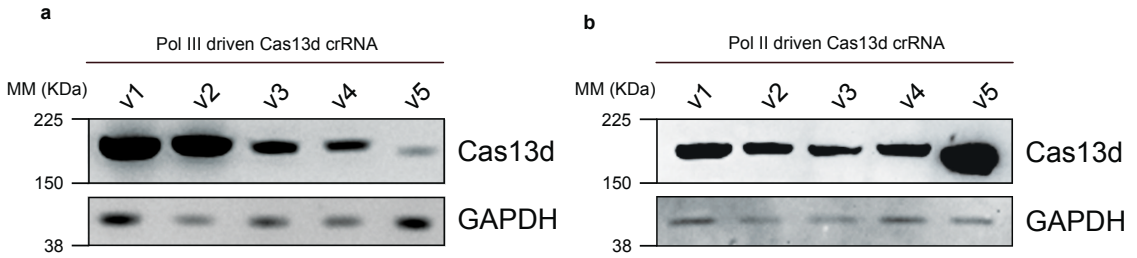

Fig. 13 | Assessment of the stability of Cas13d variants. a, Western Blot of Cas13d v1-v5, co-transfected with a pol III expressed crRNA. **b,** Western Blot of Cas13d v1-v5, co-transfected with a pol II expressed crRNA.

Interestingly, crRNA stability seemed to depend on the presence of the Cas13d protein in the same compartment, presumably to protect the crRNA from degradation (Fig. 14).

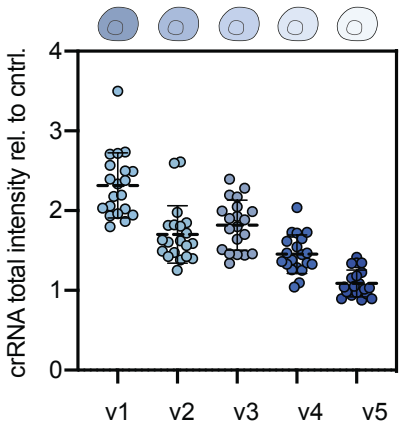

Fig. 14 | The crRNA is protected from degradation by Cas13d protein. Measurement of crRNA stability by RNA-FISH fluorescence intensity in combination with co-expressed shuttling Cas13d variants (n=20 cells, normalized to unstained cells).

5.4 Targeting a solely cytosolic RNA with Cas13d-SL

mRNAs are expressed in the nucleus and reside in the cytosol of a cell. Therefore, both nuclear and cytosolic Cas13d can target them, even if the time window for fast-exporting RNAs is fairly short for Cas13d-NLS. To test whether the shuttling Cas13d-SL system can target purely cytosolic RNAs, which should not be accessible for Cas13d-NLS, I developed a replicon-based reporter system. RNA replicons are self-amplifying RNAs derived from RNA viruses that encode a replicase complex to amplify replicon RNA exclusively in the cytosol[118].

I cloned a mGreenLantern green fluorescent protein[138], along with a puromycin resistance gene under the control of the VEE replicon 26S subgenomic promoter. Additionally, I added the interferon inhibitors B18R and E3L to the expression constructs, which should lead to sustained expression because dsRNA intermediates during replicon amplification are potent inducers of the interferon response[139, 140]. Since replicon RNA is derived from a +-strand virus, it must first be translated to produce replicase proteins nsp1-4 to replicate

the RNA. Therefore, a 5'cap and 3' polyA that are necessary for translation were enzymatically added (Fig. 15).

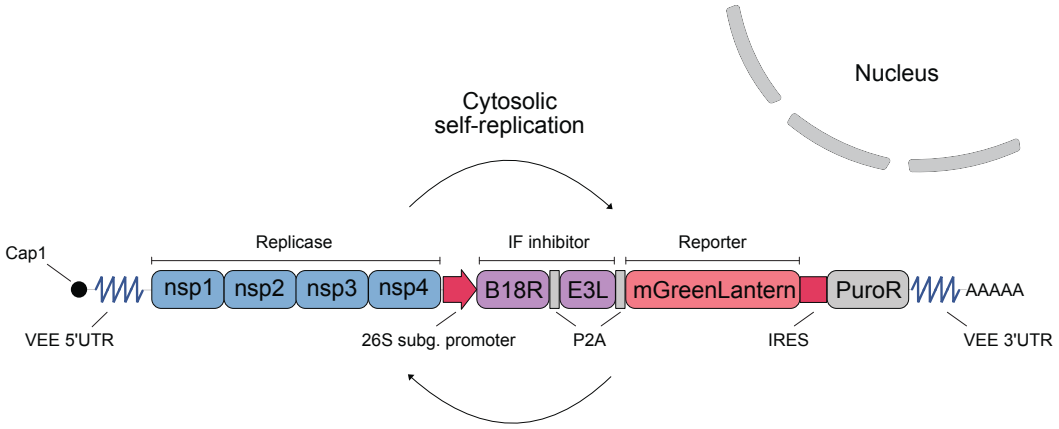

Fig. 15 | Scheme of VEE RNA virus-derived replicon. The replicase complex is composed of 4 non-structural proteins (nsp1-4) and drives solely cytosolic RNA replication. The 26S subgenomic promoter controls the expression of interferon-response blocking proteins B18R and E3L. Additionally, an mGreenLantern reporter protein and puromycin resistance gene are expressed. Replicon RNA is flanked by UTRs, capped, and polyadenylated.

I *in vitro* transcribed the replicon RNA, capped and polyadenylated it, transfected the RNA, and selected for replicon expression cells by puromycin selection. After 14 days, I imaged the cells to test for sustained replicon expression (Fig. 16a). RNA has a half-life of less than one day[136]. Therefore, non-replication-competent RNA should be rapidly degraded. Additionally, I tested by PCR or RT-PCR on extracted RNA or extracted genomic DNA that, indeed, RNA is replicated without any DNA step involved. If a DNA step would be involved, for instance, by reverse transcription of replicon RNA by endogenous retrotransposons and subsequent random integration, such an event would be detected by PCR amplification of the sequence in extracted genomic DNA. As this was not the case, I concluded that, indeed, the replicon RNA was replicated without any unintended intermediate DNA step (Fig. 16b). Furthermore, I confirmed the quality of RNA and DNA extraction, as well as proper PCR and RT-PCR conditions, by amplifying the endogenous AAVS1 locus that codes for a phosphatase mRNA as a positive control.

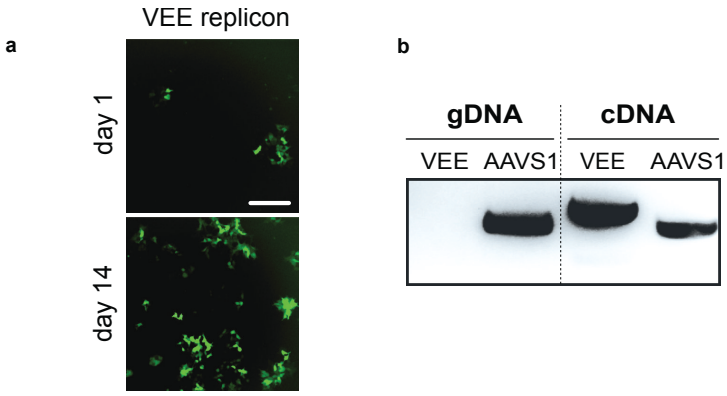

Fig. 16 | Establishing VEE Replicon. a, Stable replicon expression confirmed by long-term cultivation and fluorescence imaging of replicon-expressing cells, scale bar corresponds to 30 µm. **b,** Confirmation of solely RNA-based replicon replication by RT-PCR or PCR amplification of isolated RNA or genomic DNA.

After establishing a solely cytosolic RNA replicon expression system, I next tested Cas13d constructs to knock down replicon RNA. I first found the optimal crRNA/Cas13d-SL protein ratio (Fig. 17a), and then tested the ability to knock down replicon RNA for nine different crRNAs in combination with inactive, nuclear, and shuttling Cas13d. The knockdown efficiency was measured by reduction in replicon expressed mGreenLantern reporter, quantified by flow cytometry. Nuclear Cas13d was able to target cytosolic replicon RNA to some extent, most likely due to nuclear leakage of crRNA or protein. In contrast, the knockdown efficiency for shuttling Cas13d-SL was strongly improved across all crRNAs tested (Fig. 17b). This result supports the hypothesis that Cas13d-SL is superior to knockdown cytosolic target RNAs compared to the commonly used Cas13d-NLS.

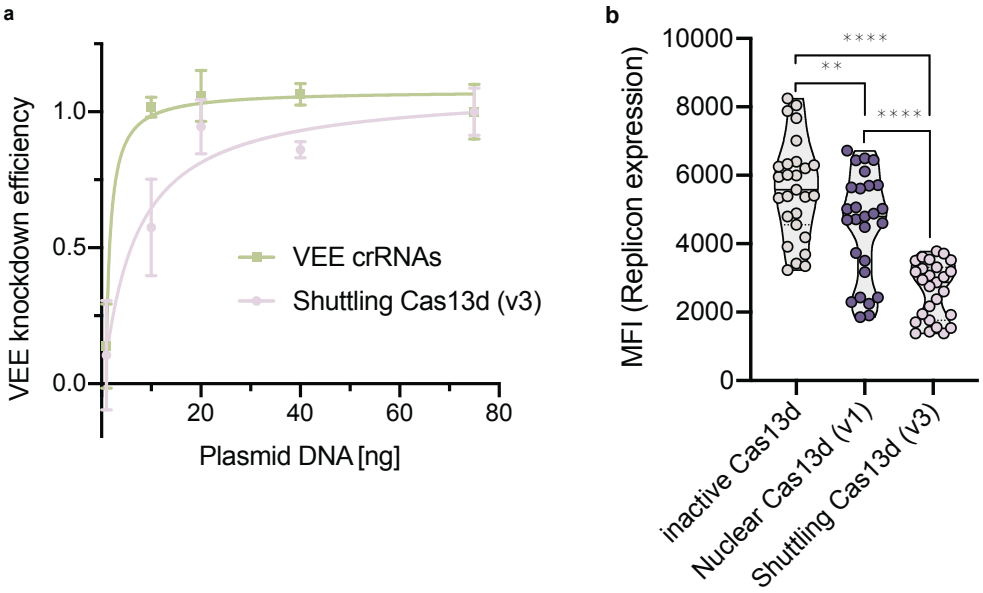

Fig. 17 | Shuttling Cas13d induced knockdown of VEE replicon. a, Optimization of crRNA to Cas13d protein ratio for targeting VEE replicon RNA, shown as mean +/- s.d. for n=3 independent biological replicates. **b,** Comparison of replicon targeting efficiency for nuclear and shuttling Cas13d, analyzed by flow cytometry-based fluorescence intensity measurement. Statistical analysis: Unpaired Student's t-test with $*P < 0.05$; $**P < 0.01$; $***P < 0.001$; $****P < 0.0001$, shown as mean +/- s.d. for 9 crRNAs, each measured n=3 independent biological replicates.

To control for transfection efficiency, for Cas13d replicon targeting experiments, I co-transfected an iRFP720 coding plasmid along with the Cas13d-SL protein/crRNA plasmids. Since the iRFP720 emission peak is clearly separated from the replicon reporting mGreenLantern (516 nm vs. 720 nm), iRFP720 should be constant under all conditions[138, 141]. Surprisingly, I found a strong correlation between replicon knockdown efficiency and iRFP720 reduction, which was unexpected because the replicon targeting crRNAs did not have any complementarity with iRFP720 (Fig. 18a). Multiple repeats of the experimental setup confirmed this observation and led to the idea that Cas13d-SL mediated replicon knockdown and iRFP720 expression are interconnected (Fig. 18b).

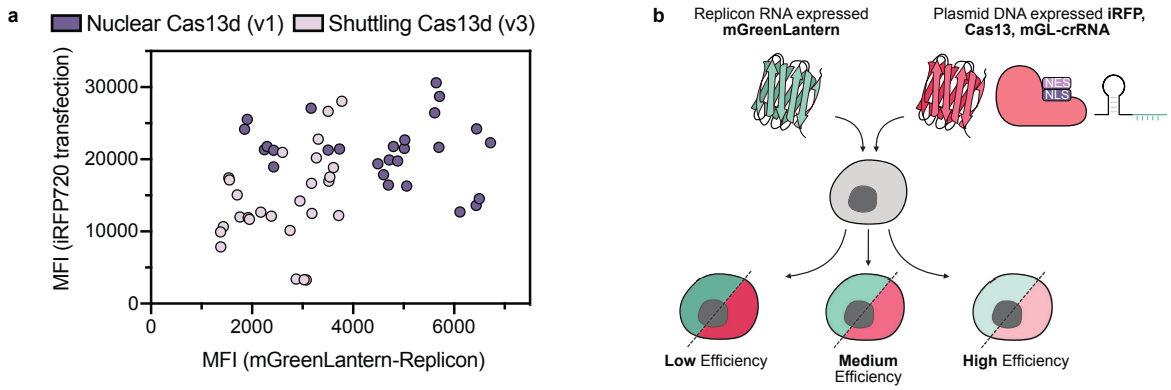

Fig. 18 | Target RNA-induced collateral cleavage of Cas13d. a, Knockdown efficiency of replicon RNA in relation to co-transfected iRFP720, quantified by flow cytometry for nuclear or shuttling Cas13d. Each dot represents one replicate of n=3 independent biological replicates for 9 different crRNAs. **b,** Schematic representation of the experimental setup and correlation between replicon knockdown and collateral iRPF720 reduction.

Additionally, I confirmed this finding for regular mRNA targets and in different mouse-derived cell lines (Fig. 19)

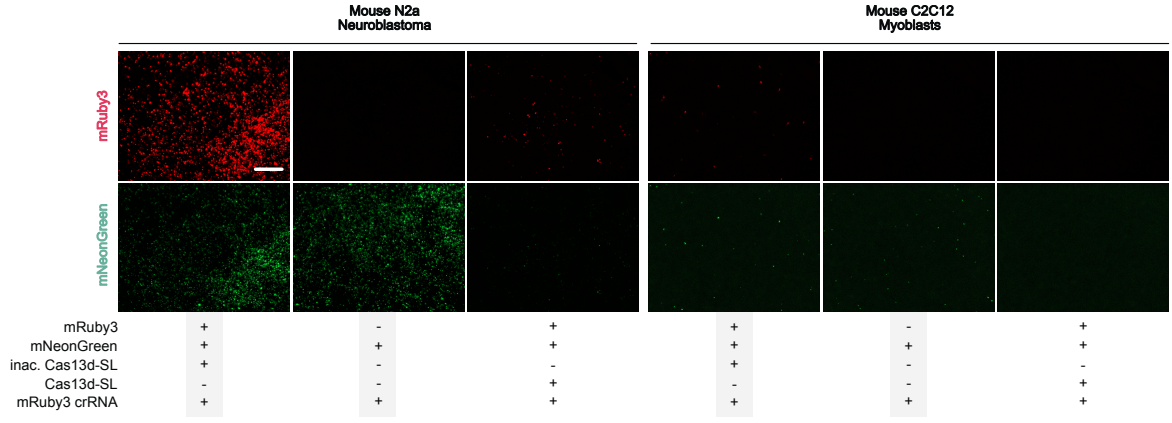

Fig. 19 | Confirmation of Cas13d-SL collateral activity in other cell lines. Collateral effect in murine cell lines by targeting mRuby3 RNA and co-transfection of an unrelated mNeonGreen coding plasmid and microscopy analysis of the resulting green fluorescence intensity, the scale bar corresponds to 100 µm.

5.5 Impact of Cas13d-SL on global cellular protein translation

This surprising finding led to the question of whether the initially described target RNA-induced collateral activity of Cas13d might be the underlying cause of this observation. It was previously described for bacteria and for purified enzymes that binding of the Cas13d/crRNA complex to a complementary target RNA activates the RNase activity of Cas13d and leads to not only on-target but also random cleavage of RNAs in proximity[55, 65, 142, 143]. This well-described biochemical mechanism is accepted *in vitro* and in bacterial cells, but the nature of Cas13ds collateral activity in eukaryotic systems is an ongoing debate[75, 76]. Multiple studies showed via transcriptomic profiling that Cas13d does not affect the eukaryotic cellular transcriptome[43, 44, 73]. Recent reports described a potential collateral effect also in mammalian cells[26, 27], but the reason for this discrepancy between studies remains elusive. Since in my luciferase reporter assay and flow cytometry-based replicon assay, the protein instead of the RNA level was analyzed, I asked if Cas13d-SL collateral activity could have a more pronounced impact on the proteome rather than the transcriptome.

To test this hypothesis, I transfected cells with an active Cas13d-SL (active Cas13d-SL protein, targeting crRNA, and target RNA) system and measured the global protein translation rate over two hours. The assay I used for this experiment is based on the irreversible labeling of nascent proteins by a puromycin analog. This puromycin derivate can subsequently be coupled to a fluorophore by click chemistry and analyzed by flow cytometry. Brighter fluorescence corresponds to a higher number of modified proteins and an increased translation rate during the observation period. Here, I found an almost 10-fold reduction in nascent protein translation in cells expressing an active Cas13d-SL system compared with an inactive version of the protein and an RNAi-based targeting system (Fig. 20).

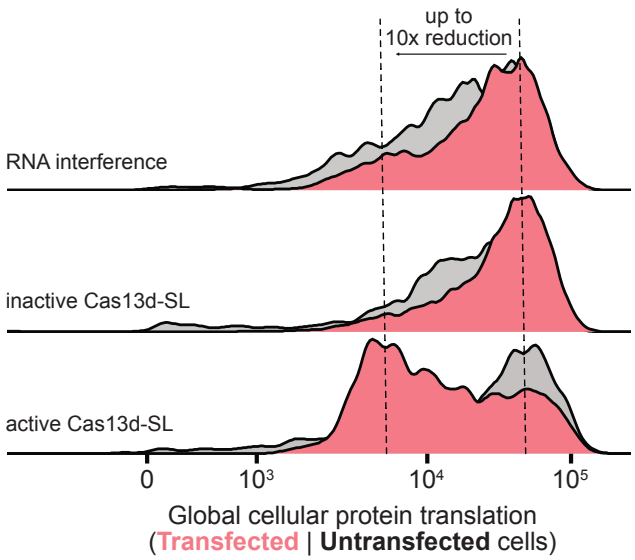

Fig. 20 | Reduction in global protein translation following Cas13d-SL activation. Flow cytometry-based quantification of nascent protein translation in cells expressing an RNAi, inactive or active Cas13d-SL targeting system.

Initially, I expected that this observation was caused by the random degradation of RNA in cells upon Cas13d-SL activation. To test this hypothesis, I transfected multiple exogenous and endogenous target RNA/crRNA combinations, extracted RNA from transfected cells, and analyzed them by gel electrophoresis. Based on previous reports about random RNA degradation by Cas13ds collateral activity, I expected an unspecific cleavage pattern in samples expressing an active Cas13d-SL system. Surprisingly, I found an additional single band at 3 kb in all targeting conditions (Fig. 21).

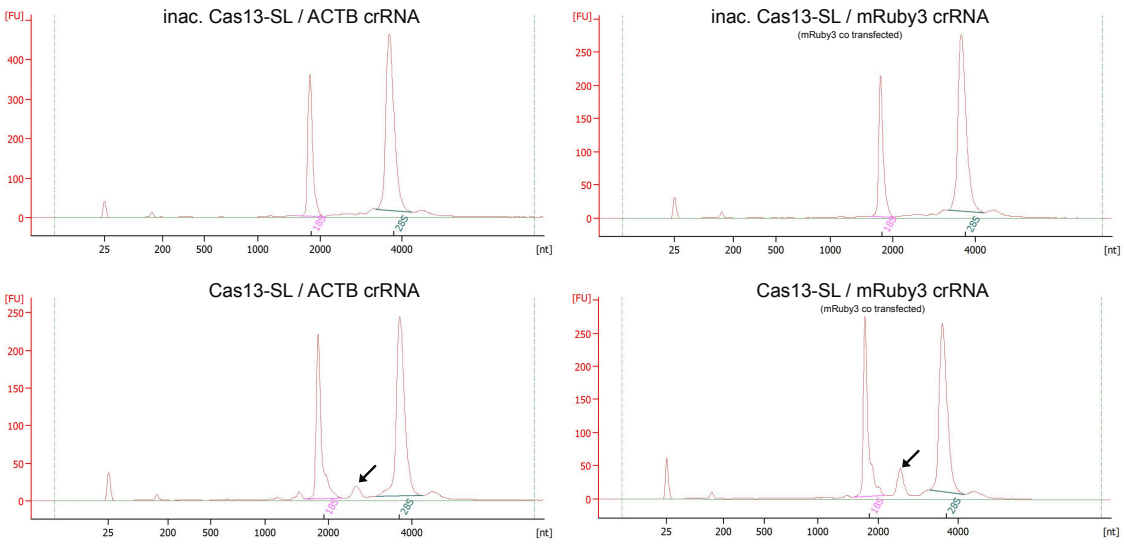

Fig. 21 | | 28S rRNA cleavage by Cas13d-SL upon activation. Bioanalyzer 2100 analysis of RNA extracted from Cas13d-SL transfected cells. The additional fragment of 3 kb is indicated by a black arrow.

This finding was subsequently confirmed for targeting several endogenous RNAs. As expected, in control conditions, expressing inactive Cas13d-SL or no Cas13d system at all, the additional band did not appear (Fig. 22).

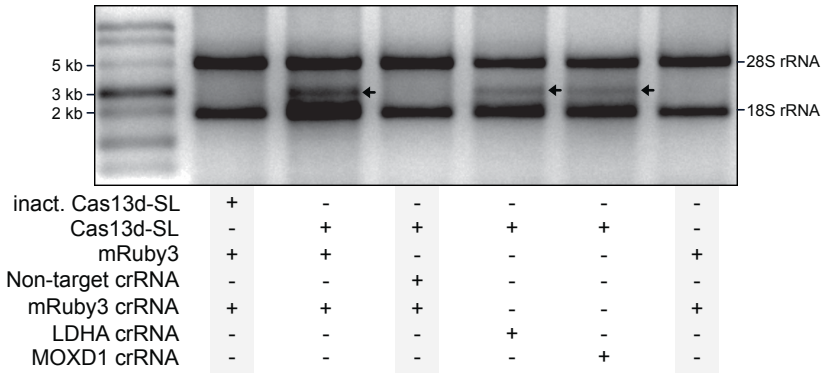

Fig. 22 | 28S rRNA cleavage by Cas13d-SL for exogenous and endogenous target RNAs. Agarose gel electrophoresis of total RNA extracted from cells expressing different crRNA/Cas13d combinations, black arrow highlights an additional band at 3 kb.

Since ribosomal RNA is by far the strongest expressed RNA in mammalian cells, it was highly suggested that the additional 3 kb band is derived from a single, specific cut in 28S rRNA, which is the RNA part of the 60S large ribosomal subunit. To further test whether the fragment was indeed derived from 28S rRNA and if the cut was induced by Cas13d-SL directly or as a subsequent cellular event, I tested whether purified Cas13d-SL protein induced the same cut in purified human 80S ribosomes (actively translating ribosomes composed of 60S and 40S ribosomal subunits). Therefore, I cloned Cas13d-SL into a bacterial expression plasmid and expressed the protein in an *Escherichia coli* (E. coli) *in vitro* transcription/translation system. In addition, I *in vitro* transcribed a target RNA and complementary crRNA. From these three components, I reconstituted an active Cas13d-SL system *in vitro* and co-incubated it with 80S ribosomes purified from HeLa cells. I analyzed these samples by gel electrophoresis and found the same cleavage pattern as for cellular samples, indicating that, indeed, 28S rRNA is the origin of this additional band and that Cas13d-SL itself, but a cellular factor, cleaves 28S rRNA at this position. (Fig. 23a).

Next, I mapped the exact cleavage position in the 28S rRNA by extracting the uncleaved and cleaved bands from the gel and sent them for RNA sequencing. By differentially mapping the NGS reads from these two conditions, I located the cleavage position between nucleotides 2165 and 2215 of 28S rRNA, which corresponds to the loop region of the ribosomal ES15L loop (Fig. 23b).

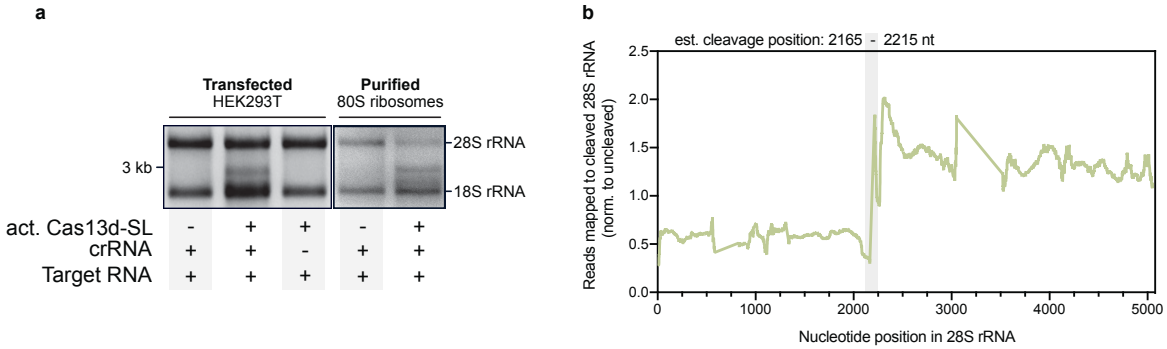

Fig. 23 | Characterization of 28S cleavage position by Cas13d-SL. a, Total RNA extracted from cells expressing an active/inactive Cas13d-SL system compared to RNA extracted from an *in vitro* assay with purified components, including purified 80S ribosomes. **b,** Differential mapping of RNA-seq reads of gel-extracted RNA from the 28S band or the additional 3 kb band.

After mapping the cleavage site in 28S rRNA, I aimed to further understand the mechanistic consequences. Therefore, I searched for the identified cleavage position in an available structure of the human ribosome (PDB ID: 6QZP[144]). Interestingly, this position is not solved in the structure, suggesting a highly unstructured region that cannot be reconstructed with sufficient probability. To still be able to set the cleavage position in the context of the entire ribosome, I modeled the missing sequence on a web server for RNA 3D structure predictions[145, 146]. Combining the available structure of the 80S ribosome with the modeled loop region revealed that the cleavage position of Cas13d-SLs is located at the tip of an exposed loop on the ribosomal surface (Fig. 24).

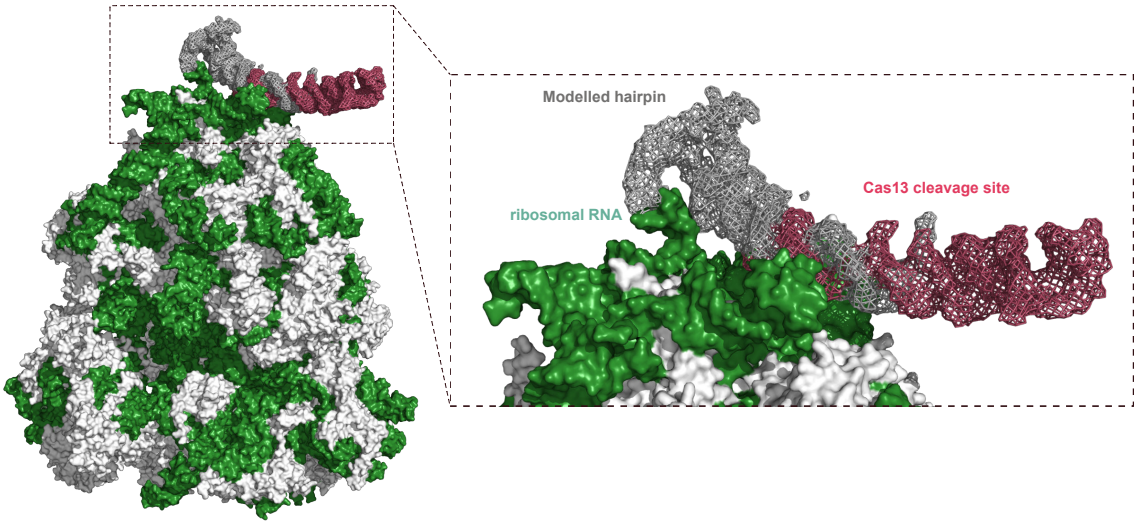

Fig. 24 | Structural mapping of the Cas13d-SLs cleavage site in 28S ribosomal RNA. The structure of human 80S ribosome (PDB ID: 6QZP) is shown. The RNA components are colored green, the protein components white, the modeled D6 loop gray, and the Cas13d cleavage site red. Additional magnification of the modeled D6 loop that is not solved in the structure.

The reason for this preferred cleavage position is unclear; however, potential explanations are discussed later. One possible explanation for this strong preference for a specific position in ribosomal RNA could be that, in my knockdown experiments, I targeted

translated mRNAs that are, by definition, in close proximity to ribosomes. Translated target RNAs could activate Cas13d-SL in proximity to the ribosome and cause its cleavage. Therefore, I cloned either a strongly expressed reporter RNA containing an optimal Kozak/ATG sequence or the same reporter RNA but without Kozak/ATG sequence. If the translation rate of the reporter RNA is a determinant of the collateral effect, a strong preference for the Kozak/ATG-containing RNA would be expected since it recruits more ribosomes. Even if the expression of the reporter without Kozak/ATG was reduced by several orders of magnitude, as expected, no difference regarding the collateral effect was detected (Fig. 25). This finding suggests that Cas13d-SL has an intrinsic affinity for the ribosome beyond its simple proximity to the target RNA.

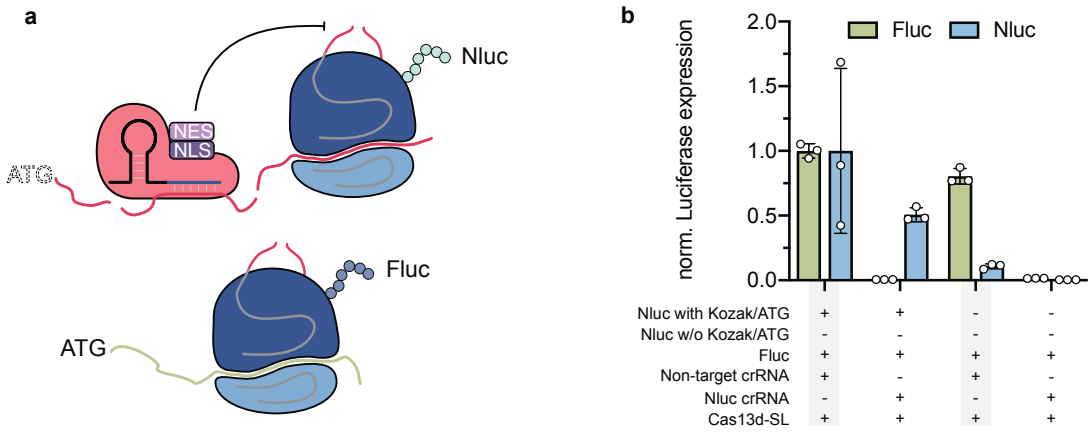

Fig. 25 | Potential mechanism of rRNA cleavage by proximity of Cas13d to translated RNAs. a, Scheme of a potential mechanism for Cas13d-SLs preference for ribosomal RNA. A highly translated target RNA brings Cas13d-SL in proximity to the ribosome, whereas a non-translated RNA does not. Co-transfected Fluc is used to read out ribosomal damage. **b,** Measurement of Fluc expression upon targeting a high or low translated Nluc RNA, shown as mean +/- s.d. for n=3 independent biological replicates.

5.6 Deciphering the impact of 28S rRNA cleavage on cellular translation

I found a strong impact of active Cas13d-SL on global cellular protein translation and precise cleavage of 28S rRNA for various combinations of crRNA/target RNA. As ribosomes are essential for protein translation, a direct relationship between these two findings is highly suggested. I aimed to set up a rescue experiment to confirm this causal relationship. Two key problems arose here. First, ribosomes are composed of multiple proteins and RNAs. Therefore, it is complicated or impossible to supplement an active Cas13d-expressing cell with additional ribosomes. Second, it is challenging to turn off Cas13d activity in a targeted cell prior to the rescue, but this is necessary to ensure that new ribosomes are not targeted by the same mechanism again.

Therefore, I decided to switch to an *in vitro* test system to overcome these limitations. The rabbit reticulocyte *in vitro* translation system has the unique advantage that exogenous factors can be added or removed from the mix and their impact on the protein translation

rate can be studied. To be able to add and remove Cas13d from the system, I coupled the Cas13d protein covalently to magnetic beads. Cas13d beads could be kept in a reaction vessel by applying magnetic force, even if the liquid was transferred. To couple Cas13d to magnetic beads, I fused it to an engineered haloalkane dehalogenase (HaloTag)[147], and a Hibit-Tag[148], which can be quantified via luminescence measurements (Fig. 26a). I expressed the enzyme in an *in vitro* transcription/translation *E. coli* cell lysate. Subsequently, I incubated the lysate with chloroalkane modified magnetic beads to covalently bind the fusion protein. This setup allowed me to add Cas13d coupled beads to the reaction and completely remove them again by simple magnetic separation. Validation experiments confirmed that it is possible to reduce the amount of protein upon applying magnetic force by 99.94% (Fig. 26b). Furthermore, I confirmed that the remaining 0.06% Cas13d protein in the supernatant did not affect the translation rate of the *in vitro* translation system (Fig. 26c).

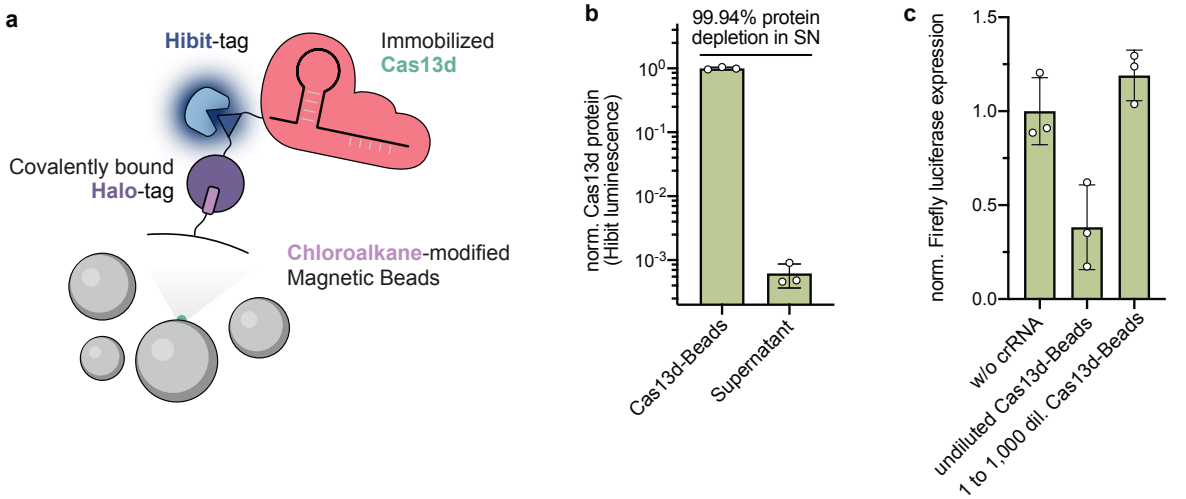

Fig. 26 | Covalent immobilization of Cas13d on magnetic beads. a, HaloTag-fused Cas13d covalently bound to chloroalkane-modified magnetic beads. Additionally, a Hibit-Tag is fused to the protein, which generates a luminescent signal that can be quantified upon incubation with recombinant LgBit. **b,** Hibit-based quantification of Cas13d-HaloTag recombinant protein and validation of protein depletion upon applying magnetic force. Shown as mean +/- s.d. for n=3 replicates. **c,** Confirmation that remaining Cas13d magnetic beads in the reticulocyte *in vitro* translation assay, after magnetic separation, do not impact Fluc mRNA translation, shown as mean +/- s.d. for n=3 independent replicates.

After establishing this tool, I next aimed to decipher whether, indeed, Cas13d-induced damage of ribosomes is the cause of translational inhibition. Co-incubation of Cas13d coupled beads along with *in vitro* transcribed crRNA, target RNA, and rabbit reticulocyte *in vitro* translation system allowed Cas13d to act similarly on the protein translation components as it would do inside a cell. Subsequently, the Cas13d beads could be removed by applying magnetic force and a translated mRNA could be added. This spatial and temporal separation of Cas13d activity and mRNA translation allowed me to measure the degree of Cas13d activity on lysate components compared to its direct activity on the translated mRNA. Additionally, I added purified 60S ribosomal subunit after removing Cas13d-beads to test for a potential rescue by untreated ribosomes (Fig. 27).

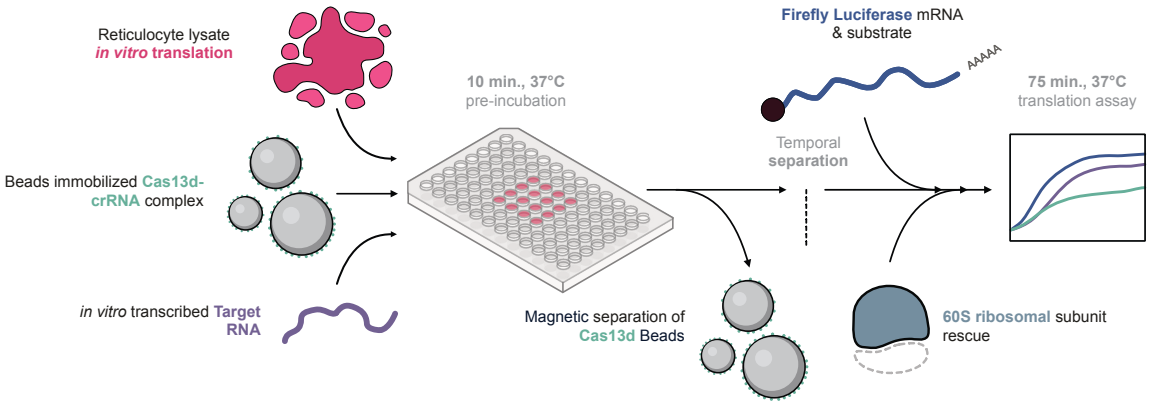

Fig. 27 | Deciphering the impact of Cas13d on protein translation in an *in vitro* system. Immobilized Cas13d/crRNA complex and *in vitro* transcribed target RNA is incubated with rabbit reticulocyte lysate. Subsequently, Cas13d is removed by magnetic separation and Firefly luciferase mRNA and D-luciferin is added to the reaction. Then, a live measurement of Firefly luciferase expression is performed. In additional rescue experiments, the purified 60S ribosomal subunit is added to the reaction after the removal of Cas13d magnetic beads.

With this system, I first aimed to confirm that Cas13d indeed has a significant impact on protein translation instead of cleaving only mRNA, as previously described. Therefore, I incubated the mammalian *in vitro* translation system with Cas13d magnetic beads, *in vitro* transcribed target RNA, crRNA and pre-incubated the lysate for 10 min. at 37°C, either by removing the beads or by keeping them in the reaction. During this pre-incubation phase, a fully active Cas13d system was resembled, which could act on translation components in the lysate. Subsequently, I added firefly luciferase coding mRNA along with substrate and measured the mRNA translation rate for 75 min. The expectation was that if Cas13ds collateral activity only acts on mRNA, the condition in which the beads were removed, firefly luciferase translation rate would not be affected. In contrast, if Cas13d impacts other cellular components, such as ribosomal RNA, temporal separation of Cas13d activity and firefly luciferase mRNA presence would still strongly affect its expression. Indeed, either the presence or removal of Cas13d beads in the reaction led to almost the same degree of inhibition of firefly luciferase expression (Fig. 28a). These results suggest that mRNA is not the main target of Cas13ds collateral activity, but other cellular RNAs.

I set up a rescue experiment to decipher which exact RNA is responsible for Cas13ds collateral effect on protein translation. My previous results suggested that 28S rRNA, the RNA component of the 60S large ribosomal subunit, is the main driver of the downstream effects of Cas13ds. Therefore, I added purified 60S ribosomes to the *in vitro* translation reaction, after removing Cas13d beads and before adding firefly luciferase mRNA. Indeed, this setup rescued the expression of firefly luciferase to almost the same level as the control conditions. Instead, if Cas13d beads were kept in the reaction and rescued with the 60S subunit, it did not lead to a substantial rescue, presumably because the newly added 60S subunit was targeted by Cas13d as well (Fig. 28b).

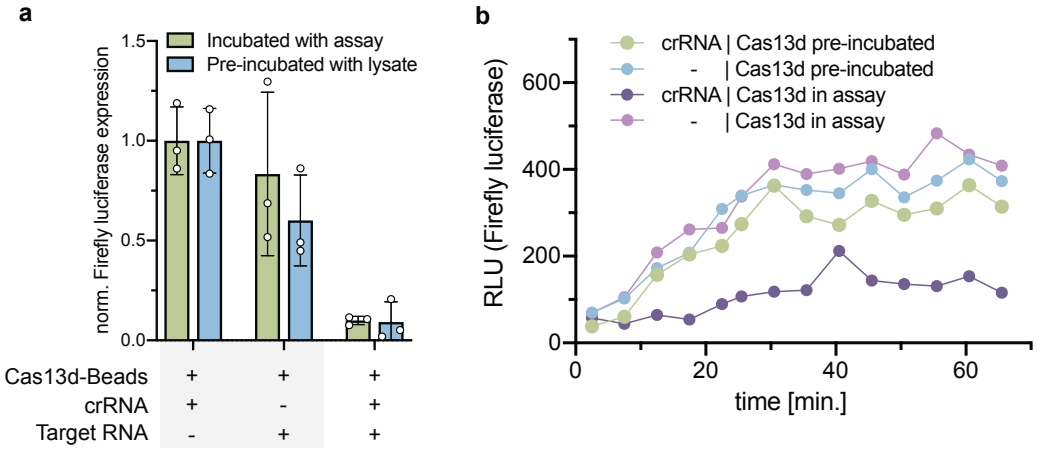

Fig. 28 | *In vitro* measurement of the impact of Cas13d on translation. a, Control conditions and active Cas13d system were incubated during the entire assay with reticulocyte lysate and Fluc mRNA, or only pre-incubated with reticulocyte lysate and removed prior to Fluc mRNA addition. The resulting Fluc expression levels were monitored. Shown as mean +/- s.d. for n=3 replicates, each dot represents the mean of the live assays last 5 measurements. **b,** Live measurement of Fluc expression for pre- or sustained incubation with Cas13d magnetic beads. Each condition was rescued with purified 60S ribosomes prior to the addition of Fluc mRNA and after Cas13d magnetic beads removal (only applies to the 'pre-incubation' condition) for n=1 replicate, each dot represents the mean of a 5 min. measurement.

In summary, these results suggest that Cas13d has a second layer of activity beyond the direct targeting of mRNA, namely, translational inhibition. Additionally, the successful 60S rescue experiments suggest that ribosomal RNA is the primary target of Cas13d upon activation by a target RNA.

5.7 Autoregulation of Cas13d-SL collateral activity

Cas13d-SL impairs the translation of cellular proteins. A system that interferes with such a fundamental process should significantly impact cell viability. Surprisingly, I never encountered a drastic effect on viability. I only found a slight impact on the cell cycle phase: Activated Cas13d-SL expressing cells remain more in G0/G1 phase compared to control conditions. Nocodazole was used as reference in this experiment, because of its well-known property to arrest cells in G2/M phase (Fig. 29).

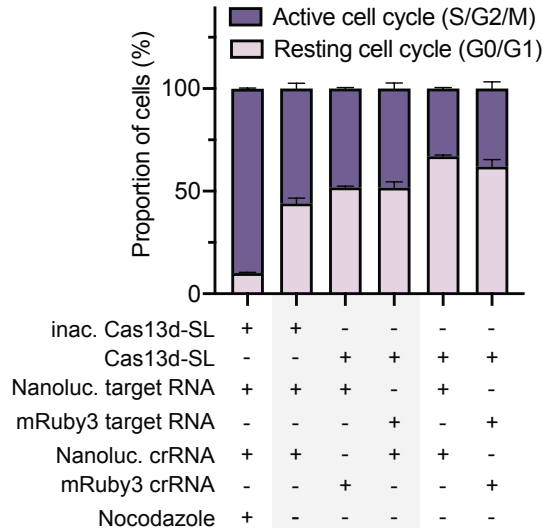

Fig. 29 | Impact of Cas13d activity on cell cycle. Analysis of cell cycle state upon treatment with different Cas13d-SL targeting systems, determined by DAPI staining intensity via flow cytometry.

Because Cas13d-SL interferes with global translation, the expression of Cas13d-SL should be regulated by its own activity (Fig. 30a). From an evolutionary point of view, such an autoregulatory loop could protect bacterial cells from being killed by an overshooting Cas13d system. Thus, such a self-regulated system might have resulted from selective pressure during evolution.

To test the hypothesis that Cas13d-SL is also self-regulated in mammalian cells, I developed a model (together with Richard Koll, Helmholtz Munich) that predicts the correlation between target RNA degradation and Cas13d-SL expression when multiple critical parameters are changed (Cas13d-SL stability/expression levels/activity and target RNA expression/expression delay). Interestingly, increasing target RNA expression in this model led to an increase in activated Cas13d-SL molecules but a decrease in total Cas13d-SL molecules (corresponding to the sum of active and inactive molecules). Additionally, a time-course analysis revealed oscillating Cas13d-SL expression as well as oscillating target RNA expression (Fig. 30b). Such an effect is a widely applicable predator-prey phenomenon in nature and is best described by the Lotka-Volterra equations[149]. This predicted oscillating interdependency of target RNA and Cas13d levels could have direct implications for Cas13d knockdown applications because it means that the time point for analysis is a strong determinant of the efficiency of the knockdown experiment. Additionally, it suggests that Cas13ds collateral activity is not infinite, since stronger target RNA expression leads to reduced Cas13d expression, and this self-regulatory system ends up in an intrinsic maximum, which cannot be exceeded. This observation might also explain why I and others did not detect massive collateral activity-induced cell death upon Cas13d activation.

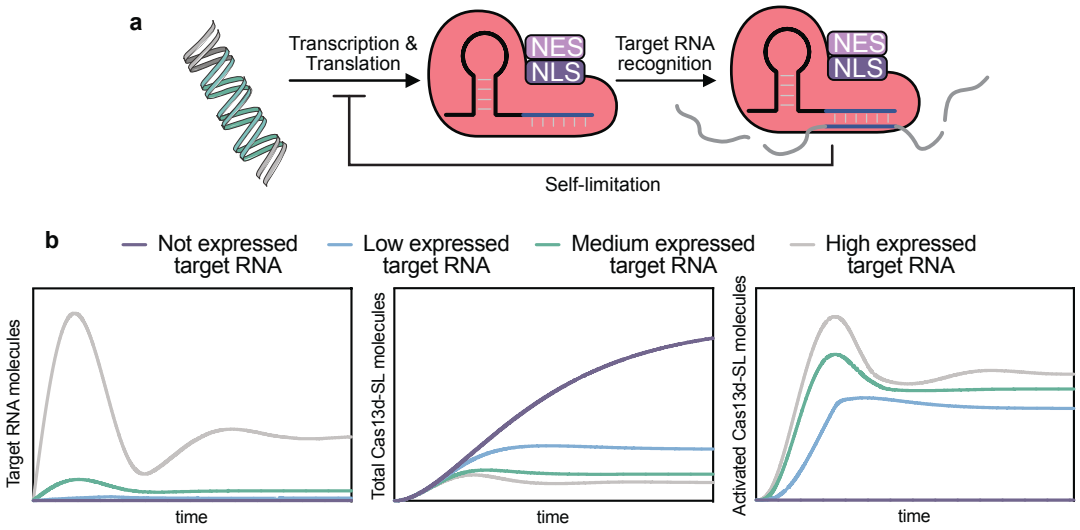

Fig. 30 | Modeling of Cas13d-SLs autoregulation. a, The translated Cas13d-SL protein binds to crRNA and target RNA, activating its collateral activity and in turn down-regulating the synthesis of Cas13d-SL, leading to an autoregulatory loop. **b,** Modeling of the impact of differentially expressed target RNAs on target RNA knockdown, total Cas13d-SL expression, and the amount of activated protein.

The oscillating nature of Cas13d-SL target RNA knockdown suggests that Cas13d-SL-based knockdown of target RNAs is limited by Cas13d-SL self-regulation. To overcome this limitation, I modeled several other situations in which different Cas13d-SL expression levels or protein stabilities were tested (Fig. 31). One condition in which a 10-fold more stable protein was assumed completely avoided the oscillating behavior described for a less stable protein variant, presumably because downregulation of the cellular translation does not impact the stable protein variant. These insights may guide future Cas13d-SL engineering efforts.

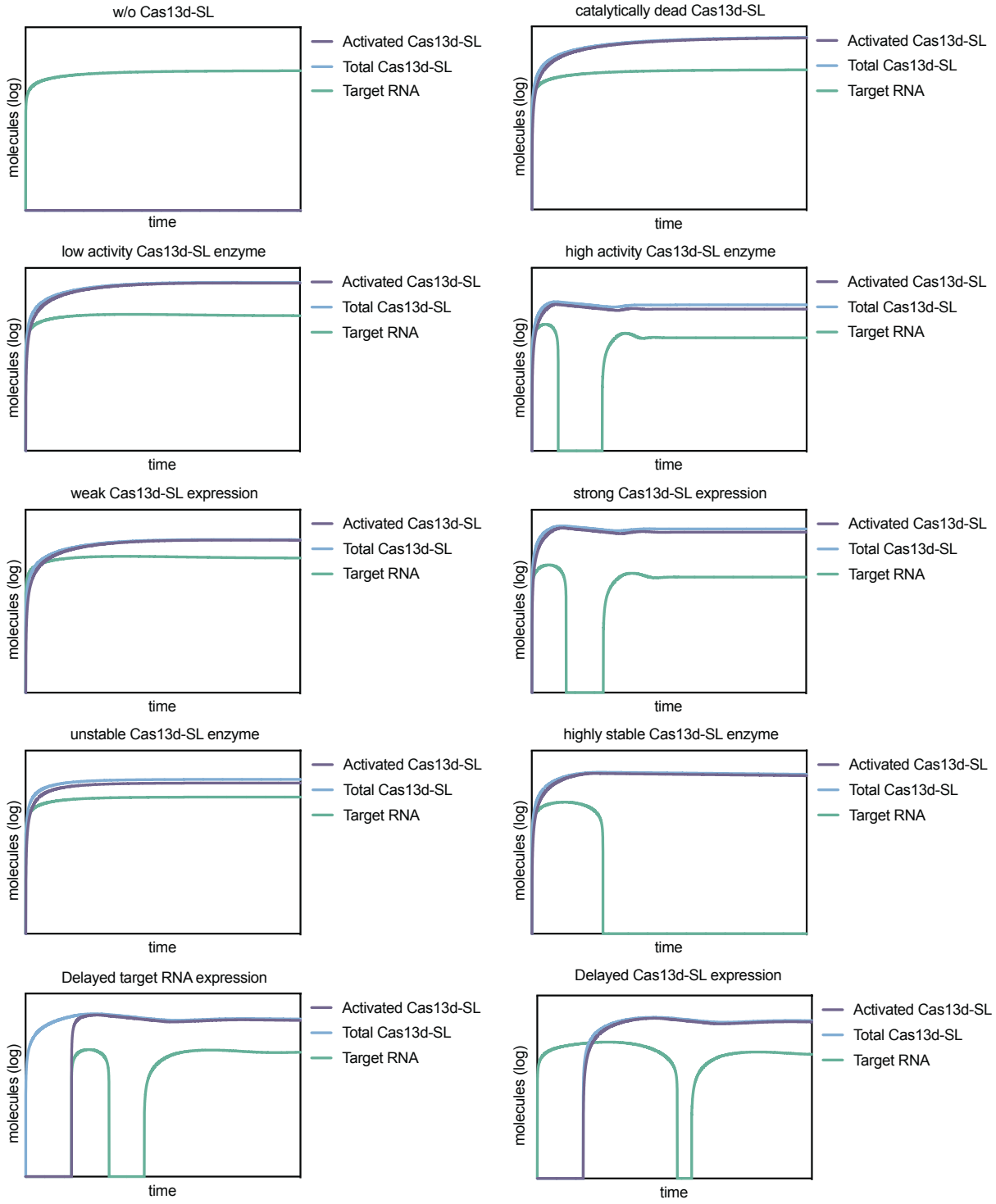

Fig. 31 | Additional modeling data for various Cas13d conditions. Time-course modeling of target RNA, total Cas13d-SL, and activated Cas13d-SL molecules for multiple expression, activity, and stability scenarios.

One of the key insights of the described model for Cas13d-SL self-regulation is the strong correlation between target RNA expression and reduction in Cas13d-SL expression. To confirm this finding experimentally, I fused Cas13d-SL to the green fluorescent protein mNeonGreen[150] and transfected it along with two crRNAs and increasing amounts of target RNA. Subsequent fluorescent imaging confirmed the predicted correlation between target RNA expression and Cas13d-SL expression and proved that this aspect of the model

is correct. As expected and predicted by the model, this observation was not applicable to inactive Cas13d-SL (Fig. 32).

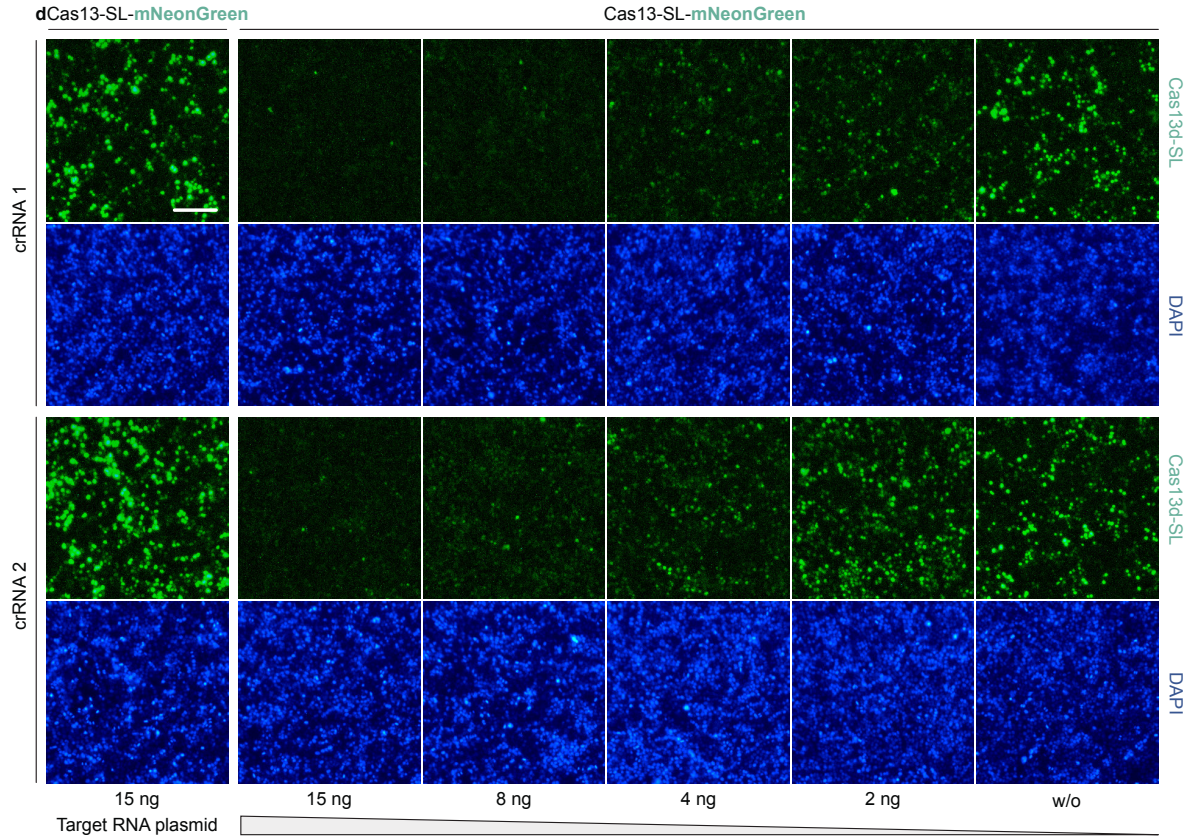

Fig. 32 | Confirmation of target RNA dependency of Cas13d-SL collateral activity. Analysis of self-regulatory expression of Cas13d-SL-mNeonGreen upon co-transfection with increasing amounts of target RNA plasmid by fluorescence microscopy, scale bar corresponds to 50 µm.

To further analyze the effect of target RNA levels on Cas13d-SL expression, I targeted different endogenous genes at varying expression levels with Cas13d-SL fused to mNeonGreen. Consistent with previous co-transfection assays, highly expressed targets induced the most potent reduction in Cas13d-SL expression (Fig. 33).

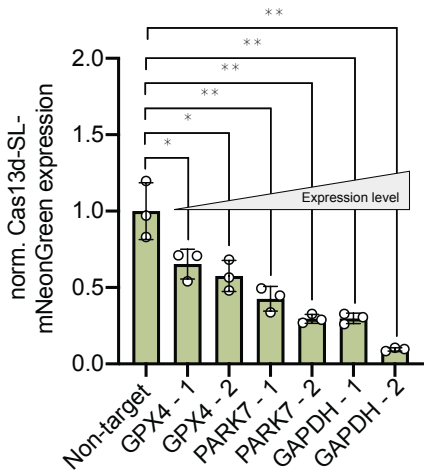

Fig. 33 | Confirmation of Cas13d-SL self-regulation for endogenous target RNAs. Different RNAs with increasing expression levels were targeted by Cas13d-SL fused to mNeonGreen and the impact on Cas13d-SL-mNeonGreen was read out by flow cytometry. Statistical analysis: Unpaired Student's t-test with $*P < 0.05$; $**P < 0.01$; $***P < 0.001$; $****P < 0.0001$, shown as mean +/- s.d. for n=3 independent biological replicates.

Since the collateral activity of Cas13d-SL could be helpful in some settings (targeting cancer cells or virus-infected cells), I explored ways to increase this effect. In the previous section, I found a strong relationship between target RNA expression and Cas13d-SL collateral activity. Depending on the application, the target RNA expression may be fixed and cannot be manipulated to increase collateral activity. Therefore, I tested the idea that targeting a single RNA with multiple crRNAs at different positions could increase collateral activity, because multiple Cas13d-SL proteins are activated from a single target RNA molecule (Fig. 34a). I transfected Cas13d-SL-mNeonGreen along with one or more (up to 38) crRNAs for the same target RNA and analyzed the impact on Cas13d-SL-mNeonGreen by flow cytometry. Indeed, increasing amounts of crRNA led to a proportional decrease in Cas13d-SL-mNeonGreen expression (Fig. 34b). This means that even low-expressed target RNAs might induce a substantial collateral effect when multiple crRNAs are co-expressed.

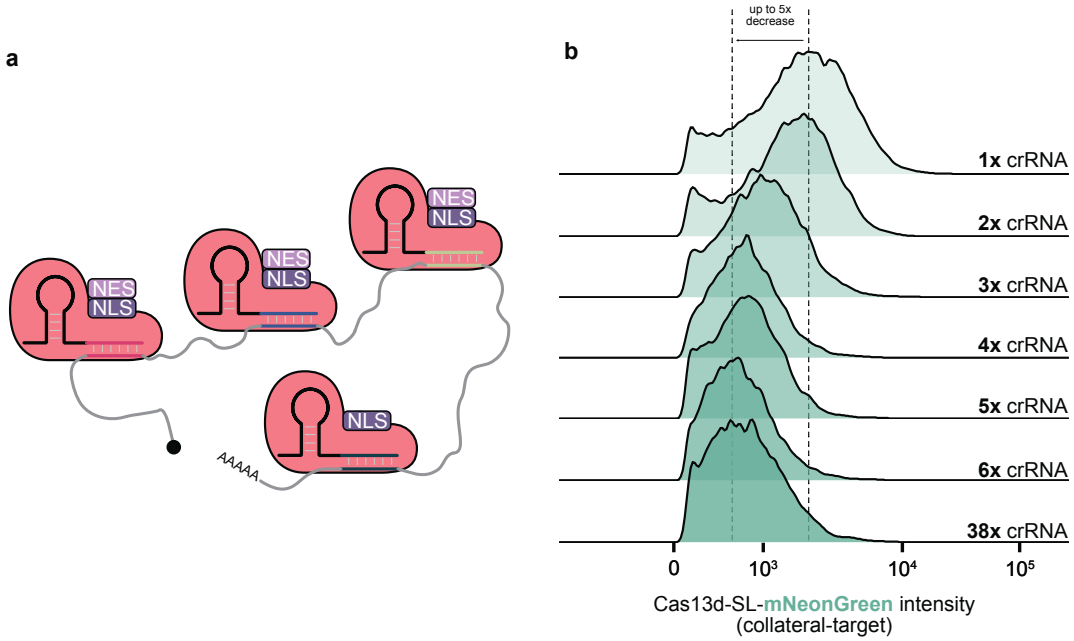

Fig. 34 | Enhancing Cas13d-SL collateral activity. a, Multiple crRNAs targeting the same RNA molecule leads to multiple activated Cas13d-SL proteins from a single target RNA. **b,** Fluorescence measurement of Cas13d-SL-mNeonGreen expression upon transfecting a single or multiple crRNAs for a co-transfected target RNA.

5.8 Development of an mRNA-based delivery system

I developed a mainly cytosolic Cas13d variant and targeted an RNA virus-derived replicon. Additionally, I found and characterized a mechanism that causes a robust Cas13d-SL-induced reduction in protein translation and might have evolved in evolution to enhance the anti-phage activity of Cas13 systems. These characteristics and the programmable nature of CRISPR systems make Cas13d-SL an ideal therapeutic tool against RNA viruses.

To explore the potential application of Cas13d-SL as an antiviral agent, I first tested different methods of delivering the system to cells. DNA-based delivery with plasmids is highly convenient in *in vitro* cell culture systems, but challenging for preclinical and clinical applications. Instead, RNA has the unique advantage that it is short-lived (in other settings, this might be disadvantageous). RNA virus targeting does not require persistent expression of Cas13d-SL, it is even preferred if Cas13d-SL mRNA and protein are quickly degraded after the infection is overcome. Additionally, mRNA cannot integrate into the genome, thereby reducing the risk of unwanted side effects. Considering these features, RNA is the preferred way to transfer Cas13d-SL to infected cells. Therefore, I decided to develop an RNA-based system.

First, I cloned a Cas13d-SL-P2A-mRuby3 reporter construct for *in vitro* transcription to monitor the proper expression of mRNA by mRuby3 red fluorescence[151]. Initial experiments showed successful, but very weak, expression of the construct (Fig. 35a). RNA has a relatively high turnover rate in mammalian cells. To increase stability, 5’ and 3’ UTR

sequences have been characterized in the past. Additionally, these UTR sequences contain regulatory elements that can improve expression rates of the coding sequences they flank[152]. I added a 5'alpha-Globin UTR and 2x 3'b beta-Globin UTR to the Cas13d-SL-P2A-mRuby3 reporter construct, which substantially increased its expression level (Fig. 35b). Transfected mRNA is endocytosed and sensed in the endosome by toll-like receptors (TLR), which can cause a strong innate immune response and therefore low mRNA expression[153]. To circumvent this issue, synthetic mRNA can be masked with chemically modified RNA bases, such as methylated pseudouridine, to replace uracil[154]. I generated N1-Methyl-Pseudouridine modified Cas13d-SL reporter mRNA, which indeed strongly increased the expression (Fig. 35c).

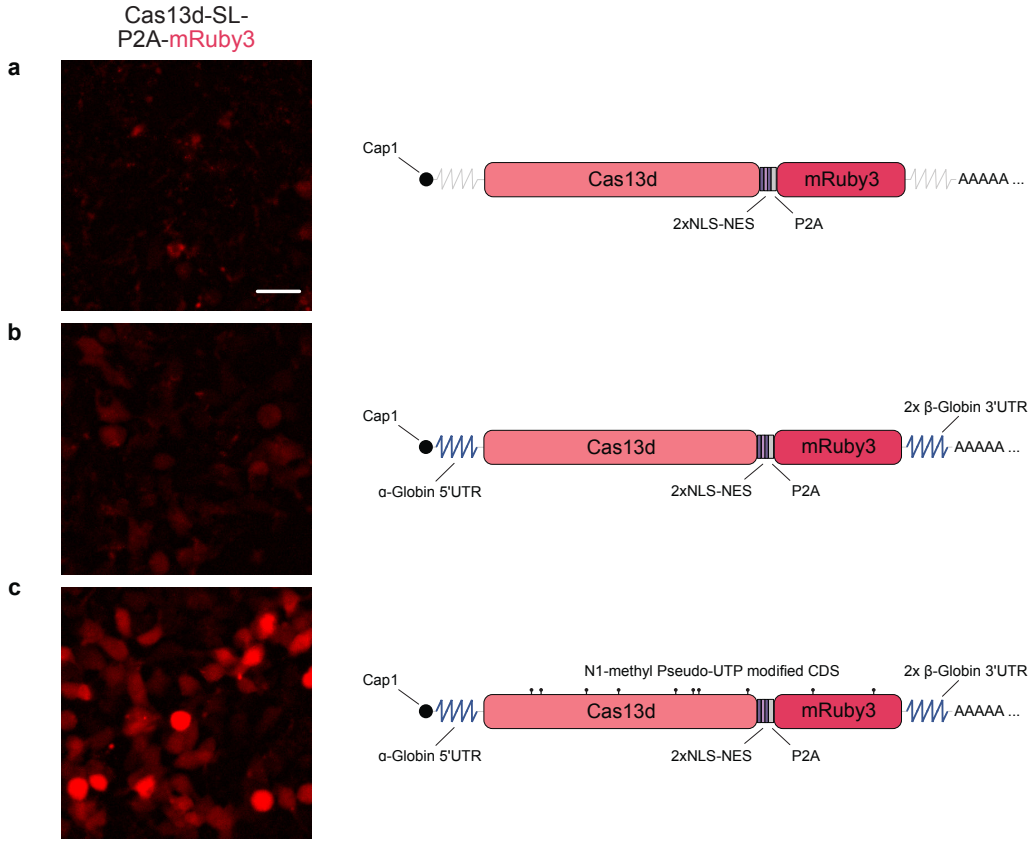

Fig. 35 | Optimization of Cas13d-SL expression from mRNA. a, Expression of Cas13d-SL-P2A-mRuby3, imaged by fluorescence microscopy, for an unmodified RNA. **b,** Compared to **a,** stabilizing UTRs were added to the mRNA. **c,** Compared to **b,** uracil was replaced by N1-methyl Pseudo-UTP, scale bar in **a-c** corresponds to 15 µm.

As expected, this optimized mRNA-based expression system did not alter the previously characterized mainly cytosolic Cas13d-SL localization (Fig. 36).

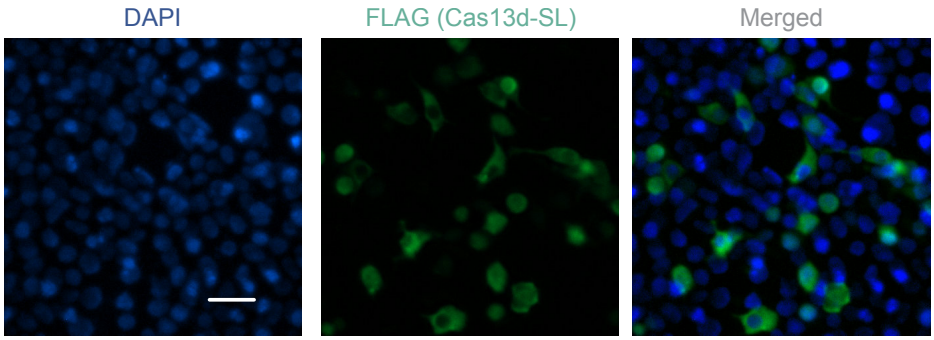

Fig. 36 | Subcellular localization of mRNA expressed Cas13d-SL. Localization analysis by immunostaining for Cas13d-SL protein and fluorescence microscopy, scale bar corresponds to 15 µm.

5.9 Targeting of SARS-CoV-2 with Cas13d-SL

After optimizing Cas13d-SL expression from mRNA, I tested the knockdown efficiency. I cloned a 30 nt fragment of the SARS-CoV-2 genome into the 3'UTR of a luciferase reporter RNA. I then formulated the optimized Cas13d-SL mRNA along with a crRNA, complementary to the cloned SARS-CoV-2 fragment, into liposomes derived from a commercially available cationic lipid (Fig. 37a). I tested the knockdown efficiency of either an *in vitro* transcribed crRNA or a chemically stabilized and synthesized crRNA. Based on previous reports for Cas9[155, 156], I expected that phosphorothioate, which was introduced at the 5' and 3' ends of the crRNA, would not interfere with crRNA function, but would increase its half-life. This system almost completely degraded the SARS-CoV-2 reporter RNA for both the modified and unmodified crRNA (Fig. 37b).

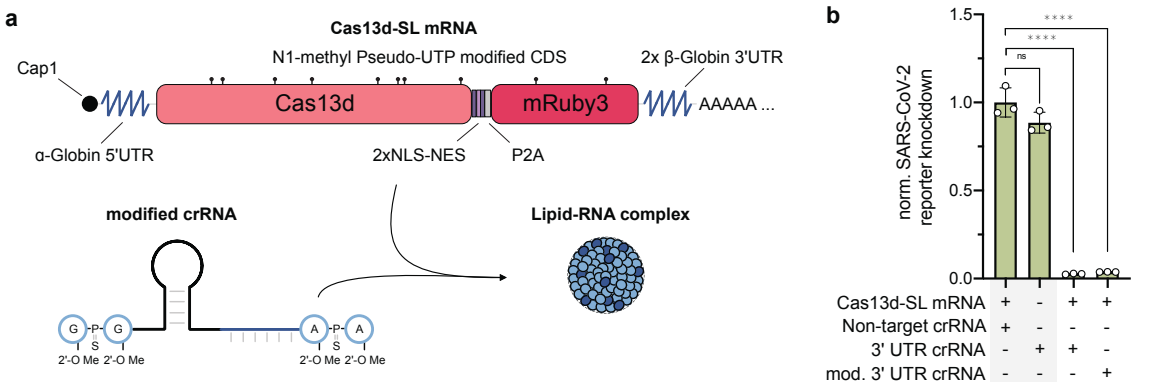

Fig. 37 | Formulation of RNA-encoded Cas13d-SL in lipid complex. a, Schematic representation of optimized Cas13d-SL mRNA along with chemically stabilized crRNA, formulated in a lipid-RNA complex. **b,** Knockdown measurement of RNA-encoded Cas13d-SL against a nanoluciferase reporter RNA with cloned SARS-CoV-2 3'UTR. Statistical analysis: Unpaired Student's t-test with $*P < 0.05$; $**P < 0.01$; $***P < 0.001$; $****P < 0.0001$, shown as mean +/- s.d. for n=3 independent biological replicates.

Next, I tested whether the system could block live SARS-CoV-2 replication. Based on my previous results, showing that multiple crRNAs for a single transcript enhance Cas13d-SL knockdown and collateral activity, I designed a set of four crRNAs targeting highly

conserved coding regions of the virus. Additionally, I designed a single crRNA targeting only the 3'UTR SARS-CoV-2. Coronaviruses such as SARS-CoV-2 harbor a discontinuous transcription mechanism[157]. The replicase complex starts to transcribe its mRNAs from the 3'end of the viral genome and jumps at specific sequences (transcription-regulatory sequence, TRS) to the far 5' part of the genome, causing the expression of mRNAs in different reading frames. Since all mRNAs start to be transcribed at the 3' end, each viral mRNA and the RNA genome can be targeted by a single 3'UTR targeting crRNA (Fig. 38).

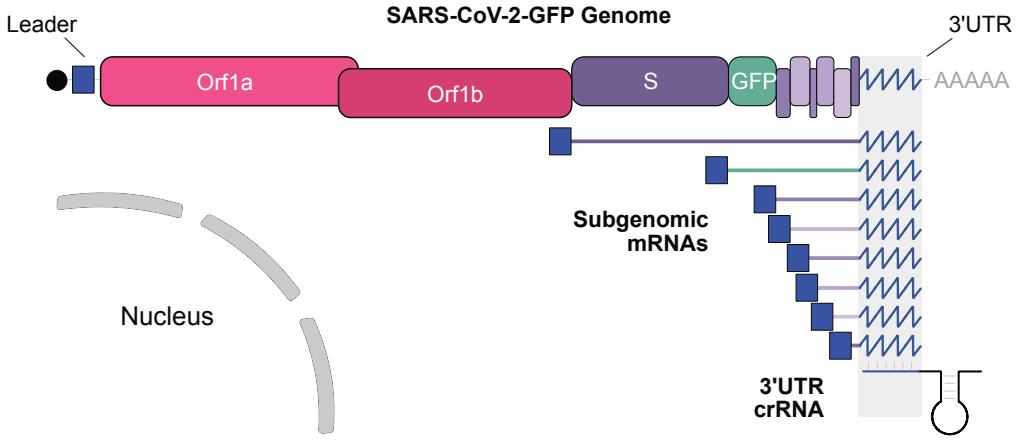

Fig. 38 | Rational targeting of the SARS-CoV-2 genome architecture. Schematic representation of SARS-CoV-2 RNA genome structure with inserted reporter GFP. Targeting of the genome and all subgenomic RNAs by 3'UTR targeting crRNA.

My collaboration partner (AG Pichlmair, Klinikum Rechts der Isar) transfected HEK293T-ACE2 cells with mRNA encoded Cas13d-SL and crRNAs targeting either the 3'UTR or a pool of four crRNAs targeting coding regions. Subsequently, the cells were infected with SARS-CoV-2 labeled with GFP, and viral infection propagation was measured through increased GFP expression. The coding sequence targeting crRNA showed a significant but moderate reduction in the viral load. Interestingly, the condition without Cas13d-SL, but with only the crRNAs alone, induced some antiviral effect, which might be a simple antisense effect. Strikingly, the 3'-UTR targeting crRNA completely inhibited SARS-CoV-2-GFP replication and depended entirely on the presence of Cas13d-SL (Fig. 39a, b).

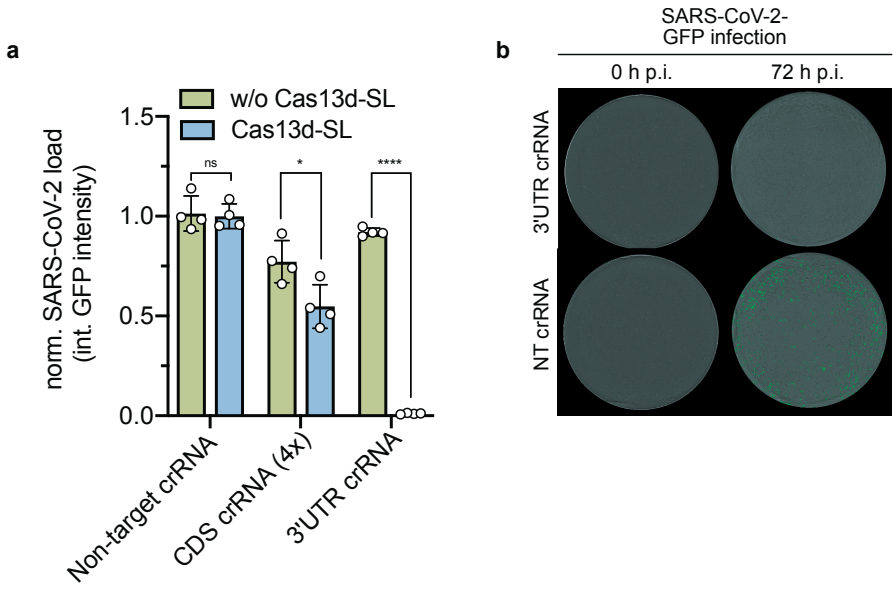

Fig. 39 | Targeting of SARS-CoV-2-GFP by Cas13d-SL. a, SARS-CoV-2-GFP replication, measured by integrated GFP intensity for either a pool of 4 crRNAs, targeting coding sequences, or a single crRNA targeting the 3'UTR. Statistical analysis: Unpaired Student's t-test with $*P < 0.05$; $**P < 0.01$; $***P < 0.001$; $****P < 0.0001$, shown as mean +/- s.d. for n=4 biological replicates. **b,** Incucyte S3 endpoint image after 72 h post-infection for targeting or non-targeting conditions.

Subsequent live measurements revealed that Cas13d-SL/3'UTR crRNA blocked SARS-CoV-2-GFP replication throughout the entire time course of the experiment (Fig. 40a). Ultimately, these results were confirmed for the severe SARS-CoV-2 Delta subtype. Cells were transfected with Cas13d-SL mRNA, chemically stabilized 3'-UTR crRNA, and subsequently infected with SARS-CoV-2-Delta. Two days after the infection, RNA was isolated from infected cells and analyzed by RNA sequencing. Sequencing results confirmed the strong inhibition of viral load upon Cas13d-SL treatment and the expected homogeneous reduction of all SARS-CoV-2-Delta transcripts containing the 3'-UTR target sequence (Fig. 40b). For all SARS-CoV-2 experiments, the same 3'-UTR crRNA was used, revealing that the system was fairly robust against viral mutations.

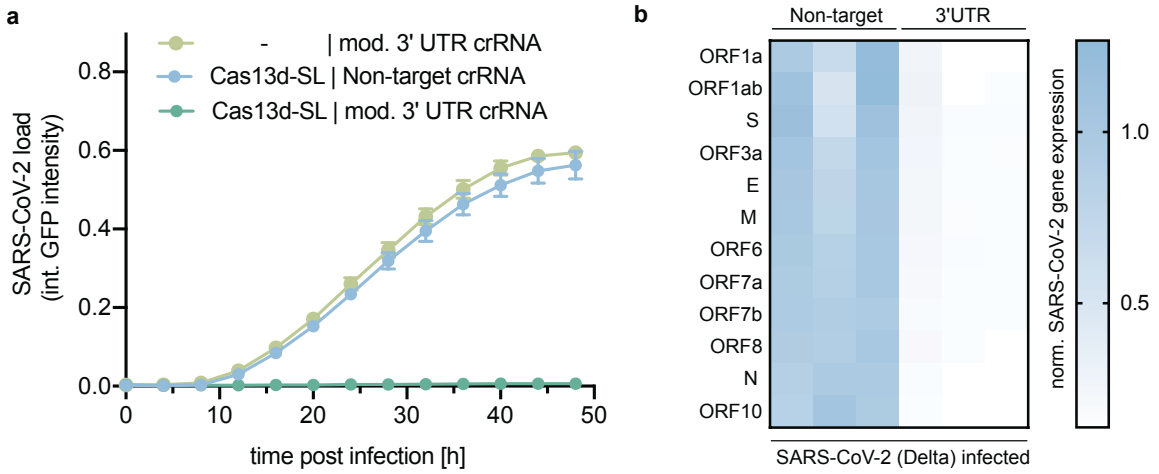

Fig. 40 | Longitudinal and variant-specific inhibition of SARS-CoV-2 by Cas13d-SL. a, Live measurement of SARS-CoV-2-GFP viral load by integrated GFP intensity over 48 h under different targeting conditions, shown as mean +/- s.d. for n=4 biological replicates. **b,** RNA-seq analysis of SARS-CoV-2 (Delta) subgenomic mRNAs expression after 48 h of treatment with Cas13d-SL along with a non-target or 3'UTR target crRNA for n=3 biological replicates.

These results confirm that Cas13d-SL can be formulated in a therapeutically relevant mRNA format and applied as a highly efficient and programmable antiviral system against different variants of SARS-CoV-2 and most likely for a wide variety of RNA viruses.

6 Discussion

CRISPR/Cas13d is one of the first RNA targeting CRISPR systems described with great potential in fundamental research and clinical applications. Here, I engineered a novel Cas13d system with cytosolic localization, characterized its biological activity, and applied it as an antiviral system.

6.1 Optimization of Cas13d RNA targeting

To review the divergent information on the optimal Cas13d crRNA, I initially characterized crRNAs ranging from 22 nt to 30 nt. I found that a crRNA length of 22 nt, as suggested in most studies[45, 73], was not optimal in my experimental setup. Instead, I found an optimal length of 26 nt. The recommendation to use a 22 nt crRNA could have historical reasons since the original study in which Cas13d was described performed the biochemical characterization for a different ortholog of the Cas13d family (RspCas13d) instead of the ortholog used in mammalian cells (RfxCas13d)[45]. Presumably, RspCas13d prefers a 22 nt crRNA, whereas RfxCas13d prefers a 26 nt. Interestingly, I also found that a longer crRNAs decreased the efficiency as well. Most likely, longer crRNAs tend to misfold and therefore decrease the efficiency. Furthermore, the addition of a tRNA or ribozyme upstream of the U6 terminator increased the knockdown efficiency. My intention in adding these motifs to the crRNA was to cleave off the 4-6 uracil added by the U6 terminator to the crRNA, as they can partially pair with the highly conserved AAAC motif at the very 3'end of the direct repeat of the crRNA. In fact, the addition of these motifs significantly increased the efficiency. Instead of avoiding mispairing, these motifs might also support proper folding of the crRNA since tRNAs, in particular, fold in highly stable structures. During this characterization, I had an astonishing finding: a C/T mutation at position 25 of the crRNA direct repeat when I isolated crRNAs from transfected cells and sequenced them. Given that purposely mutating this position almost completely abolished the activity of the crRNA, understanding the cause of this alteration might open new directions for improving the Cas13d system. I hypothesize that this position is recognized by an endogenous enzyme and is post-transcriptionally modified. If this is true, it could be either a random effect or a cellular rescue mechanism to avoid unwanted Cas13d cleavage.

6.2 Engineering of Cas13d subcellular localization

The initial study, which characterized Cas13d, compared different localization tags fused to Cas13d and concluded that an NLS is optimal[45]. Historically, CRISPR RNAs were expressed from a U6 promoter because this promoter has been the workhorse for Cas9 gRNA expression for multiple applications[10, 36, 37]. For RNA targeting applications, a more diverse localization portfolio may be required. My characterization confirmed previous reports that the knockdown efficiency for nuclear Cas13d is preferred[45, 74]. From a cell

biological point of view, this is quite surprising in the case of mRNA targeting since transcribed RNAs are exported rapidly and leave only a very short time window for nuclear Cas13d to degrade its target RNA[158]. Additionally, the size of Cas13d (approximately 160 kDa) exceeded the limit for passive diffusion between the cytoplasm and nucleus. Therefore, nuclear import signals have to be added, but the nuclear import of such a large protein is challenging and can only be achieved by the fusion of multiple nuclear localization signals[92]. In sum, these challenges make it surprising that Cas13d is most active in the nucleus and support the hypothesis that crRNA localization is the driver of Cas13ds nuclear preference.

Interestingly, altering crRNA locations has never been discussed so far, neither for Cas13 nor for any other CRISPR system. The most obvious way to achieve cytosolic localization was to express the crRNA from a pol II promoter. As shown in this work for GAPDH mRNA, pol II transcripts are highly efficiently transported out of the nucleus. Three elements are essential for the export of pol II transcripts: 5' Cap, Exon-Exon-Junction (EEJ) complex, and 3' polyA[159]. Here, I found that even if the pol II crRNA was exported efficiently, the resulting knockdown efficiency was very low. Presumably, one or more of these elements, which are important for nuclear export, interfere with proper crRNA function. I used the CAG promoter for pol II-dependent crRNA expression. The CAG promoter is composed of the CBh core promoter, CMV enhancer, and β-actin intron[160]. Therefore, the resulting crRNA is 5'capped, and the EEJ complex is bound upstream of the crRNA and could avoid binding of Cas13d to the crRNA. Pol II transcripts usually code for proteins. The ribosome binds to the 5' cap and starts scanning for the Kozak/ATG sequence. During translation, EEJ complexes are removed from the transcript – if this does not happen, the RNA is degraded via the non-sense-mediated decay (NMD) pathway[161]. A transcript expressing noncoding pol II crRNA may not be bound by the ribosome, leading to NMD-mediated degradation of the transcript. Even if the knockdown efficiency for pol II crRNAs was not satisfactory, it is interesting to note that an NES-fused Cas13d was much more efficient than an NLS-fused Cas13d with it, further supporting the hypothesis that the location of the crRNA determines the location preferences of the Cas13d enzyme. Additionally, I explored the possibility of exporting crRNAs from the nucleus in a pol II-independent manner. Many viruses, such as HIV, have developed alternative RNA export routes[162]. One of these is the minihelix motif of adenoviruses[137, 163]. Unfortunately, the minihelix-modified crRNA was hardly exported. Further optimization of this strategy is needed, such as adding multiple minihelix motifs or motifs from other viruses that might be used (e.g., Constitutive Transport Element, CTE[164]). An aspect that I did not further investigate here is the crRNA processing capability of Cas13d. Cas13d can process crRNAs from a larger transcript[45]. This means that export motifs are cleaved off from the crRNA after binding to the enzyme. I expect this to not affect export efficiency since these crRNAs were combined with NES-Cas13d. Therefore, the enzyme binds to the crRNA after its nuclear export. If pre-crRNA

processing interferes with export, processing mutants have been described to avoid this activity.

The most efficient crRNA export strategy I developed here is based on a nucleocytoplasmic shuttling system. Other than, for example, mitochondrial transport, nuclear and cytosolic proteins are transported in a folded state[165]. Folded export is essential since unfolding of Cas13d during import/export would release the crRNA from the RNP complex. Interestingly, various biological processes rely on shuttling proteins, such as viruses or even optogenetic tools, to transport cargos[97, 162]. This study is the first to use designed shuttling proteins to transport RNA cargos across the nuclear membrane. The exact balance between the NLS and NES signals for optimal shuttling is challenging to predict because it mainly relies on the shuttling protein. Large proteins may need additional NLS signals to be imported into the nucleus, whereas smaller proteins may need to be fused to additional NES signals to avoid accumulation in the nucleus. Currently, the optimal NLS/NES composition for each protein needs to be tested experimentally; however, design principles might be developed in the future if more experimental data for other designed shuttling proteins become available. Even if multiple designs were tested here, the crRNA export efficiency was not perfect and probably can never be perfect. The system relies on the equilibrium between protein import and export. Because the protein is present in both compartments by design, the efficiency of crRNA export will never reach 100%. If this is sufficient, it likely depends on the particular application and the protein. Perhaps, better export strategies can be built on this knowledge in the future. The localization variants v1-v5 I tested here showed an optimal knockdown efficiency for v3 with two NLS and one NES. My interpretation of these results is that the NLS-only fused variant v1 has crRNA and protein in the same location, but the target mRNA is quickly exported. Therefore, mRNA targeting is possible but inefficient. NES only v5 contains the protein and target RNA in the same place, but the crRNA is missing. Besides binding to crRNA that leaks from the nucleus, Cas13d-NES cannot target RNA. Intermediate variants v2-v4 are located to varying degrees in the nucleus or cytosol and are, therefore, capable of targeting mRNA. In line with this interpretation is the finding that Cas13d fused to an NLS is most stable with a pol III crRNA, but Cas13d fused to an NES is most stable with a pol II crRNA. In both cases, the protein and crRNA are located in the same compartment, presumably stabilizing each other in an RNP complex.

6.3 RNA replicon targeting with Cas13d-SL

I established a novel VEE replicon system that expresses two interferon response blocking proteins (B18R[139] and E3L[140]) and, therefore, could be maintained in culture for several months instead of two weeks for a normal VEE replicon. Notably, the cells were under constant selective pressure. Consequently, cells that lose replicon RNA do not survive.

Thus, it is unclear which percentage of cells would keep the replicon RNA without selection. Interestingly, only a small number of cells started to express the replicon immediately after transfection, and within this population, significant differences in expression levels were detected. This suggests that a significant fraction of *in vitro* transcribed replicon RNA is non-functional. Replicon RNA is 12 kb in size, which is a significant challenge to transcribe for standard formulations of T7 polymerase. Therefore, truncated *in vitro* transcribed RNA products are generated, but complete replicon RNA must be transcribed since the full-length 3'UTR is essential for replication. Further improvements are needed to yield full-length replicon RNA, such as T7 polymerase mutants or optimized nucleotide and buffer conditions.

As expected, NLS-Cas13d was almost unable to degrade cytosolic replicon RNA. Only a slight effect was observed, presumably because of leakage of the RNP complex from the cytosol. However, Cas13d-SL was highly efficient in degrading replicon RNA because of its semi-cytosolic localization. I co-transfected iRFP720 coding plasmid, initially to gate for transfected cells. Surprisingly, iRFP720 expression was reduced in all conditions expressing Cas13d-SL compared to nuclear Cas13d and correlated with the knockdown efficiency of replicon RNA. Since iRFP720 and replicon RNA do not share any common sequence motif and since the effect was consistently measured across nine different Cas13d crRNAs, it is strongly suggested that Cas13ds collateral activity is the cause of this phenomenon. Most likely, efficient targeting of replicon RNA results in more activated Cas13d molecules, leading to stronger collateral activity and, therefore, reduced iRFP720 expression. One could argue that this observation is limited to the particular case of replicon targeting. Therefore, I targeted normal mRNAs in murine cell lines to additionally exclude any species effect. Here I observed the same effect, suggesting a species-conserved mechanism.

6.4 Biological characterization of Cas13d-SL collateral activity

To gain a deeper understanding of the effect observed during replicon targeting, I performed an unbiased measurement of the global protein translation. If the effect is indeed caused by Cas13d collateral activity, one would expect it not to be limited to iRFP720 but to the global transcriptome or proteome. Since an effect on the transcriptome should also be visible in the proteome, but not vice versa, I analyzed global cellular protein translation during Cas13d-SL targeting. Strikingly, I observed an almost 10-fold reduction in protein translation in Cas13d-SL targeting conditions. As it is still controversial whether Cas13d collateral activity exists in mammalian cells, this effect is surprisingly pronounced and raises several questions. Most importantly: What is different in my experimental setup compared to other studies, enabling such a strong effect?

First, I targeted an exogenously transfected RNA expressed from a plasmid. Multiple plasmid copies enter a transfected cell, and the RNA is expressed from a strong CAG promoter. Both of these factors cause very high expression levels of the target RNA. In subsequent experiments, I showed that Cas13d-SL collateral activity is related to target RNA expression, as more Cas13d-SL molecules can be activated from a higher expressed target RNA. Most other studies targeted low-expressed endogenous targets[45, 73, 74]. Therefore, Cas13ds collateral activity might be below a certain detection level in these conditions.

Second, the reduced expression of iRFP720 in replicon-targeting experiments for Cas13d-SL compared to Cas13d fused to an NLS only suggests that Cas13d-SL exhibits higher collateral cleavage activity. The original idea for designing Cas13d-SL was to maximize its knockdown activity by bringing the system into the cytosol, where most of the mRNA targets are present. Because higher on-target cleavage is correlated with higher collateral cleavage, Cas13d-SL induces a stronger collateral effect than Cas13d-NLS, which has been used in other studies.

Third, throughout this study, I mainly analyzed the impact of Cas13d-SL targeting at the protein level, even if Cas13d is an RNase. This is because reading out protein levels is straightforward and therefore eases the analysis of a wide variety of constructs. Most previous studies analyzed the consequences of Cas13d targeting on the RNA level by RT-qPCR or transcriptomics. Here, I found not only a strong inhibition of cellular protein translation but also linked it to a Cas13d-induced cut in 28S rRNA and confirmed that 28S rRNA could rescue Cas13d-induced collateral cleavage. This suggests that, indeed, the protein level might be much more affected than the RNA level and could therefore explain why previous studies did not take note of this effect. Generally, this might also question some of my results for the knockdown efficiency of different Cas13d constructs against a co-transfected nanoluciferase because the global inhibition of protein translation might contribute to a second layer of nanoluciferase knockdown beyond the direct targeting of the target RNA. It is complicated to decipher how much of the effect is induced by directly targeting the mRNA and how much is caused by Cas13d-SL collateral activity, as both activities are co-dependent. Additional experiments are required to carefully analyze the RNA and protein levels in a targeting experiment.

One of the key findings to support this argument is the precise cutting of the 28S rRNA, which was directly caused by Cas13d-SL. An off-target effect based on simple mispairing of Cas13d crRNA, as it is widely described for Cas9[11, 166, 167], could be a potential explanation for this result. This explanation is highly unlikely because the same 28S rRNA cut became visible for multiple crRNAs and depended on the presence of a target RNA.

Instead, it is very likely that the cut was induced by Cas13d-SLs collateral activity due to an unknown structure or sequence preferences.

Another critical question in this context is whether the identified 28S cut is the only or at least the primary target of the collateral activity. Since ribosomal RNA is the highest expressed RNA, making up 80% of cellular RNA, it is the only RNA directly visible on a simple gel when loaded with extracted total RNA. Therefore, it could be possible that the identified 28S cut is the most prominent target due to its high expression, but not the only target. The only conclusion that can be drawn from this finding is that within ribosomal RNA, Cas13d prefers a specific position in 28S rRNA, as no random degradation pattern was found. Since protein translation is such a fundamental cellular process, it could indeed be that 28S rRNA is the primary target of Cas13ds collateral activity because of evolutionary selection for an essential process. Cas13d is a bacterial system; therefore, this process must be conserved in the bacterial host if it is selected during evolution. Sequence alignment of the bacterial equivalent to human 28S rRNA, 23S rRNA from *Ruminococcus flavefaciens strain XPD3002* does not show clear sequence conservation, neither between the expected cleavage position in 28S rRNA nor any other sequence. This suggests that the cleavage position in the human 28S rRNA has reasons other than a conserved mechanism, such as simple accessibility. Another explanation could be that not sequence similarities, but structural similarities between bacterial and human ribosomes, guide Cas13d to this position in human 28S rRNA. Since the structure of *Ruminococcus flavefaciens strain XPD3002* has not yet been solved, this possibility cannot be excluded but needs to be further explored. Furthermore, an unbiased sequencing approach is highly recommended to elucidate whether 28S rRNA is indeed the main target of Cas13d-SL collateral activity or just the most obvious target. Subsequently discussed ribosomal rescue experiments indicated that 28S rRNA cleavage is the primary driver of the downstream cellular consequences of Cas13d activation, even if this does not exclude additional effects. This raises the question of the exact function of the target position in the 28S rRNA. No particular function has been assigned to the ES15L loop in the literature[144, 168]. The structure seems to be surface-exposed, supporting the hypothesis that Cas13d is not guided to the position for functional reasons but for accessibility reasons. In addition, the ES15L loop is a ribosomal expansion element that was extended during evolutionary development[105]. Interestingly, the ES15L loop is hardly conserved between humans and other mammals and seems to be unstructured because it is not solved in ribosomal structures[144]. In summary, this information also questions whether the position in rRNA is cleaved by Cas13d on purpose.

Intriguingly, the identified cleavage position is precisely located where some species have a ‘hidden break’ in their rRNA, and others have an intron to avoid breaking of the rRNA[106, 107]. This correlation leads one to speculate that human rRNA might also have a hidden

break in this position, but an intron avoids the break here. If this is true, further speculation could be made that the observed Cas13d-induced rRNA cleavage is related to this phenomenon.

6.5 Identification of 28S rRNA as the major cause of translational inhibition

Prior to this study it was known that the RNase domain of Cas13d is exposed on the surface upon activation of the enzyme by recognizing a target RNA[55, 65]. In bacteria, this activity leads to a dormancy effect but not to cell death[70]. Cas13d is believed to randomly cleave RNA without specificity for sequences, RNA species, or motifs. Here, I question this expectation, at least for heterologous mammalian hosts. The clear cut in 28S rRNA suggests that it is involved in the observed translational inhibition. A similarly plausible explanation is that Cas13d indeed cleaves RNA randomly. Unspecific degradation of mRNA, tRNA, and rRNA would presumably also lead to a substantial reduction in global protein translation. To dissect these co-dependencies and identify the actual cause of Cas13d-induced translational inhibition, I set up an *in vitro* translation system in which Cas13d can be supplemented or removed to test for its influence. Coupling Cas13d to magnetic beads allowed me to remove it from the system by applying magnetic force and to study if and what kind of damage it leaves behind in the *in vitro* translation system before adding the translated mRNA.

In this experimental setup, it became clear that incubation of *the in vitro* translation lysate with activated Cas13d had a drastic impact on the subsequently added mRNA, even if Cas13d and translated mRNA were spatially and temporally separated. This excludes the possibility that Cas13d degrades only mRNA, as stated in the literature. However, pre-incubation of the translation system in the absence of translated mRNA compared to constant incubation together with translated mRNA resulted in a similar reduction in translation efficiency. This suggests that the effect on the translational machinery is much more important than the direct cleavage of mRNA – if relevant at all.

Narrowing down the collateral activity of Cas13d on the components of the translation machinery instead of mRNA raises the question of which component is mainly affected by Cas13d. The degradation of tRNAs could lead to a translational block similar to rRNA degradation. To further answer this question, I attempted to rescue damaged *in vitro* translation lysate by adding an unaffected 60S ribosomal subunit. Since conditions supplemented with 60S ribosomal subunit were almost as translationally competent as the Cas13d-untreated *in vitro* translation system, this strongly suggests that, indeed, ribosomes are the primary cause of Cas13d-induced translational inhibition. Some technical uncertainties remain: Do beads coupled with Cas13d behave in the same manner

as free Cas13d? And could the remaining Cas13d protein in the supernatant after removal of Cas13d beads still have an impact, even if reduced by several orders of magnitude?

The experimental setup established here enables to easily add and remove Cas13d and study its impact, but if this setup indeed allows drawing conclusions for the cellular conditions remains open to discussion. It is impossible to completely remove Cas13d from a cellular system before a certain mRNA is expressed. This complicates the translation of the results obtained from the cell extract to a cellular situation but should be attempted because it could shed light on the exact consequences of Cas13d activation in mammalian cells. Different inducible promoter systems could be harnessed for such an attempt.

Together with my previous results on 28S rRNA cleavage, I hypothesize the following model to explain Cas13d-induced collateral activity in mammalian cells: Translated Cas13d protein binds to a crRNA. The binary complex searches for a complementary target RNA. The resulting ternary complex activates Cas13ds RNase activity, cleaving the target RNA and 28S rRNA. Damaged ribosomes are less competent in translating cellular proteins, leading to target RNA-induced cellular shutdown.

Depending on the application, it might be desirable to block Cas13ds collateral activity. Recently, Cas13d mutants were generated, which seem to have a lower intrinsic affinity for RNA and, therefore, are less collateral active[169]. Another option would be to directly target the ribosomal mechanism uncovered here by reducing ribotoxic stress. In fact, several specific RNA targeting tools exist. Therefore, it might be preferable not to block Cas13ds natural collateral activity but instead to harness it for novel applications that could profit from RNA-induced cell shutdown. Examples of such applications could be cancer treatment, elimination of misdifferentiated cells in cell replacement therapies, or – as it was done here – targeted antiviral therapies.

6.6 Self-regulation of Cas13d-SL

My model for Cas13d-SL activation and its impact on translation led me to hypothesize that Cas13d-SL should be subjected to an autoregulatory loop. Strong Cas13d-SL activation leads to a strong reduction in global protein translation and, therefore, a strong reduction in newly synthesized Cas13d-SL, which in turn leads to a weakening of the collateral effect on translation and subsequent increased Cas13d expression. This mutual dependency was computationally modeled to simulate different scenarios. On the one hand, this model provided interesting insights into the potential interaction, but on the other hand, it was limited to some key variables and could not model the entire complexity of the cellular situation. Some variables that were not integrated into the model but might be relevant in a natural biological system could be the regeneration rate of defective ribosomes,

energy consumption during this process, on-target activity of the crRNA, and many more. Even if a model cannot represent the whole reality of a cell, successful validation of one of the essential findings and reasonable prediction of multiple other scenarios suggests that the model can provide valuable insights into the consequences of Cas13d-SLs collateral activity in mammalian cells.

A direct experimental consequence of the model's prediction that the degree of Cas13d-SL collateral activity is strongly correlated with target RNA expression was to target a single RNA molecule with multiple crRNAs. The idea here was that endogenous target RNA expression could not be manipulated. However, when Cas13d-SLs activation is dependent on target RNA expression, it might be possible to boost Cas13d-SLs collateral activity artificially by retargeting the fragments of an already cleaved target RNA with additional crRNAs. Indeed, this strategy increased Cas13d-SLs collateral activity, but a saturation effect became visible for 5-6 crRNAs already. Thus, it is likely that the effect cannot be enhanced infinitely, but this might also depend on the target RNA. Very long target RNAs may be more susceptible to this strategy since longer fragments should be degraded more slowly than short fragments, and therefore increase the time window in which an additional crRNA can bind and activate Cas13d-SL.

I suggest that Cas13d-SL autoregulation is the underlying cause of why I and other studies did not detect drastically reduced viability of activated Cas13d-SL expressed cells as one would expect for a protein translation inhibiting system. I carried out these experiments in robust cell lines (HEK293T, N2a, C2C12). However, it remains unclear whether more sensitive cell types, such as primary or stem cells, are equally tolerant to Cas13d-SL activation.

6.7 Establishment of Cas13d-SL as a programmable antiviral therapy

Following the development of Cas13d-SL and the characterization of the biological consequences of its activation, I applied Cas13d-SL as a programmable antiviral system. Initially, I transferred the system to an mRNA-based expression system. Therefore, I analyzed the effect of multiple elements previously shown to improve the expression level from mRNA. One key element was the addition of stabilizing UTRs to Cas13d-SL mRNA. These UTRs not only protect RNA from degradation but also contain regulatory elements to improve translation efficiency[152], which might be cell-type dependent to a certain degree. The UTRs I used were only tested in HEK293T cells. It remains to be tested whether they improve translation efficiency in other cell lines and, most importantly, *in vivo.* The other aspect that might contribute to expression levels is the coding itself. Here, I used human codon-optimized sequences designed from ideal codon usage, but for an mRNA expression system, other regulatory motifs might be considered; for example, splicing

motifs, polyadenylation signals, or internal Kozak sequences should be avoided. Taken together, there is still room for improving the expression of Cas13d-SL from mRNA.

Targeting SARS-CoV-2-GFP with Cas13d-SL and a 3'UTR targeting crRNA almost completely blocked viral replication. A pool of four crRNAs targeting different coding sequences in SARS-CoV-2-GFP mRNAs substantially reduced viral load. Surprisingly, the crRNA control condition also led to a 20% reduction. A simple antisense effect of crRNAs may explain this surprising finding. Complementary binding of crRNAs to the SARS-CoV-2 genome or mRNAs could induce endogenous degradation mechanisms, such as RNAi, or simply interfere with proper translation or replication of the targeted viral fragment, thereby slowing viral replication. Because these effects are complicated to predict, an active degradation mechanism based on Cas13d-SL is still preferred. A potential risk of targeting viral RNAs with only a single crRNA, as I did here for the 3'UTR crRNA, is that escape mutants might appear. Previous studies have shown that Cas13d accepts a single mismatch in its crRNA/target RNA duplex but not two consecutive mismatches. This implies that a virus must acquire two consecutive mismatches to escape Cas13d-SL targeting. In particular, 3'UTRs could be susceptible to such alterations since mutations do not lead to mutated protein products. This theoretical consideration needs to be evaluated in long-term experiments, as the short-term experiment performed in this study did not indicate such a problem, but it cannot be excluded. In the case of SARS-CoV-2, the 3'UTR is highly conserved between multiple coronavirus subtypes, suggesting a regulatory function. Therefore, in the particular case of coronaviruses, escape from a 3'UTR crRNA is unlikely.

I have extensively characterized the collateral activity of Cas13d-SL and hypothesized that it might be advantageous for antiviral therapy. Collateral activity is highly conserved in all Cas13 subtypes and orthologs studied to date; therefore, it could be a crucial feature of the CRISPR/Cas13 defense system. Previous studies suggested that Cas13 exhibits this activity to slow down phage replication after recognition of a phage nucleic acid by blocking phage and host protein expression[55, 70]. Because phages in bacteria and viruses in humans are closely related, it is very likely that the collateral activity of Cas13d-SL strongly contributes to the antiviral effect against SARS-CoV-2 measured in this study.

Another observation I made was that the effect of Cas13d-SL targeting was more pronounced in the case of the SARS-CoV-2-GFP fluorescent live assay compared to the measurement of the SARS-CoV-2 delta endpoint by RNA-seq. The different properties of these two viral strains may explain this finding. SARS-CoV-2-GFP might be attenuated by the expression of the GFP transgene and, therefore, be more susceptible to Cas13d-SL targeting. Another explanation corresponds to previous sections of this study. For SARS-CoV-2-GFP, the protein level was measured, assuming that GFP expression levels

correlated with the viral load. SARS-CoV-2 delta replication was assayed at the transcriptome level using RNA-Seq. I found that Cas13d-SL strongly affected cellular protein translation upon activation. Therefore, it could be that the second layer of Cas13d targeting of cellular protein translation covers a much higher viral replication in the SARS-CoV-2-GFP targeting condition. This possibility must be considered when further dissecting the different layers of Cas13d-SL targeting of RNA viruses.

The pioneering work I have done here to establish Cas13d-SL as a programmable and broadly applicable antiviral therapy requires further development. One of the critical questions in this regard is whether the system is similarly efficient in a more complex *in vivo* situation compared with well-controlled cell culture conditions. Multiple additional aspects arise *in vivo*, such as a possible immune reaction against the bacteria-derived foreign Cas13d protein or natural barriers that must be overcome, such as the mucus of the lungs[170, 171]. Low-immunogenic Cas13d variants could be developed by rational design or high-throughput screening of protein variants to overcome this potential limitation. Another aspect is the relatively high amount of 150 ng of RNA for 25,000 cells used for virus-targeting experiments. This amount is probably not transferable to *in vivo* conditions. Therefore, more efficient expression systems must be developed.

Here, I used a liposome-based delivery system composed of a cationic lipid to deliver Cas13d-SL to cells infected with SARS-CoV-2. Liposomes are constructed from double membranes with an aqueous core where the RNA is located. The cationic lipid component binds to the cell membranes via simple electrostatic interactions, inducing endocytosis[172]. This mechanism has been well established for decades for cell culture experiments but is difficult to transfer to *in vivo* systems because of the relatively unstable double membrane and missing cellular tropism. Therefore, novel delivery modalities must be developed and tested to transfer Cas13d-SL *in vivo*. Two main technologies exist for RNA delivery *in vivo*: Virus-like particles (VLPs)[173, 174], and derivatives thereof and lipid nanoparticles (LNPs)[175, 176]. Especially the latter are currently in focus because of their successful use in SARS-CoV-2 mRNA vaccines[177]. Technically, LNPs are similar to liposomes but other than liposomes, they do not consist of an aqueous core or a double membrane. Instead, RNA is directly complexed by the lipid, thereby increasing its stability compared to that of liposomes[172]. Generally, the established Cas13d-SL mRNA system can be adapted to LNPs in a relatively simple manner. One limitation of all current RNA delivery vehicles is to program target cell types. In summary, it remains to be seen whether LNPs will be the delivery vehicle of choice or if other technologies will emerge for the efficient transport of Cas13d-SL mRNA into infected cells.

Besides these technical challenges, this study showed the great promise Cas13d-SL may hold as programmable antiviral therapy.

7 Conclusion & Outlook

CRISPR/Cas13 is the first RNA targeting CRISPR system described. It is simple to program and is applicable in many organisms, opening doors to a wide variety of RNA targeting applications, including RNA knockdown and post-transcriptional modifications. Previous studies on Cas13 in eukaryotes lacked a deeper understanding of how Cas13 functions in a compartmentalized cell compared to its non-compartmentalized prokaryotic origin[43-45]. Furthermore, Cas13s collateral activity in eukaryotes remains elusive. To address this research gap, I combined multiple molecular, biochemical, and cellular technologies, uncovering the consequences of CRISPR/Cas13 activation in mammalian cells. Based on these results, I developed a framework to apply CRISPR/Cas13 for next-generation programmable antivirals.

My initial characterization of RNA knockdown by Cas13d in mammalian cells highlights the importance of carefully designing expression constructs when transferring bacterial systems to eukaryotes. The human U6 promoter is terminated by six consecutive uracils that are partially added to the transcript. In the case of Cas13ds crRNA, these additional nucleotides interfere with the correct folding of the crRNA. The addition of a cleavage motif upstream of the terminator sequence rescued this effect. In addition, compartmentalization was not considered when the system was transferred to mammalian cells. U6 transcripts remain in the nucleus, whereas, in most cases, the target RNA of interest is located mainly in the cytosol. Such targeting constraints have not yet been considered. Therefore, the crRNA relocalization strategies I developed here might open new possibilities for subcellular RNA knockdown by Cas13d. A wide variety of focused RNA degradation applications, such as synaptic RNA, centrosomal RNA, or mitochondrial RNA knockdown, could be envisioned. These strategies are not limited to Cas13d but could also be a valuable approach for other programmable RNA targeting tools such as Cas7-11[51, 178, 179]. Strikingly, relocating the crRNA not only shifted the activity of Cas13d to the cytosol but also significantly enhanced its knockdown efficiency. Since multiple studies reported moderate knockdown efficiency for different Cas13 subtypes, this new enzyme variant could be a tool to improve RNA targeting in mammalians. An interesting observation I made during this process was that Cas13d accepts insertions at every relevant position of its crRNA (5', 3', direct repeat). This finding may be important for future RNA targeting applications beyond knockdown. Similar to the SAM system for Cas9-based transcriptional activation[180], one could envision crRNA modifications that bring effector molecules in proximity to the Cas13d binding site.

The most promising crRNA export strategy I developed was based on a shuttling enzyme variant. To date, shuttling enzymes have not been explored for cell engineering

applications. Beyond crRNA transport, several other applications could be envisioned. Shuttling proteins could promote the export of mRNA to the cytosol or the import of proteins into the nucleus to manipulate gene regulation. Shuttling proteins might even transport co-factors or metabolites to certain positions inside the cell. In general, insights into crRNA localization might be valuable for directing different CRISPR systems to subcellular localizations, such as mitochondria. A recent study showed that the limitation of mitochondrial targeting by Cas9 is the missing import of gRNA[181]. Shuttling and other similar systems may help to overcome this limitation.

I found that the stability of the Cas13d protein was strongly enhanced by the presence of a crRNA. Presumably, the crRNA acts as a scaffold structure for the protein. As similar observations were made for Cas9[9], it can be speculated that this is a general feature of all CRISPR systems. If this is correct, new directions for optimizing CRISPR enzymes could be to strengthen the crRNA/protein complex, for example, by fusing RNA binding proteins.

To test the cytosolic knockdown ability of Cas13d, I established a solely cytosolic RNA replicating system based on the VEE replicon. I added two interferon response inhibiting proteins (B18R[139] and E3L[140]) which allowed me to culture these cells for several weeks. This newly developed system might also be helpful in situations where extended, but not infinite, gene expression is desired. For instance, advanced gene editing tools, such as Base and Prime Editing, involve multiple steps of enzymatic activity and cellular response and, therefore, might profit from such a system[182, 183].

One of the key findings of this study is that Cas13d strongly impairs global protein translation upon activation. Such a mechanism has not been previously described and may open new directions in antiviral/antiphage research. Tackling such a fundamental process as protein translation leads to a situation in which viral or phage proteins can no longer be produced and is, therefore, a highly efficient way to block viral/phage propagation. Further investigation of other Cas13 subtypes or phage defense systems using a similar mechanism could shed new light on the bacteria-phage arm-race. In particular, ribosomes are of great interest in this regard. Ribosomes are critical for cellular protein translation; therefore, any ribosome-interfering mechanism can severely affect host and pathogen protein expression. To gain insight into the impact of Cas13d on protein translation, I used a mammalian *in vitro* translation assay. This system might be a valuable tool to further investigate the Cas13d-ribosome relationship since it allows noninvasive addition or removal of factors from the system to test for their function. I coupled Cas13d to magnetic beads to remove the enzyme from the *in vitro* translation assay or added new 60S ribosomes. Beyond these two components, it would be interesting to see if other molecules could rescue the effect, such as 28S rRNA itself.

Upon noticing that collateral activity is also present in mammalian cells and might impact Cas13d itself, a complex self-regulatory interplay was suggested. Interestingly, this aspect has never been discussed to date, neither for natural nor heterologous Cas13 expression systems. From a biological perspective, this could be an essential feature since bacteria are not multicellular, and therefore an altruistic system, as initially suggested for Cas13d, would be surprising. Instead of killing phage-infected cells and therefore protecting the bacterial population by overshooting Cas13 activity, nature might have created a system that is self-regulating to slow down phage replication without destroying the host cell. Targeting protein translation as a central hub in cellular organization would be an efficient way to design a phage and a self-regulating system. Targeting a general pathway such as protein translation would also mean that the cellular consequences are highly complex to predict. Therefore, I co-developed a mathematical model to pre-test the impact of multiple parameters on targeted knockdown and self-regulation. This model provides valuable information on the dependencies between Cas13d expression, stability, activity on target RNA knockdown, and self-regulation. One key aspect of this model was that Cas13d self-regulation is strongly correlated with target RNA expression, which I could experimentally confirm. Furthermore, the model suggests that target RNA knockdown could be strongly enhanced if Cas13d protein stability was increased, presumably because the already translated protein is no longer affected by the collateral effects of activated Cas13d molecules. In conclusion, modeling complex situations such as Cas13ds self-regulation can help test hypotheses and preselect research activities without laborious experimental testing. However, experimental confirmation of the key insights is necessary and can help optimize the model further. Similar models could be applied to a wide variety of problems at the intersection of fundamental research and bioengineering. Cellular differentiation and reprogramming are other examples of complex interactions in which modeling could help make informed decisions.

To apply Cas13d-SL in a potential therapeutic setting, I transferred the system from a DNA expressed to an mRNA-expressed tool. The major advantage of mRNA is its short half-life and minimal risk of integration into the genome; therefore, it has a beneficial safety profile. Other than DNA, mRNA is relatively unstable and can trigger a robust immune response when transferred from an exogenous source. Decades of research have explored the use of mRNA to express therapeutic proteins or vaccines[121, 154, 184, 185]. When adapting Cas13d-SL for mRNA expression, I incorporated many of these improvements, namely, a native 5'cap structure, modified uracil, stabilizing UTRs, and a genetically encoded 3' polyA. The addition of these elements remarkably enhanced the efficiency of Cas13d-SL expression from mRNA. Recent interest in mRNA-based protein expression shed light on further improvements, such as large-scale screening of UTR motifs[186], and stabilization of RNA by circularization[187]. Adding these latest advancements to Cas13d-SL mRNA could further improve its efficiency and increase its half-life. In general, the optimization steps I

performed showed that careful design is required when transferring a DNA-based expression to an mRNA-based expression system. Several parameters can and should be optimized to obtain an optimal expression system. This is particularly important for non-coding RNAs, such as Cas13d-SL crRNA. The optimal design of non-coding RNAs is hardly described yet. In this study, I incorporated chemically stabilized motifs at the 5' and 3' end of the crRNA to improve its half-life. Beyond this, internal motifs could be added to further improve the stability.

Ultimately, I used Cas13d-SL as a programmable antiviral system. Previous studies reported moderate efficiency of such an approach because it relied on the leakage of crRNA from the nucleus to target cytosolic RNA viruses. To overcome this limitation, I developed Cas13d-SL, a nucleocytoplasmic shuttling enzyme. One of the key findings here was that crRNA design should be closely coupled with viral biology. Instead of targeting conserved regions, targeting regions present in multiple viral transcripts can be advantageous because a single crRNA can then efficiently block viral replication. In general, the proof-of-concept study for SARS-CoV-2 in this work confirmed the great potential of Cas13d-SL as a broad-spectrum antiviral system. Other RNA viruses beyond SARS-CoV-2 should be targeted to further explore this potential, such as the clinically relevant class of *Bunyavirales*, including Hantavirus. Other than conventional therapeutic approaches, such as small molecule or antibody-based therapies, Cas13d-SL does not target a protein structure but directly targets the viral RNA genome. Targeting genetic information has the significant advantage of relying on simple antisense pairing of crRNA and target RNA, which is easily predictable instead of complex molecular docking simulations or screenings, as it is the case for protein targeting approaches. Currently, 2.5 mio. RNA viruses are known, along with their genetic sequences[188]. Within days multiple crRNAs for each virus could be computed to be prepared for viral spillover infections. Thus, the programmable nature of Cas13d-SL could open the door to a new class of broad-spectrum antivirals with a huge potential to combat existing viral threats and future pandemic preparedness programs.

In this work, I tested and optimized Cas13d variants for targeted knockdown in mammalian cells. I developed shuttling Cas13d-SL as the first cytosolic Cas13d variant, described a novel mechanism of target RNA-induced cleavage of 28S rRNA, and applied this system as a programmable antiviral. Based on this study, two key questions remain: First, is 28S rRNA the only collateral target or the most pronounced target? Unbiased sequencing approaches such as Nanopore direct RNA sequencing of Cas13d-SL treated cells could reveal other potential targets and possible conserved sequence motifs which are targeted. Second, is Cas13d-SL an efficient antiviral system *in vivo*? The initial results in a well-controlled *in vitro* system suggested that Cas13d-SL is highly efficient in blocking viral replication. In an *in vivo* model, multiple additional aspects come into place, such as

tissue distribution, immune response, and finding a suitable delivery vehicle. If these challenges can be overcome, Cas13d-SL will be a major advance in the treatment of numerous virus-borne diseases.

8 Material & Methods

8.1 Molecular cloning

Chemically competent *E. coli* K-12 DH5α strain and NEB Stable Competent *E.coli* cells were used for plasmid DNA transformation. For chemical transformation, bacterial cells were first heat-shocked, then recovered in SOC Outgrowth Medium (NEB) at 37 °C, and finally plated on lysogeny broth (LB) agar plates with the appropriate antibiotics (1:1000 ratio) and incubated overnight at 37 °C or 30 °C. Transfected clones were inoculated in 2 mL 2X LB medium with the respective antibiotics (1:1000 ratio) and incubated at 37 °C. Using the Monarch Plasmid Miniprep Kit (NEB), plasmid DNA was purified according to the manufacturer´s protocol. Fragments for DNA cloning were generated by PCR or restriction digests. PCRs were performed with Q5 Hot Start High-Fidelity 2X Master Mix (NEB) or KOD One PCR Master Mix (Merck Millipore) in a 25 µL reaction volume according to the manufacturer´s protocol. DNA restriction digests were generated by plasmid DNA digest in a total volume of 30 µL using restriction enzymes (NEB and ThermoFisher) according to the manufacturer's protocol at 37 °C for 60 min. to overnight. Subsequently, the resulting DNA fragments were analyzed by agarose gel electrophoresis and extracted from the gel (Monarch Gelex kit). Plasmids were cloned with a 1:3 insert to backbone ratio by ligation or Gibson assembly using Instant Sticky-end Ligase Master Mix (NEB) or NEBuilder HiFi DNA Assembly Master Mix (NEB).

8.2 Mammalian cell culture

(HEK293T-ACE2 cell line generation was performed by AG Pichlmair)

Cells were cultured at 37 °C, 5 % CO_2 in an H_2O-saturated atmosphere. HEK293T cells were maintained in DMEM (Gibco) supplemented with 10 % FBS and 1 % Penicillin-Streptomycin. To passage the cells at 90 % confluence, cells were washed with DPBS (Gibco) and detached with 0.05 % Trypsin-EDTA (Gibco). Cells were further cultivated at an appropriate density. For transfection experiments, viable cells were counted using Trypan Blue solution (Sigma Aldrich) to stain nonviable cells and plated on 96-well, 48-well or 6-well plates. For generating HEK293T-ACE2 cells, ACE2 sequence was amplified from an ACE2 expression vector (provided by S. Pöhlmann) and cloned into the lentiviral vector pWPI-puro. HEK293T cells were transduced and selected with puromycin.

8.3 Plasmid transfection

The day before transfection, HEK293T cells were passaged, and 2.5 x10^4 cells per well for 96-well format, 7 x10^4 cells per well for 48-well format, or 5.0 x10^4 cells per well for 8-well-format were seeded. For 96-well format and 8-well format, a total of 75 ng DNA per well was transfected, while for 48-well format, a total of 150 ng per was transfected. JetOptimus DNA transfection reagent (Polyplus transfection) was used according to the manufacturer´s protocol. The transfection reagent was added to the sample using a ratio

of 1.5 at 90 % confluency. The medium was changed every 24 hr after transfection, and cells were analyzed after 2-3 days.

8.4 Knockdown of nanoluciferase reporter

Protein isolation of samples was performed using 5X passive Lysis buffer (Promega). Therefore, the medium was removed completely from the plate. 5X passive Lysis buffer was diluted with water, and 100 µL of the mixture was added to every well. The plate was incubated for 10 min while shaking. After incubation, the plate was centrifuged for 5 min at 1000 rpm. The supernatant was harvested for further experiments. Finally, 10 µL protein was diluted in 40 µL PBS, and the samples were analyzed using the NanoLuc-Assay (Promega) according to the manufacturer´s protocol.

8.5 Knockdown measurement of endogenous TFRC via flow cytometry

Samples were transfected in a 48-well plate. After 3 d, the media was removed, and the cells were treated with 300 µL of Accutase (Gibco). The samples were transferred in Eppendorf Tubes and centrifuged for 10 min. After removing the supernatant, the cells were resuspended in 150 µL antibody solution. For the antibody solution, the TFRC antibody BLD-334105 (Biozol, 1:2000) was diluted in FACS buffer (1xPBS, 5% (v/v) FBS, 2 mM EDTA). After the cells were incubated for 30 min at 4 °C, the samples were centrifuged for 10 min. The supernatant was removed, and the cells were washed 2x with PBS. Next, the cells were resuspended in FACS buffer and passed through a cell strainer into a Corning Falcon Test Tube (Fisher Science). Fluorescence-activated cell sorting (FACS) was performed on the BD FACSaria II and controlled with the BD FACSDiva Software (Version 6.1.3, BD Biosciences).

8.6 Sequencing analysis of expressed crRNA

RNA from crRNA transfected cells was extracted (Monarch Total RNA Miniprep Kit, NEB), reverse transcribed, and amplified in a one-step reaction (Luna Universal Probe One-Step RT-qPCR, NEB) with primers binding in the crRNA scaffold and spacer part. The resulting PCR product was gel extracted (Monarch DNA Gel Extraction Kit, NEB) and sent for amplicon sequencing. Genewiz (Leipzig) performed library preparation and MiSeq sequencing. The resulting sequencing reads were mapped with Geneious Prime to the expected crRNA sequence. The Consensus sequence and mutation rate were calculated in Geneious Prime from the mapped sequencing reads. Subsequently, a crRNA variant containing C/T mutation was cloned and compared to unmodified crRNA in a nanoluciferase knockdown assay.

8.7 Imaging of Cas13d localization and quantification

Cas13d transfected cells were fixed with 10 % formalin-solution (Sigma-Aldrich) for 10 min at 37 °C and washed 3x with PBS 48-72 h post transfection, permeabilized (1% BSA, 0.5%

Triton X-100 in PBS) and stained with 1:500 diluted appropriate primary and fluorophore coupled secondary antibody. Additionally, cellular membranes were stained with Wheat Germ Agglutinin CF488A (Thermo Fisher). Subsequently, cells were DAPI stained (1:1000) and imaged with an EVOS Cell Imaging (Thermo Fisher) or CellInsight NTX High Content Analysis (ThermoFisher Scientific) device. Nuclear and cytosolic fluorescence intensities were manually analyzed using Fiji (Image J).

8.8 Fluorescence *in situ* hybridization (FISH) analysis of crRNA and GAPDH mRNA localization

The localization of CRISPR/Cas13d, its crRNA, and GAPDH was visualized by RNA FISH staining. Transfected cells in an 8-well slide were fixed with 10 % formalin-solution (Sigma-Aldrich) for 10 min at 37 °C and washed 3x with PBS. The cells were permeabilized with ice-cold 70 % ethanol at 4 °C for 4 h and then incubated with pre-hybridization-solution (2x saline sodium citrate (SSC), 10% formamide, 1:20 ribonucleoside vanadyl complex (VRC)) for 15 min at 37 °C. Atto488 labeled crRNA probe (Metabion), and Quasar labeled GAPDH probe (Stellaris) were mixed with FISH hybridization buffer (ddH_2O, 2x SSC, 10 % formamide, 15 mg/ml tRNA, 50 % dextran sulfate, 50 mg/ml BSA, 10 mM VRC) and incubated at 37 °C overnight. The next day, the samples were washed 3x with pre-hybridization buffer, followed by 3x with PBS and imaged. For stability quantification of the crRNA, cells were fixed, stained by RNA FISH, and imaged. Total crRNA staining intensity was manually measured in Fiji (ImageJ).

8.9 Western Blot analysis of protein stability

After removing all media from 96 well plates, protein samples were obtained by adding 50 µL of M-PER Mammalian Protein Extractions Reagent (Thermo Fisher Scientific) supplemented with protease inhibitor (1:100) (ThermoFisher Scientific). After incubating for 10 min at room temperature, 20 µL of supernatant was taken out and incubated at 95°C 1:1 with Laemmli buffer (Sigma Aldrich). The samples were loaded onto a 15-4 % gradient gel (Invitrogen). The gel was run in NuPAGE Running Buffer (Thermo Fisher Scientific). The SDS gel was blotted to a PDVF membrane (Bio-Rad) in a wet blotting chamber (Invitrogen) overnight at 4°C, 15 V. Next, the membrane was incubated in 5 % blocking buffer (PBS-T, 5 % milk powder). Then, the membrane was washed 3x in PBS-T (10x PBS, 1 % Tween 20) and incubated at 4 °C overnight in 5 % milk powder solution with the primary antibody (1:1000) or 2-5 h at room temperature. After washing the membrane 3x, it was incubated in milk powder solution with the secondary antibody conjugated to peroxidase (1:5000) for 2-5 h at room temperature. For signal detection, Amersham ECL Prime Detection Reagent (Sigma-Aldrich) was pipetted onto the membrane. Fusion (VILBER) was used to visualize chemoluminescence.

8.10 VEE replicon cell line generation

The VEE replicon (Merck Millipore) was modified via PCR and restriction digest to add mGreenLantern and puromycin resistance under the control of the 26S subgenomic promoter. The resulting plasmid was *in vitro* transcribed with HiScribe T7 Quick High Yield RNA Synthesis Kit (NEB) and afterward capped with the One-Step Capping and 2´-O-Methylation Kit (NEB) according to the manufacturer´s protocol in a 40 µL reaction with 15 µg of transcribed RNA supplemented with 1 µL RNase Inhibitor. RNA Poly-A-Tailing was performed using *E. coli* Poly(A) Polymerase (NEB) of capped RNA according to the manufacturer´s manual. To generate a "stable" cell line in HEK293T, the *in vitro* transcribed, capped, and poly-adenylated VEE replicon fused to mGreenLantern was transfected using JetMessenger RNA transfection reagent (Polyplus transfection) according to the manufacturer´s protocol. Transfected cells were selected by adding 1 µg/mL Puromycin-Dihydrochloride (Gibco) to the media 3 days post transfection. After successful selection, the cells were cultured in medium with 4 µg/mL Puromycin. 14 days after selection, stable fluorescence was confirmed by imaging. Additionally, RNA-dependent replication without DNA was confirmed by RT-PCR amplification of extracted RNA (Monarch Total RNA Isolation Kit, NEB) for VEE replicon and AAVS1 control gene and compared to PCR amplification of genomic DNA template (Wizard Genomic DNA Purification Kit, Promega) with the same primer sets.

8.11 Knockdown measurement of VEE replicon

replicon cells were transfected with Cas13d, crRNAs and iRFP720 coding plasmids. After 72 h, cells were treated with 300 µl Accutase (Gibco) for 15 min at room temperature. FACS buffer (1xPBS, 5% (v/v) FBS, 2 mM EDTA) was added to the cells and passed through a cell strainer into a Corning Falcon Test Tube (Fisher Science). FACS was performed on the BD FACSaria II and controlled with the BD FACSDiva Software (Version 6.1.3, BD Biosciences).

8.12 Collateral activity analysis of Cas13d-SL in murine cell lines

Mouse-derived Neuro2A cells and C2C12 cells were transfected with Cas13d-SL and fluorescent reporter constructs (JetOptimus; Polyplus). 48 h after transfection, cells were imaged at an EVOS Cell Imaging (Thermo Fisher) device for fluorescence intensity at 530 and 586 nm.

8.13 Assay of global cellular protein translation

HEK293T cells were seeded in a 48 well plate and transfected 24 h later with nanoluciferase, crRNA, and Cas13d-SL or RNAi coding plasmids. 72h later, global protein translation was measured with Protein Synthesis Assay Kit (Cayman Chemicals) according to the manufacturer´s protocol. Briefly, cells were collected and incubated with O-Propargyl-Puromycin (OPP) for 30 min. During this incubation step, OPP was added to the C-terminus of nascent proteins. Subsequently, cells were fixed, washed, and 5-FAM

staining solution was added to induce click-chemistry-based modification of OPP in labeled proteins. Cells were washed, and fluorescence intensity at 530 nm was measured by flow cytometry. The resulting fluorescence intensity is proportional to actively translated protein.

8.14 rRNA cleavage analysis in cells

Cells were seeded, transfected with Cas13d-SL, and according crRNAs. 48 h after transfection, total RNA was extracted (Monarch RNA Miniprep Kit, NEB). For each condition, 2 µg RNA was mixed with 2x RNA loading dye (NEB), incubated at 70°C for 20 min. and subsequently, run on a 2% agarose gel and imaged. Selected RNA samples were analyzed on a Bioanalyzer 2100 (Agilent) according to the manufacturer´s protocol.

8.15 Cas13d protein production and purification, crRNA, and target RNA production

Cas13d coding sequence was cloned along with a 6xHis tag into a pET28a vector and expressed with NEBExpress Cell-free *E. coli* Protein Synthesis System (NEB) overnight at 30°C. Subsequently, Cas13d protein was purified with NEBExpress Ni Spin Columns and stored at -20°C. Templates for crRNA production were generated by polymerase extension of two overlapping oligonucleotides coding for T7 promoter and crRNA sequence. The crRNA was *in vitro* transcribed from PCR reactions by QuickYield HiScribe T7 *in vitro* Transcription Kit (NEB) and purified with Monarch RNA Cleanup kit (NEB). Target RNA sequences were generated accordingly but with a PCR product template instead of overlapping oligonucleotides.

8.16 rRNA cleavage analysis of purified total RNA and purified ribosomes

100 ng Purified target RNA, crRNA, and Cas13d protein were mixed with NEB 4 buffer and purified 80S human ribosomes isolated from HeLa cells (a gift from AG Beckmann, LMU Munich). The reactions were incubated for 30 min. at 37°C; subsequently, the reaction was stopped by the addition of EDTA, and the samples were treated with Proteinase K for 30 min. The samples were then mixed with 2x RNA loading dye and denatured at 70°C for 20 min. and analyzed on a 2% agarose gel.

8.17 Mapping of 28S rRNA cleavage site

Total RNA was extracted from cells and transfected with an active Cas13d-SL system. The RNA was then run on an agarose gel, and the 28S rRNA band at 5 kb, along with the band of interest at 3 kb, was cut out of the gel and extracted with Monarch RNA cleanup kit (NEB) by adding additional cleanup buffer and incubating the gel piece at 50°C for 10 min. Subsequently, both extracted RNAs were sent for RNA sequencing. RNA sequencing library preparation and Illumina paired-end sequencing was performed by GENEWIZ (Leipzig, Germany). RNA-seq reads were mapped to 28S rRNA with Geneious Prime software, and

differential reads (5 kb vs. 3 kb band) were calculated for each position. A drop in sequence coverage for the 3 kb band indicated the cleavage position.

8.18 Modeling and visualization of the rRNA cleavage site

The human 80S ribosome (PDB ID: 6QZP) was visualized, and missing structure information for the ribosomal ES15L motif was identified. The 3D structure of the missing sequence was modeled (https://rnacomposer.cs.put.poznan.pl) and manually added to the solved structure. The expected cleavage position was indicated in the modeled structure.

8.19 Cas13-HaloTag protein production, immobilization, and purity analysis

Cas13d, fused to Hibit and HaloTag, was cloned into a pET28 expression vector and expressed with NEBExpress Cell-free *E. coli* Protein Synthesis System (NEB) overnight at 30°C. The reaction was then incubated with 100 µl PBS washed HaloTag magnetic beads (Promega) for 2 h at room temperature to induce covalent binding of Cas13d-HaloTag to the beads. Protein-coupled beads were washed seven times with BSA containing wash buffer in PBS by applying magnetic force and stored at 4°C in Tris-HCl buffer supplemented with 20 mM $MgCl_2$. Subsequently, successful expression was confirmed via Hibit Assay (Promega). Additionally, sufficient washing of magnetic beads was monitored by protein depletion in the supernatant.

8.20 Impact of 28S rRNA cleavage on protein translation *in vitro* and 60S ribosomal rescue

Target RNA, crRNA, and Cas13d-HaloTag coupled magnetic beads were produced, as described in the previous sections. 200 ng crRNA, 500 ng target RNA, 1 µl murine RNase inhibitor (NEB), 5 µl 1:10 diluted Cas13d-HaloTag beads, 1 µl amino acid mix, 35 µl Rabbit Reticulocyte Lysate System (Nuclease Treated; Promega) were prepared in a 96 well plate. To activate Cas13d and induce its impact on the lysate, the reaction was then incubated at 37°C for 10 min under constant shaking to avoid settling of the magnetic beads. Magnetic force was applied to the plate, and either the supernatant without protein beads was transferred to a new well or the beads containing reaction was kept in the same well. To validate the successful depletion of Cas13d-HaloTag coupled beads in the supernatant, Hibit assay (Promega) was performed. Subsequently, 500 ng firefly luciferase coding mRNA and 5 µl D-luciferin (Carl Roth) were added to the supernatant or beads containing reactions. Under constant shaking at 37°C, firefly luciferase expression was monitored for 1:15 h in real-time in a Cytation 3 plate reader (Biotek). In a rescue experiment, purified 60S ribosomal subunit (Biovision) was added either to the supernatant without Cas13d beads or to the Cas13d beads containing reaction, along with firefly luciferase mRNA and D-luciferin substrate.

8.21 Modeling of Cas13d-SL autoregulation

(Developed by Richard Koll)

A discrete model was developed, inspired by the predator-prey relation with key equations:

- The idle generation and decay of agents is described by the following formula:
  N_t = N_(t-1) * 0.5^(1/h) + g (N_t: abundance at time t, h: halflife, g: generation rate)
- Cas13 destroys RNA according to the following formula:
  v_ti = v_(t-1)i * (x/E(v_t)) (v_t: vector of RNA abundances at time t, v_ti: abundance of RNA i at time t, E(v_t): total amount of RNA, x: cutting capacity of all Cas13 protiens combined)

Predictions were modeled for different input criteria and data exported to CSV files. These files were imported into GraphPad Prism and visualized.

8.22 Analysis of Cas13d-SL autoregulation for endogenous and exogenous transcripts

Increasing amounts of nanoluciferase target RNA coding plasmid were co-transfected with crRNA and Cas13d-SL fused to mNeonGreen. After 24 h, cells were fixed, DAPI stained, and imaged at an EVOS Cell Imaging (Thermo Fisher). The same experimental setup was used to test the impact on Cas13d-SL-mNeonGreen when targeting endogenous target RNAs. 72 h after transfection, the cells were collected and analyzed by flow cytometry for Cas13d-SL-mNeonGreen expression.

8.23 Amplification of Cas13d-SLs collateral activity

To amplify the collateral impact on Cas13d-SL-mNeonGreen, 38 crRNAs were pool cloned. Briefly, oligonucleotides coding for 38 crRNAs were designed with Gibson Assembly Overhangs, complementary to a human U6 expression vector, and ordered as oPool (IDT). The oligonucleotides were cloned into the expression vector and transformed. Resulting clones were scraped from the agar plate, and plasmid DNA was isolated. Subsequently, isolated plasmid DNA was transfected along with Cas13d-SL expression plasmid and target RNA coding plasmid. 48 h post transfection, cells were collected and analyzed via flow cytometry for Cas13d-SL-mNeonGreen expression. Pools of two to six crRNAs were pooled manually, but besides this, they were treated equally.

8.24 Cell Cycle determination of Cas13d-SL expressing cells

Cas13d-SL expression cells were harvested and DAPI stained. DAPI staining intensity indicates different cell cycle phases due to beginning, ongoing, or finished chromosomal replication and, therefore, different DNA content in each cell cycle phase. Cells were analyzed via flow cytometry, and gates were set depending on their DAPI staining

intensity. Nocodazole-treated cells for 18 h were used as technical control and gating aid for the G2/M phase.

8.25 Cas13 mRNA generation and crRNA modification

For standard *in vitro* transcription HiScribe T7 Quick High Yield RNA Synthesis Kit (NEB) and HiScribe T7 High Yield RNA Synthesis Kit (NEB) were used according to the manufacturer´s protocol. For mRNAs containing modified nucleotides, the HiScribe T7 High Yield RNA Synthesis Kit was used following the manufacturer´s protocol for modified nucleotides with N1-methyl-pseudouridine, CTP, ATP, and GTP at a concentration of 10 mM. RNA capping was performed using the One-Step Capping and 2´-O-Methylation Kit (NEB) according to the manufacturer´s protocol in a 40 µL reaction with 15 µg of transcribed RNA with 1 µL RNase Inhibitor added to the mix. RNA Poly-A-Tailing was genetically encoded or performed with 1x *E.coli* Poly(A) Polymerase Reaction Buffer (NEB), 10 mM ATP (NEB), 1 µL *E.coli* Poly(A) Polymerase (NEB), and 10 µg of capped RNA in a 20 µl reaction volume and incubated at 37 °C for 30 min. Each reaction was cleaned up using Monarch RNA Cleanup Kit (NEB) before proceeding with the next step. mRNAs were quality controlled on an agarose gel as described in previous sections.

8.26 RNA transfection and optimization for Reporter knockdown

The day before transfection, cells were seeded at a density of 2.5 x10^4 cells per well for 96-well format. A total amount of 150 ng RNA per well was transfected. JetMessenger RNA transfection reagent (Polyplus) was used according to the manufacturer´s protocol. The transfection reagent was added at a 1.5 ratio.

8.27 Virus strains, stock preparation, plaque assay, and *in vitro* infection

(performed by AG Pichlmair)

SARS-CoV-2 (delta) and SARS-CoV-2-GFP strains (PMID: **35833542**) were produced by infecting Vero E6 cells cultured in DMEM medium (10% FCS, 100 µg ml−1 Streptomycin, 100 IU ml−1 penicillin) for 2 days (MOI of 0.01). Viral stocks were collected and spun twice (1,000g for 10 min) before storage at −80 °C. The titer of viral stock was determined by plaque assay. Confluent monolayers of Vero E6 cells were infected with serial five-fold dilutions of virus supernatants for 1 h at 37 °C. The inoculum was removed and replaced with serum-free MEM (Gibco, Life Technologies) containing 0.5% carboxymethylcellulose (Sigma-Aldrich). Two days after infection, cells were fixed for 20 min at room temperature with formaldehyde added directly to the medium to a final concentration of 5%. Fixed cells were washed extensively with PBS before staining with water containing 1% crystal violet and 10% ethanol for 20 min. After rinsing with PBS, the number of plaques was counted, and the virus titer was calculated. Unless otherwise stated, all infections were performed by addition of inoculum to the supernatant of cells, corresponding to MOI 3 (SARS-CoV-2-GFP) or MOI 0.5 (wild-type).

8.28 SARS-CoV-2-GFP reporter virus assays

(performed by AG Pichlmair)

HEK293T-ACE2 cells were seeded into 96-well plates 1 day before transfection at the density of 25k cells/well. The cells were transfected with Cas13d-SL mRNA (100 ng/well) and crRNAs (50 ng/well) one day before infection using JetMessenger reagent (Polyplus), according to the manufacturer's instructions. Immediately following infection with SARS-CoV-2-GFP, the plate was placed in the IncuCyte S3 Live-Cell Analysis System (Sartorius), where images of phase, green, and red channels were captured at regular time intervals at 4× magnification. Cell viability was assessed as cell confluence per well (phase area). Virus growth was assessed as GFP integrated intensity normalized to cell confluence per well (GFP integrated intensity/phase area). Basic image analysis and image export were performed using the IncuCyte S3 software (Essen Bioscience; version 2019B Rev2).

8.29 SARS-CoV-2 delta infection and expression analysis

(viral infection was performed by AG Pichlmair)

HEK293T-ACE2 cells were seeded into 24-well plates at the density of 150k cells/well. One day post-seeding, the cells were transfected with 400 ng of Cas13d-SL mRNA and 200 ng of crRNAs per well. One day post-transduction, the medium was exchanged prior to infection with SARS-CoV-2 delta strain at MOI 0.5. RNA was isolated from infected cells by Trizol/Chloroform extraction 48 h post infection. RNA sequencing library preparation and Illumina paired-end sequencing was performed by GENEWIZ (Leipzig, Germany). Sequencing reads were processed in Geneious Prime by mapping them to SARS-CoV-2 reference sequence NC_045512 and calculating expression differences for the different conditions.

8.30 Materials

Tab. 1: Cell lines and bacterial strains

Description	**Supplier / Source**
C2C12	Jessica Giehrl-Schwab
E. coli DH5a	Annerose Kurz-Drexler
HEK293T	ATCC
HEK293T-ACE2	AG Pichlmair, Klinikum Rechts der Isar
NEB Stable Cells	NEB
Neuro2A	ATCC

Tab. 2: Relevant chemicals, enzymes, antibodies, and kits

Description	**Supplier**
10% Formalin solution	Sigma-Aldrich
2′-O-Methylation	NEB
5x Passive Lysis buffer	Promega
60S ribosomal subunit	Biovision
80S human ribosomes	AG Beckmann
Accutase	Thermo Scientific
Amersham ECL Prime Detection Reagent	Merck Millipore
Carbenicillin	Carl Roth
Chloroform	Merck Millipore
crRNA FISH Probe	Custom-made, Metabion
D-luciferin	Carl Roth
DMEM	Thermo Scientific
DPBS	Thermo Scientific
E. coli polyA polymerase	NEB
FBS	Thermo Scientific
FLAG antibody	Merck Millipore
GAPDH FISH Probe	Stellaris
HaloTag magnetic beads	Promega
Halt Protease Inhibitor	Sigma Aldrich
HiScribe T7 Quick High Yield RNA Synthesis Kit	NEB
Instant Sticky End Ligase Master Mix	NEB
JetMessenger	PolyPlus
JetOptimus DNA transfection reagent	PolyPlu
KOD One PCR Master Mix	Merck Millipore
Laemmli buffer	Sigma Aldrich
Luna Universal Probe One-Step RT- qPCR	NEB
M-PER Mammalian Protein Extractions Reagent	Thermo Scientific
Milk Powder	Carl Roth
Monarch DNA Cleanup Kit	NEB
Monarch DNA Miniprep Kit	NEB
Monarch Gel Extraction Kit	NEB
Monarch RNA Cleanup Kit	NEB
Monarch Total RNA Miniprep	NEB
Murine RNase Inhibitor	NEB
N1-methyl-pseudouridine	Jena Bioscience

Nano-Glo® HiBiT Lytic Detection System	Promega
NanoGlo Assay	Promega
NEBExpress Cell-free *E. coli* Protein Synthesis System	NEB
NEBExpress Ni Spin Columns	NEB
NEBuilder DNA HiFi Assembly Mix	NEB
Nocodazole	Sigma Aldrich
NuPage SDS Gel 4-15%	Thermo Scientific
oPool	IDT
PDFV membrane	Merck Millipore
Penicillin/Streptomycin	Thermo Scientific
Protein Synthesis Assay Kit	Cayman Chemicals
Puromycin	Thermo Scientific
Q5 Hot Start High-Fidelity 2X Master Mix	NEB
QuickYield HiScribe T7 *in vitro* Transcription Kit	NEB
Rabbit Reticulocyte Lysate System	Promega
Restriction Enzymes	NEB
Ribonucleoside vanadyl complex	NEB
RNA Loadingy Dye	NEB
SOC Outgrowth Medium	NEB
TFRC antibody	Biozol, BLD-334105
Trizol	Qiagen
Trypsin	Thermo Scientific
Vaccina Virus Capping	NEB
VEE replicon vector (Simplicon)	Merck Millipore
Wheat Germ Agglutinin CF488A	Thermo Scientific
Wizard Genomic DNA Purification Kit	Promega
Yeast tRNA	Thermo Scientific

Tab. 3: Software

Description	**Supplier**
FACS data	FlowJo
Graphics	Affinity Designer
Image analysis	Fiji (ImageJ)
Plasmid Design	Geneious Prime
References	EndNote
Statistics	Graphpad Prism

Tab. 4: Relevant plasmids

Construct name
miRNA_mRuby3
pbs-U6-RfxCas13d-_3'tRNA-Nluc-G1
pbs-U6-RfxCas13d-_3'tRNA-Nluc-G2
pbs-U6-RfxCas13d-3'tRNA-GAPDH-G2
pbs-U6-RfxCas13d-3'tRNA-GPX4-G1
pbs-U6-RfxCas13d-3'tRNA-GPX4-G2
pbs-U6-RfxCas13d-3'tRNA-LDHA-G1
pbs-U6-RfxCas13d-3'tRNA-LDHA-G2
pbs-U6-RfxCas13d-3'tRNA-MOXD1-G1
pbs-U6-RfxCas13d-3'tRNA-MOXD1-G2
pbs-U6-RfxCas13d-C/D-Box-mNG_3'tRNA
pbs-U6-RfxCas13d-empty_3'tRNA
pbs-U6-RfxCas13d-empty_3'tRNA invSV40pA
pbs-U6-RfxCas13d-mGL-1_3'tRNA
pbs-U6-RfxCas13d-mGL-2_3'tRNA
pbs-U6-RfxCas13d-mRuby3-Guide3_3'tRNA invSV40pA
pbs-U6-RfxCas13d-mRubyoPool_HCV
pbs-U6-RfxCas13d-Multiplex-mNeonGreen-Guide
pbs-U6-RfxCas13d-Nluc-G1-22bp_3'tRNA
pbs-U6-RfxCas13d-Nluc-G1-24bp_3'tRNA
pbs-U6-RfxCas13d-Nluc-G1-26bp_3'tRNA
pbs-U6-RfxCas13d-Nluc-G1-28bp_3'tRNA
pbs-U6-RfxCas13d-Nluc-G1-28bp_3'tRNA
pbs-U6-RfxCas13d-Nluc-G2_3'tRNA invSV40pA
pbs-U6-RfxCas13d-Nluc-G2_HDV
pbs-U6-RfxCas13d-Park7oPool_HCV
pbs-U6-RfxCas13d-TFRC-G1_3'tRNA
pbs-U6-RfxCas13d-TFRC-G2_3'tRNA
pbs-U6-RfxCas13d-VEEV-3'UTR-G1-26nt_3'tRNA
pbs-U6-RfxCas13d-VEEV-3'UTR-G1-26nt_3'tRNA
pbs-U6-RfxCas13d-VEEV-3'UTR-G2-26nt_3'tRNA
pbs-U6-RfxCas13d-VEEV-5'UTR-G1-26nt_3'tRNA
pbs-U6-RfxCas13d-VEEV-5'UTR-G2-26nt_3'tRNA
pbs-U6-RfxCas13d-VEEV-5'UTR-G2-26nt_3'tRNA
pbs-U6-RfxCas13d-VEEV-mGL-G3-26nt_3'tRNA
pbs-U6-RfxCas13d-VEEV-nsp2-G1-26nt_3'tRNA

pbs-U6-RfxCas13d-VEEV-nsp2-G1-26nt_3'tRNA
pbs-U6-RfxCas13d-VEEV-nsp4-G1-26nt_3'tRNA
pbs-U6-RfxCas13d-VEEV-nsp4-G1-26nt_3'tRNA
pbs-U6-RfxCas13d-wotRNA-Nluc-G1
pbs-U6-RfxCas13d-wotRNA-Nluc-G1-fullinvSV40
pbs-U6-RfxCas13d-wotRNA-Nluc-G2
pbs-U6-RfxCas13d-wotRNA-Nluc22nt-G1
pbs-U6-VARdm-RfxCas13d-Nluc-G2-3'tRNA
pCAG_Cas13preDR_Nluc-G2_preDR
pCAG_dRfxCas13d_NES_FLAG
pCAG_dRfxCas13d_NLS-NES-FLAG
pCAG_dRfxCas13d_NLS-NES-FLAG-mNG-NLS
pCAG_dRfxCas13d_NLS-NES-FLAG-NES
pCAG_dRfxCas13d_NLS-NES-FLAG-NLS
pCAG_dRfxCas13d_NLSv2
pCAG_RfxCas13d_NES_FLAG
pCAG_RfxCas13d_NES_FLAG-P2A-mRuby3
pCAG_RfxCas13d_NLS-NES-FLAG
pCAG_RfxCas13d_NLS-NES-FLAG-mNG-NLS
pCAG_RfxCas13d_NLS-NES-FLAG-NES
pCAG_RfxCas13d_NLS-v2-FLAG-PEST
pCAG_RfxCas13d_NLSv3_FLAG
pCAG_T7-5_betaglob-Apatmer-RfxCas13d_NLS-NES_FLAG
pCAG-Kozakdel-FLuc-PEST-bpA
pCAG-Kozakdel-NLuc-PEST-bpA
pETM-11_RfxCas13d_FLAG-HaloTag_Hibit
pETM-11_RfxCas13d_NLS_FLAG-6xHis
T7-VEE-B18R-P2A-E3L-P2A-mGL-IRES-PuroR

.

9 Supplementary Data

Suppl. Tab. 1: List of most relevant crRNAs

2a	AACCCCTACCAACTGGTCGGGGTTTGAAACCTGGATAGGGGTCACAGACACT AACCCCTACCAACTGGTCGGGGTTTGAAACCTGGATAGGGGTCACAGACACTCC AACCCCTACCAACTGGTCGGGGTTTGAAACCTGGATAGGGGTCACAGACACTCCCA AACCCCTACCAACTGGTCGGGGTTTGAAACCTGGATAGGGGTCACAGACACTCCCAG G AACCCCTACCAACTGGTCGGGGTTTGAAACCTGGATAGGGGTCACAGACACTCCCAG GTT AACCCCTACCAACTGGTCGGGGTTTGAAACGATCTTCAGGCCGTTCTCGCCG AACCCCTACCAACTGGTCGGGGTTTGAAACGATCTTCAGGCCGTTCTCGCCGCT AACCCCTACCAACTGGTCGGGGTTTGAAACGATCTTCAGGCCGTTCTCGCCGCTCA AACCCCTACCAACTGGTCGGGGTTTGAAACGATCTTCAGGCCGTTCTCGCCGCTCAGC AACCCCTACCAACTGGTCGGGGTTTGAAACGATCTTCAGGCCGTTCTCGCCGCTCAGC AC
2b	AACCCCTACCAACTGGTCGGGGTTTGAAACGATCTTCAGGCCGTTCTCGCCGCTCAGC AC AACCCCTACCAACTGGTCGGGGTTTGAAACCTGGATAGGGGTCACAGACACTCCCAG GTT
4a	AACCCCTACCAACTGGTCGGGGTTTGAAACCCTCACAAATGAAAGCAGTTGGCTGTTG AACCCCTACCAACTGGTCGGGGTTTGAAACTCCACGAGCAGAATACAGCCACTGTAAA
5b	AACCCCTACCAACTGGTCGGGGTTTGAAACAGTCCACGCCGTTGATGCTGCCGAAGAT GTGCAAGTCCTCGCCGTGGGCGTGATCCGAAAGGTGACCC AACCCCTACCAAACCCGGATCCGGGCGTGATCCGAAAGGTGACCCGCTAGCGGGAAC T GGTCGGGGTTTGAAACAGTCCACGCCGTTGATGCTGCCGAAGATGTGCA GGGCGTGATCCGAAAGGTGACCCGGATCCAACCCCTACCAACTGGTCGGGGTTTGAA A CAGTCCACGCCGTTGATGCTGCCGAAGATGTGCA
6b	AACCCCTACCAACTGGTCGGGGTTTGAAACCTGGATAGGGGTCACAGACACT AACCCCTACCAACTGGTCGGGGTTTGAAACGATCTTCAGGCCGTTCTCGCCG

	GGGCACTCTTCCGTGGTCTGGTGGATAAATTCGCAAGGGTATCATGGCGGACGACCG GGGTTCGAACCCCGGATCCGGCCGTCCGCCGTGATCCATGCGGTTACCGCCCGCGTGT CGAACCCAGGTGTGCGACGTCAGACAACGGGGGAGCGCTCCTAGTCCGGACAAGTAA ACCCCTACCAACTGGTCGGGGTTTGAAACCTGGATAGGGGTCACAGACACT GGGCACTCTTCCGTGGTCTGGTGGATAAATTCGCAAGGGTATCATGGCGGACGACCG GGGTTCGAACCCCGGATCCGGCCGTCCGCCGTGATCCATGCGGTTACCGCCCGCGTGT CGAACCCAGGTGTGCGACGTCAGACAACGGGGGAGCGCTCCTAGTCCGGACAAGTAA ACCCCTACCAACTGGTCGGGGTTTGAAACGATCTTCAGGCCGTTCTCGCCG CAAGTAAACCCCTACCAACTGGTCGGGGTTTGAAACCTGGATAGGGGTCACAGACACT CCCAGGTTCAAGTAAACCCCTACCAACTGGTCGGGGTTTGAAAC CAAGTAAACCCCTACCAACTGGTCGGGGTTTGAAACGATCTTCAGGCCGTTCTCGCCG CTCAGCACCAAGTAAACCCCTACCAACTGGTCGGGGTTTGAAAC
11	AACCCCTACCAACTGGTCGGGGTTTGAAACCTGGATAGGGGTCACAGACACTCCCAG GTT AACCCCTACCAACTGGTCGGGGTTTGAAACGATCTTCAGGCCGTTCTCGCCGCTCAGC AC
14c, 15	AACCCCTACCAACTGGTCGGGGTTTGAAACGTAACCTTTATCAAGCCACGAGGTGT AACCCCTACCAACTGGTCGGGGTTTGAAACGTAACCTTTATCAAGCCACGAGGTGT AACCCCTACCAACTGGTCGGGGTTTGAAACACCTAGCAAAACATGCGACACCATAC AACCCCTACCAACTGGTCGGGGTTTGAAACTGGGCTTCTCTCATGCGCCGCCCATC AACCCCTACCAACTGGTCGGGGTTTGAAACAGGTAATTGGTCTGGGCTTCTCTCAT AACCCCTACCAACTGGTCGGGGTTTGAAACAAAATAAAAATTTTAAGGCGGCATGC AACCCCTACCAACTGGTCGGGGTTTGAAACGCGAGTTCTATGTAAGCAGCTTGCCA AACCCCTACCAACTGGTCGGGGTTTGAAACCAGGCAACAAAACTGGTCCATCCCCA AACCCCTACCAACTGGTCGGGGTTTGAAACAGGCAACAAAACTGGTCCATCCCCAA
17	AACCCCTACCAACTGGTCGGGGTTTGAAACATGGTCTGCACGCCCTCATAAGGTCTGC CC AACCCCTACCAACTGGTCGGGGTTTGAAACATATGACATCAGAAGACTTTAAAATTGC AG AACCCCTACCAACTGGTCGGGGTTTGAAACCTCATGGCCTCTCTGTATCACTGGCTCAA C
24	AACCCCTACCAACTGGTCGGGGTTTGAAACCTGGATAGGGGTCACAGACACTCCCAG GTT

	AACCCCTACCAACTGGTCGGGGTTTGAAACGATCTTCAGGCCGTTCTCGCCGCTCAGC AC
25	AACCCCTACCAACTGGTCGGGGTTTGAAAC ATTTGTCTGTTTATTCCCACAAGGTAGC AACCCCTACCAACTGGTCGGGGTTTGAAAC TAGCGCTTCACCACGCAGCCGTTCTTGT AACCCCTACCAACTGGTCGGGGTTTGAAACAGGAAATGAGCTTGACAAAGTGGTCGTT GA AACCCCTACCAACTGGTCGGGGTTTGAAACTATTTGGCAGGTTTTTCTAGACGGCAGG TC AACCCCTACCAACTGGTCGGGGTTTGAAACAAACCTATTTCATGAGCCAACAGAGC AACCCCTACCAACTGGTCGGGGTTTGAAACTCTTTAAGAACAAGTGGAGCCTTCAC
28b	ACCCCTACCAACTGGTCGGGGTTTGAAACGCATTAATACAGCCACCATCGTAACAAT (modified and unmodified)
30	ACCCCTACCAACTGGTCGGGGTTTGAAACGCATTAATACAGCCACCATCGTAACAAT TACCCCTACCAACTGGTCGGGGTTTGAAACCCACATAATAAGCTGCAGCACCAGCTGT TACCCCTACCAACTGGTCGGGGTTTGAAACGCATTAATACAGCCACCATCGTAACAAT TACCCCTACCAACTGGTCGGGGTTTGAAACACAGAGATTATAAGAGCCCACATGGAAA AACCCCTACCAACTGGTCGGGGTTTGAAACCACCAATAATGATAGAGTCAGCACACAA
31	ACCCCTACCAACTGGTCGGGGTTTGAAACGCATTAATACAGCCACCATCGTAACAAT

Suppl. Tab. 2: List of Cas13d fused localization tags (inc. FLAG tag)

RfxCas13d	MIEKKKSFAKGMGVKSTLVSGSKVYMTTFAEGSDARLEKIVEGDSIRSVNEGEAFS AEMADKNAGYKIGNAKFSHPKGYAVVANNPLYTGPVQQDMLGLKETLEKRYFGE SADGNDNICIQVIHNILDIEKILAEYITNAAYAVNNISGLDKDIIGFGKFSTVYTYDEFK DPEHHRAAFNNNDKLINAIKAQYDEFDNFLDNPRLGYFGQAFFSKEGRNYIINYGN ECYDILALLSGLRHWVVHNNEEESRISRTWLYNLDKNLDNEYISTLNYLYDRITNELT NSFSKNSAANVNYIAETLGINPAEFAEQYFRFSIMKEQKNLGFNITKLREVMLDRKD MSEIRKNHKVFDSIRTKVYTMMDFVIYRYYIEEDAKVAAANKSLPDNEKSLSEKDIF VINLRGSFNDDQKDALYYDEANRIWRKLENIMHNIKEFRGNKTREYKKKDAPRLPR ILPAGRDVSAFSKLMYALTMFLDGKEINDLLTTLINKFDNIQSFLKVMPLIGVNAKFV EEYAFFKDSAKIADELRLIKSFARMGEPIADARRAMYIDAIRILGTNLSYDELKALADT FSLDENGNKLKKGKHGMRNFIINNVISNKRFHYLIRYGDPAHLHEIAKNEAVVKFVL GRIADIQKKQGQNGKNQIDRYYETCIGKDKGKSVSEKVDALTKIITGMNYDQFDKK RSVIEDTGRENAEREKFKKIISLYLTVIYHILKNIVNINARYVIGFHCVERDAQLYKEKG

	YDINLKKLEEKGFSSVTKLCAGIDETAPDKRKDVEKEMAERAKESIDSLESANPKLYA NYIKYSDEKKAEEFTRQINREKAKTALNAYLRNTKWNVIIREDLLRIDNKTCTLFRNK AVHLEVARYVHAYINDIAEVNSYFQLYHYIMQRIIMNERYEKSSGKVSEYFDAVND EKKYNDRLLKLLCVPFGYCIPRFKNLSIEALFDRNEAAKFDKEKKKVSGNS
V1	PPKKKRKVEDGEGPAAKRVKLDSGAAPAAKKKKLDYKDDDDK
V2	PPKKKRKVEDGEGPAAKRVKLDSGAAPAAKKKKLDYKDDDDKLQLPPLERLTL
V3	PPKKKRKVEDGEGLQLPPLERLTLSGAAPAAKKKKLDYKDDDDK
V4	PPKKKRKVEDGEGLQLPPLERLTLSGAAPAAKKKKLDYKDDDDKLQLPPLERLTL
V5	LQLPPLERLTLGSGDYKDDDDK

10 List of Tables and Figures

11 Acronyms

ASO	Antisense oligonucleotides
BSA	Bovine serum albumin
CAG	CMV enhancer CBA promoter and rabbit β-globin acceptor site
Cas9/13	CRISPR-associated protein 9/13
CMV	Cytomegalovirus
cDNA	Complementary DNA
CRISPR	Clustered Regularly Interspaced Short Palindromic Repeats
crRNA	CRISPR RNA
CTE	Constitutive Transport Element
DAPI	4’ , 6-Diamidin-2-phenylindol
DMEM	Dulbecco´s modified eagle medium
E. coli	Escherichia coli
FACS	Fluorescence-activated cell sorting
FBS	Fetal Bovinse Serum
FISH	Fluorescence in situ hybridization
Fluc	Firefly luciferase
gDNA	Genomic DNA
gRNA	guide RNA
HDR	Homology directed repair
HEK293T	Human embryonic kidney 293, large T
HIV	Human immunodeficiency virus
IVT	in vitro transcription
IRES	internal ribosome-entry sequence
kDa	Kilo Dalton
LNP	Lipid nanoparticles
NES	Nuclear export signal
NHEJ	Non-homologous end joining
NLS	Nuclear localization signal
Nluc	Nanoluciferase
NMD	Non-sense mediated decay
nsp	Non-structural proteins
NT	Non-target
mGL	mGreenLantern
mNG	mNeonGreen
mRNA	Messenger RNA
OPP	O-Propargyl-Puromycin
PBS-T	Phosphate-buffered saline with Tween-20
pol I	RNA Polymerase I
pol II	RNA polymerase II
pol III	RNA polymerase III
PUF	Pumilio family
RNAi	RNA interference
RNP	Ribonucleoprotein
rRNA	Ribosomal RNA

RT	Reverse transcription
SD	Standard deviation
SL	Shuttling
SSC	Saline sodium citrate
SV40	simian virus 40
TALE	Transcription activator-like effector
tracrRNA	Trans-activating crRNA
UTR	Untranslated region
VEE	Venezuelan equine encephalitis
VLP	Virus-like particles
VRC	Ribonucleoside vanadyl complex

12 References

1. Bothmer, A. et al. Characterization of the interplay between DNA repair and CRISPR/Cas9-induced DNA lesions at an endogenous locus. *Nat Commun* **8**, 13905 (2017).
2. Merkert, S. & Martin, U. Targeted genome engineering using designer nucleases: State of the art and practical guidance for application in human pluripotent stem cells. *Stem Cell Res* **16**, 377-386 (2016).
3. Cathomen, T. & Keith Joung, J. Zinc-finger Nucleases: The Next Generation Emerges. *Mol Ther* **16**, 1200-1207 (2008).
4. Kim, Y.G., Cha, J. & Chandrasegaran, S. Hybrid restriction enzymes: zinc finger fusions to Fok I cleavage domain. *Proc Natl Acad Sci U S A* **93**, 1156-1160 (1996).
5. Boch, J. et al. Breaking the code of DNA binding specificity of TAL-type III effectors. *Science* **326**, 1509-1512 (2009).
6. Boch, J. TALEs of genome targeting. *Nat Biotechnol* **29**, 135-136 (2011).
7. Bitinaite, J., Wah, D.A., Aggarwal, A.K. & Schildkraut, I. FokI dimerization is required for DNA cleavage. *Proc Natl Acad Sci U S A* **95**, 10570-10575 (1998).
8. Mojica, F.J., Diez-Villasenor, C., Garcia-Martinez, J. & Soria, E. Intervening sequences of regularly spaced prokaryotic repeats derive from foreign genetic elements. *J Mol Evol* **60**, 174-182 (2005).
9. Jinek, M. et al. A programmable dual-RNA-guided DNA endonuclease in adaptive bacterial immunity. *Science* **337**, 816-821 (2012).
10. Cong, L. et al. Multiplex genome engineering using CRISPR/Cas systems. *Science* **339**, 819-823 (2013).
11. Hsu, P.D. et al. DNA targeting specificity of RNA-guided Cas9 nucleases. *Nat Biotechnol* **31**, 827-832 (2013).
12. Mocellin, S. & Provenzano, M. RNA interference: learning gene knock-down from cell physiology. *J Transl Med* **2**, 39 (2004).
13. McJunkin, K. et al. Reversible suppression of an essential gene in adult mice using transgenic RNA interference. *Proc Natl Acad Sci U S A* **108**, 7113-7118 (2011).
14. Boettcher, M. & McManus, M.T. Choosing the Right Tool for the Job: RNAi, TALEN, or CRISPR. *Mol Cell* **58**, 575-585 (2015).
15. Shapiro, E., Biezuner, T. & Linnarsson, S. Single-cell sequencing-based technologies will revolutionize whole-organism science. *Nat Rev Genet* **14**, 618-630 (2013).
16. Biasco, L., Baricordi, C. & Aiuti, A. Retroviral integrations in gene therapy trials. *Mol Ther* **20**, 709-716 (2012).
17. Barbier, A.J., Jiang, A.Y., Zhang, P., Wooster, R. & Anderson, D.G. The clinical progress of mRNA vaccines and immunotherapies. *Nat Biotechnol* **40**, 840-854 (2022).
18. Gross, M. (Elsevier, 2021).
19. Rohner, E., Yang, R., Foo, K.S., Goedel, A. & Chien, K.R. Unlocking the promise of mRNA therapeutics. *Nat Biotechnol* **40**, 1586-1600 (2022).
20. Fire, A. et al. Potent and specific genetic interference by double-stranded RNA in Caenorhabditis elegans. *Nature* **391**, 806-811 (1998).
21. Agrawal, N. et al. RNA interference: biology, mechanism, and applications. *Microbiol Mol Biol Rev* **67**, 657-685 (2003).
22. Wilson, R.C. & Doudna, J.A. Molecular mechanisms of RNA interference. *Annu Rev Biophys* **42**, 217-239 (2013).

23. Hu, B. et al. Therapeutic siRNA: state of the art. *Signal Transduct Target Ther* **5**, 101 (2020).
24. Dana, H. et al. Molecular Mechanisms and Biological Functions of siRNA. *Int J Biomed Sci* **13**, 48-57 (2017).
25. Moore, C.B., Guthrie, E.H., Huang, M.T. & Taxman, D.J. Short hairpin RNA (shRNA): design, delivery, and assessment of gene knockdown. *Methods Mol Biol* **629**, 141-158 (2010).
26. Neumeier, J. & Meister, G. siRNA Specificity: RNAi Mechanisms and Strategies to Reduce Off-Target Effects. *Front Plant Sci* **11**, 526455 (2020).
27. Stojic, L. et al. Specificity of RNAi, LNA and CRISPRi as loss-of-function methods in transcriptional analysis. *Nucleic Acids Res* **46**, 5950-5966 (2018).
28. Crooke, S.T., Liang, X.H., Baker, B.F. & Crooke, R.M. Antisense technology: A review. *J Biol Chem* **296**, 100416 (2021).
29. Rinaldi, C. & Wood, M.J.A. Antisense oligonucleotides: the next frontier for treatment of neurological disorders. *Nat Rev Neurol* **14**, 9-21 (2018).
30. Singh, N.N., Luo, D. & Singh, R.N. Pre-mRNA Splicing Modulation by Antisense Oligonucleotides. *Methods Mol Biol* **1828**, 415-437 (2018).
31. Liang, X.H. et al. Antisense oligonucleotides targeting translation inhibitory elements in 5' UTRs can selectively increase protein levels. *Nucleic Acids Res* **45**, 9528-9546 (2017).
32. Liang, X.H., Sun, H., Nichols, J.G. & Crooke, S.T. RNase H1-Dependent Antisense Oligonucleotides Are Robustly Active in Directing RNA Cleavage in Both the Cytoplasm and the Nucleus. *Mol Ther* **25**, 2075-2092 (2017).
33. Prakash, V. Spinraza-a rare disease success story. *Gene Ther* **24**, 497 (2017).
34. Wang, Y., Wang, Z. & Tanaka Hall, T.M. Engineered proteins with Pumilio/fem-3 mRNA binding factor scaffold to manipulate RNA metabolism. *FEBS J* **280**, 3755-3767 (2013).
35. Choudhury, R., Tsai, Y.S., Dominguez, D., Wang, Y. & Wang, Z. Engineering RNA endonucleases with customized sequence specificities. *Nat Commun* **3**, 1147 (2012).
36. Chavez, A. et al. Highly efficient Cas9-mediated transcriptional programming. *Nat Methods* **12**, 326-328 (2015).
37. Gilbert, L.A. et al. CRISPR-mediated modular RNA-guided regulation of transcription in eukaryotes. *Cell* **154**, 442-451 (2013).
38. Khosravi, H.M. & Jantsch, M.F. Site-directed RNA editing: recent advances and open challenges. *RNA Biol* **18**, 41-50 (2021).
39. Jiang, K. et al. Programmable eukaryotic protein synthesis with RNA sensors by harnessing ADAR. *Nat Biotechnol* (2022).
40. Yi, Z. et al. Engineered circular ADAR-recruiting RNAs increase the efficiency and fidelity of RNA editing in vitro and in vivo. *Nat Biotechnol* **40**, 946-955 (2022).
41. Han, S. et al. RNA-protein interaction mapping via MS2- or Cas13-based APEX targeting. *Proc Natl Acad Sci U S A* **117**, 22068-22079 (2020).
42. Chritton, J.J. & Wickens, M. Translational repression by PUF proteins in vitro. *RNA* **16**, 1217-1225 (2010).
43. Abudayyeh, O.O. et al. RNA targeting with CRISPR-Cas13. *Nature* **550**, 280-284 (2017).
44. Cox, D.B.T. et al. RNA editing with CRISPR-Cas13. *Science* **358**, 1019-1027 (2017).
45. Konermann, S. et al. Transcriptome Engineering with RNA-Targeting Type VI-D CRISPR Effectors. *Cell* **173**, 665-676 e614 (2018).
46. Amitai, G. & Sorek, R. CRISPR-Cas adaptation: insights into the mechanism of action. *Nat Rev Microbiol* **14**, 67-76 (2016).

47. McGinn, J. & Marraffini, L.A. Molecular mechanisms of CRISPR-Cas spacer acquisition. *Nat Rev Microbiol* **17**, 7-12 (2019).
48. Newsom, S., Parameshwaran, H.P., Martin, L. & Rajan, R. The CRISPR-Cas Mechanism for Adaptive Immunity and Alternate Bacterial Functions Fuels Diverse Biotechnologies. *Front Cell Infect Microbiol* **10**, 619763 (2020).
49. Hille, F. et al. The Biology of CRISPR-Cas: Backward and Forward. *Cell* **172**, 1239-1259 (2018).
50. Zetsche, B. et al. Cpf1 is a single RNA-guided endonuclease of a class 2 CRISPR-Cas system. *Cell* **163**, 759-771 (2015).
51. van Beljouw, S.P.B. et al. The gRAMP CRISPR-Cas effector is an RNA endonuclease complexed with a caspase-like peptidase. *Science* **373**, 1349-1353 (2021).
52. Klompe, S.E., Vo, P.L.H., Halpin-Healy, T.S. & Sternberg, S.H. Transposon-encoded CRISPR-Cas systems direct RNA-guided DNA integration. *Nature* **571**, 219-225 (2019).
53. Strecker, J. et al. RNA-guided DNA insertion with CRISPR-associated transposases. *Science* **365**, 48-53 (2019).
54. Shmakov, S. et al. Discovery and Functional Characterization of Diverse Class 2 CRISPR-Cas Systems. *Mol Cell* **60**, 385-397 (2015).
55. Abudayyeh, O.O. et al. C2c2 is a single-component programmable RNA-guided RNA-targeting CRISPR effector. *Science* **353**, aaf5573 (2016).
56. Hu, Y. et al. Metagenomic discovery of novel CRISPR-Cas13 systems. *Cell Discov* **8**, 107 (2022).
57. Smargon, A.A. et al. Cas13b Is a Type VI-B CRISPR-Associated RNA-Guided RNase Differentially Regulated by Accessory Proteins Csx27 and Csx28. *Mol Cell* **65**, 618-630 e617 (2017).
58. Yan, W.X. et al. Cas13d Is a Compact RNA-Targeting Type VI CRISPR Effector Positively Modulated by a WYL-Domain-Containing Accessory Protein. *Mol Cell* **70**, 327-339 e325 (2018).
59. Xu, C. et al. Programmable RNA editing with compact CRISPR-Cas13 systems from uncultivated microbes. *Nat Methods* **18**, 499-506 (2021).
60. Silas, S. et al. Direct CRISPR spacer acquisition from RNA by a natural reverse transcriptase-Cas1 fusion protein. *Science* **351**, aad4234 (2016).
61. Mohr, G. et al. A Reverse Transcriptase-Cas1 Fusion Protein Contains a Cas6 Domain Required for Both CRISPR RNA Biogenesis and RNA Spacer Acquisition. *Mol Cell* **72**, 700-714 e708 (2018).
62. Schmidt, F. et al. Noninvasive assessment of gut function using transcriptional recording sentinel cells. *Science* **376**, eabm6038 (2022).
63. Schmidt, F., Cherepkova, M.Y. & Platt, R.J. Transcriptional recording by CRISPR spacer acquisition from RNA. *Nature* **562**, 380-385 (2018).
64. Toro, N., Mestre, M.R., Martinez-Abarca, F. & Gonzalez-Delgado, A. Recruitment of Reverse Transcriptase-Cas1 Fusion Proteins by Type VI-A CRISPR-Cas Systems. *Front Microbiol* **10**, 2160 (2019).
65. East-Seletsky, A. et al. Two distinct RNase activities of CRISPR-C2c2 enable guide-RNA processing and RNA detection. *Nature* **538**, 270-273 (2016).
66. Zhang, B. et al. Two HEPN domains dictate CRISPR RNA maturation and target cleavage in Cas13d. *Nat Commun* **10**, 2544 (2019).
67. Chen, J.S. et al. CRISPR-Cas12a target binding unleashes indiscriminate single-stranded DNase activity. *Science* **360**, 436-439 (2018).

68. Samai, P. et al. Co-transcriptional DNA and RNA Cleavage during Type III CRISPR-Cas Immunity. *Cell* **161**, 1164-1174 (2015).
69. Tamulaitis, G. et al. Programmable RNA shredding by the type III-A CRISPR-Cas system of Streptococcus thermophilus. *Mol Cell* **56**, 506-517 (2014).
70. Meeske, A.J., Nakandakari-Higa, S. & Marraffini, L.A. Cas13-induced cellular dormancy prevents the rise of CRISPR-resistant bacteriophage. *Nature* **570**, 241-245 (2019).
71. Mahas, A., Aman, R. & Mahfouz, M. CRISPR-Cas13d mediates robust RNA virus interference in plants. *Genome Biol* **20**, 263 (2019).
72. Jing, X. et al. Implementation of the CRISPR-Cas13a system in fission yeast and its repurposing for precise RNA editing. *Nucleic Acids Res* **46**, e90 (2018).
73. Kushawah, G. et al. CRISPR-Cas13d Induces Efficient mRNA Knockdown in Animal Embryos. *Dev Cell* **54**, 805-817 e807 (2020).
74. Truong, D.J. et al. Non-invasive and high-throughput interrogation of exon-specific isoform expression. *Nat Cell Biol* **23**, 652-663 (2021).
75. Kelley, C.P., Haerle, M.C. & Wang, E.T. Negative autoregulation mitigates collateral RNase activity of repeat-targeting CRISPR-Cas13d in mammalian cells. *Cell Rep* **40**, 111226 (2022).
76. Ai, Y., Liang, D. & Wilusz, J.E. CRISPR/Cas13 effectors have differing extents of off-target effects that limit their utility in eukaryotic cells. *Nucleic Acids Res* **50**, e65 (2022).
77. Wang, Q. et al. The CRISPR-Cas13a Gene-Editing System Induces Collateral Cleavage of RNA in Glioma Cells. *Adv Sci (Weinh)* **6**, 1901299 (2019).
78. Zhou, H. et al. Glia-to-Neuron Conversion by CRISPR-CasRx Alleviates Symptoms of Neurological Disease in Mice. *Cell* **181**, 590-603 e516 (2020).
79. Li, S. et al. Screening for functional circular RNAs using the CRISPR-Cas13 system. *Nat Methods* **18**, 51-59 (2021).
80. Zhang, Y. et al. Optimized RNA-targeting CRISPR/Cas13d technology outperforms shRNA in identifying functional circRNAs. *Genome Biol* **22**, 41 (2021).
81. Fareh, M. et al. Reprogrammed CRISPR-Cas13b suppresses SARS-CoV-2 replication and circumvents its mutational escape through mismatch tolerance. *Nat Commun* **12**, 4270 (2021).
82. Blanchard, E.L. et al. Treatment of influenza and SARS-CoV-2 infections via mRNA-encoded Cas13a in rodents. *Nat Biotechnol* **39**, 717-726 (2021).
83. Abbott, T.R. et al. Development of CRISPR as an Antiviral Strategy to Combat SARS-CoV-2 and Influenza. *Cell* **181**, 865-876 e812 (2020).
84. Freije, C.A. et al. Programmable Inhibition and Detection of RNA Viruses Using Cas13. *Mol Cell* **76**, 826-837 e811 (2019).
85. Zeng, L. et al. Broad-spectrum CRISPR-mediated inhibition of SARS-CoV-2 variants and endemic coronaviruses in vitro. *Nat Commun* **13**, 2766 (2022).
86. Yang, L.Z. et al. Dynamic Imaging of RNA in Living Cells by CRISPR-Cas13 Systems. *Mol Cell* **76**, 981-997 e987 (2019).
87. Abudayyeh, O.O. et al. A cytosine deaminase for programmable single-base RNA editing. *Science* **365**, 382-386 (2019).
88. Wilson, C., Chen, P.J., Miao, Z. & Liu, D.R. Programmable m(6)A modification of cellular RNAs with a Cas13-directed methyltransferase. *Nat Biotechnol* **38**, 1431-1440 (2020).
89. Du, M., Jillette, N., Zhu, J.J., Li, S. & Cheng, A.W. CRISPR artificial splicing factors. *Nat Commun* **11**, 2973 (2020).
90. Johnson, A.E. & van Waes, M.A. The translocon: a dynamic gateway at the ER membrane. *Annu Rev Cell Dev Biol* **15**, 799-842 (1999).

91. Endo, T. & Yamano, K. Transport of proteins across or into the mitochondrial outer membrane. *Biochim Biophys Acta* **1803**, 706-714 (2010).
92. Silver, P.A. How proteins enter the nucleus. *Cell* **64**, 489-497 (1991).
93. Fu, X. et al. The Rules and Functions of Nucleocytoplasmic Shuttling Proteins. *Int J Mol Sci* **19** (2018).
94. Cavazza, T. & Vernos, I. The RanGTP Pathway: From Nucleo-Cytoplasmic Transport to Spindle Assembly and Beyond. *Front Cell Dev Biol* **3**, 82 (2015).
95. Lui, K. & Huang, Y. RanGTPase: A Key Regulator of Nucleocytoplasmic Trafficking. *Mol Cell Pharmacol* **1**, 148-156 (2009).
96. Li, J., Yu, M., Zheng, W. & Liu, W. Nucleocytoplasmic shuttling of influenza A virus proteins. *Viruses* **7**, 2668-2682 (2015).
97. Kaberniuk, A.A., Baloban, M., Monakhov, M.V., Shcherbakova, D.M. & Verkhusha, V.V. Single-component near-infrared optogenetic systems for gene transcription regulation. *Nat Commun* **12**, 3859 (2021).
98. Lafontaine, D.L. Noncoding RNAs in eukaryotic ribosome biogenesis and function. *Nat Struct Mol Biol* **22**, 11-19 (2015).
99. Pelletier, J., Thomas, G. & Volarevic, S. Ribosome biogenesis in cancer: new players and therapeutic avenues. *Nat Rev Cancer* **18**, 51-63 (2018).
100. Jones, T.D. et al. A deimmunised form of the ribotoxin, alpha-sarcin, lacking CD4+ T cell epitopes and its use as an immunotoxin warhead. *Protein Eng Des Sel* **29**, 531-540 (2016).
101. Szewczak, A.A., Moore, P.B., Chang, Y.L. & Wool, I.G. The conformation of the sarcin/ricin loop from 28S ribosomal RNA. *Proc Natl Acad Sci U S A* **90**, 9581-9585 (1993).
102. Endo, Y., Gluck, A. & Wool, I.G. Ribosomal RNA identity elements for ricin A-chain recognition and catalysis. *J Mol Biol* **221**, 193-207 (1991).
103. Donovan, J., Rath, S., Kolet-Mandrikov, D. & Korennykh, A. Rapid RNase L-driven arrest of protein synthesis in the dsRNA response without degradation of translation machinery. *RNA* **23**, 1660-1671 (2017).
104. Wilson, D.N. & Doudna Cate, J.H. The structure and function of the eukaryotic ribosome. *Cold Spring Harb Perspect Biol* **4** (2012).
105. Anger, A.M. et al. Structures of the human and Drosophila 80S ribosome. *Nature* **497**, 80-85 (2013).
106. Melen, G.J., Pesce, C.G., Rossi, M.S. & Kornblihtt, A.R. Novel processing in a mammalian nuclear 28S pre-rRNA: tissue-specific elimination of an 'intron' bearing a hidden break site. *EMBO J* **18**, 3107-3118 (1999).
107. Azpurua, J. et al. Naked mole-rat has increased translational fidelity compared with the mouse, as well as a unique 28S ribosomal RNA cleavage. *Proc Natl Acad Sci U S A* **110**, 17350-17355 (2013).
108. Vasu, K. & Nagaraja, V. Diverse functions of restriction-modification systems in addition to cellular defense. *Microbiol Mol Biol Rev* **77**, 53-72 (2013).
109. Meeske, A.J. & Marraffini, L.A. RNA Guide Complementarity Prevents Self-Targeting in Type VI CRISPR Systems. *Mol Cell* **71**, 791-801 e793 (2018).
110. Jung, D. & Alt, F.W. Unraveling V(D)J recombination; insights into gene regulation. *Cell* **116**, 299-311 (2004).
111. Nishana, M. & Raghavan, S.C. Role of recombination activating genes in the generation of antigen receptor diversity and beyond. *Immunology* **137**, 271-281 (2012).
112. Payne, S. Introduction to RNA viruses. *Viruses*, 97 (2017).

113. Rampersad, S. & Tennant, P. Replication and expression strategies of viruses. *Viruses*, 55 (2018).
114. Zanotti, G. & Grinzato, A. Structure of filamentous viruses. *Curr Opin Virol* **51**, 25-33 (2021).
115. Mosley, V.M. & Wyckoff, R.W. Electron micrography of the virus of influenza. *Nature* **157**, 263 (1946).
116. Lee, W.M. et al. Human rhinovirus species and season of infection determine illness severity. *Am J Respir Crit Care Med* **186**, 886-891 (2012).
117. Nyakarahuka, L. et al. How severe and prevalent are Ebola and Marburg viruses? A systematic review and meta-analysis of the case fatality rates and seroprevalence. *BMC Infect Dis* **16**, 708 (2016).
118. Khromykh, A.A. Replicon-based vectors of positive strand RNA viruses. *Curr Opin Mol Ther* **2**, 555-569 (2000).
119. Lundstrom, K. Replicon RNA Viral Vectors as Vaccines. *Vaccines (Basel)* **4** (2016).
120. Nguyen, H.T., Falzarano, D., Gerdts, V. & Liu, Q. Construction of a Noninfectious SARS-CoV-2 Replicon for Antiviral-Drug Testing and Gene Function Studies. *J Virol* **95**, e0068721 (2021).
121. Vogel, A.B. et al. Self-Amplifying RNA Vaccines Give Equivalent Protection against Influenza to mRNA Vaccines but at Much Lower Doses. *Mol Ther* **26**, 446-455 (2018).
122. Pushko, P. et al. Replicon-helper systems from attenuated Venezuelan equine encephalitis virus: expression of heterologous genes in vitro and immunization against heterologous pathogens in vivo. *Virology* **239**, 389-401 (1997).
123. Kim, D.Y. et al. Enhancement of protein expression by alphavirus replicons by designing self-replicating subgenomic RNAs. *Proc Natl Acad Sci U S A* **111**, 10708-10713 (2014).
124. Li, Y. et al. In vitro evolution of enhanced RNA replicons for immunotherapy. *Sci Rep* **9**, 6932 (2019).
125. Bush, K. Beta-lactamase inhibitors from laboratory to clinic. *Clin Microbiol Rev* **1**, 109-123 (1988).
126. Lew, W., Chen, X. & Kim, C.U. Discovery and development of GS 4104 (oseltamivir): an orally active influenza neuraminidase inhibitor. *Curr Med Chem* **7**, 663-672 (2000).
127. Westendorf, K. et al. LY-CoV1404 (bebtelovimab) potently neutralizes SARS-CoV-2 variants. *Cell Rep* **39**, 110812 (2022).
128. Murdin, A.D., Barreto, L. & Plotkin, S. Inactivated poliovirus vaccine: past and present experience. *Vaccine* **14**, 735-746 (1996).
129. Bester, J.C. Measles and Measles Vaccination: A Review. *JAMA Pediatr* **170**, 1209-1215 (2016).
130. Loetscher, P., Pratt, G. & Rechsteiner, M. The C terminus of mouse ornithine decarboxylase confers rapid degradation on dihydrofolate reductase. Support for the pest hypothesis. *J Biol Chem* **266**, 11213-11220 (1991).
131. Reiter, N.J. et al. Structure of a bacterial ribonuclease P holoenzyme in complex with tRNA. *Nature* **468**, 784-789 (2010).
132. Wu, H.N. et al. Human hepatitis delta virus RNA subfragments contain an autocleavage activity. *Proc Natl Acad Sci U S A* **86**, 1831-1835 (1989).
133. Kalderon, D., Roberts, B.L., Richardson, W.D. & Smith, A.E. A short amino acid sequence able to specify nuclear location. *Cell* **39**, 499-509 (1984).
134. Dang, C.V. & Lee, W.M. Identification of the human c-myc protein nuclear translocation signal. *Mol Cell Biol* **8**, 4048-4054 (1988).

135. Fukuda, M. et al. CRM1 is responsible for intracellular transport mediated by the nuclear export signal. *Nature* **390**, 308-311 (1997).
136. Yang, E. et al. Decay rates of human mRNAs: correlation with functional characteristics and sequence attributes. *Genome Res* **13**, 1863-1872 (2003).
137. Gwizdek, C. et al. Exportin-5 mediates nuclear export of minihelix-containing RNAs. *J Biol Chem* **278**, 5505-5508 (2003).
138. Campbell, B.C. et al. mGreenLantern: a bright monomeric fluorescent protein with rapid expression and cell filling properties for neuronal imaging. *Proc Natl Acad Sci U S A* **117**, 30710-30721 (2020).
139. Kim, Y.G. et al. Recombinant Vaccinia virus-coded interferon inhibitor B18R: Expression, refolding and a use in a mammalian expression system with a RNA-vector. *PLoS One* **12**, e0189308 (2017).
140. Rivas, C., Gil, J., Melkova, Z., Esteban, M. & Diaz-Guerra, M. Vaccinia virus E3L protein is an inhibitor of the interferon (i.f.n.)-induced 2-5A synthetase enzyme. *Virology* **243**, 406-414 (1998).
141. Shcherbakova, D.M. & Verkhusha, V.V. Near-infrared fluorescent proteins for multicolor in vivo imaging. *Nat Methods* **10**, 751-754 (2013).
142. Gootenberg, J.S. et al. Nucleic acid detection with CRISPR-Cas13a/C2c2. *Science* **356**, 438-442 (2017).
143. Gootenberg, J.S. et al. Multiplexed and portable nucleic acid detection platform with Cas13, Cas12a, and Csm6. *Science* **360**, 439-444 (2018).
144. Natchiar, S.K., Myasnikov, A.G., Kratzat, H., Hazemann, I. & Klaholz, B.P. Visualization of chemical modifications in the human 80S ribosome structure. *Nature* **551**, 472-477 (2017).
145. Antczak, M. et al. New functionality of RNAComposer: an application to shape the axis of miR160 precursor structure. *Acta Biochim Pol* **63**, 737-744 (2016).
146. Popenda, M. et al. Automated 3D structure composition for large RNAs. *Nucleic Acids Res* **40**, e112 (2012).
147. Los, G.V. et al. HaloTag: a novel protein labeling technology for cell imaging and protein analysis. *ACS Chem Biol* **3**, 373-382 (2008).
148. Schwinn, M.K. et al. CRISPR-Mediated Tagging of Endogenous Proteins with a Luminescent Peptide. *ACS Chem Biol* **13**, 467-474 (2018).
149. Lotka, A.J. Elements of physical biology. (Williams & Wilkins, 1925).
150. Shaner, N.C. et al. A bright monomeric green fluorescent protein derived from Branchiostoma lanceolatum. *Nat Methods* **10**, 407-409 (2013).
151. Bajar, B.T. et al. Improving brightness and photostability of green and red fluorescent proteins for live cell imaging and FRET reporting. *Sci Rep* **6**, 20889 (2016).
152. Orlandini von Niessen, A.G. et al. Improving mRNA-Based Therapeutic Gene Delivery by Expression-Augmenting 3' UTRs Identified by Cellular Library Screening. *Mol Ther* **27**, 824-836 (2019).
153. Dalpke, A. & Helm, M. RNA mediated Toll-like receptor stimulation in health and disease. *RNA Biol* **9**, 828-842 (2012).
154. Kariko, K., Buckstein, M., Ni, H. & Weissman, D. Suppression of RNA recognition by Toll-like receptors: the impact of nucleoside modification and the evolutionary origin of RNA. *Immunity* **23**, 165-175 (2005).
155. Ryan, D.E. et al. Improving CRISPR-Cas specificity with chemical modifications in single-guide RNAs. *Nucleic Acids Res* **46**, 792-803 (2018).

156. Riesenberg, S., Helmbrecht, N., Kanis, P., Maricic, T. & Paabo, S. Improved gRNA secondary structures allow editing of target sites resistant to CRISPR-Cas9 cleavage. *Nat Commun* **13**, 489 (2022).
157. Sola, I., Almazan, F., Zuniga, S. & Enjuanes, L. Continuous and Discontinuous RNA Synthesis in Coronaviruses. *Annu Rev Virol* **2**, 265-288 (2015).
158. Lefaudeux, D., Sen, S., Jiang, K., Hoffmann, A. & Group, U.R. Kinetics of mRNA nuclear export regulate innate immune response gene expression. *Nat Commun* **13**, 7197 (2022).
159. Carmody, S.R. & Wente, S.R. mRNA nuclear export at a glance. *J Cell Sci* **122**, 1933-1937 (2009).
160. Miyazaki, J. et al. Expression vector system based on the chicken beta-actin promoter directs efficient production of interleukin-5. *Gene* **79**, 269-277 (1989).
161. Lykke-Andersen, S. & Jensen, T.H. Nonsense-mediated mRNA decay: an intricate machinery that shapes transcriptomes. *Nat Rev Mol Cell Biol* **16**, 665-677 (2015).
162. Blissenbach, M., Grewe, B., Hoffmann, B., Brandt, S. & Uberla, K. Nuclear RNA export and packaging functions of HIV-1 Rev revisited. *J Virol* **84**, 6598-6604 (2010).
163. Gwizdek, C. et al. Minihelix-containing RNAs mediate exportin-5-dependent nuclear export of the double-stranded RNA-binding protein ILF3. *J Biol Chem* **279**, 884-891 (2004).
164. Pasquinelli, A.E. et al. The constitutive transport element (CTE) of Mason-Pfizer monkey virus (MPMV) accesses a cellular mRNA export pathway. *EMBO J* **16**, 7500-7510 (1997).
165. Kim, Y.H., Han, M.E. & Oh, S.O. The molecular mechanism for nuclear transport and its application. *Anat Cell Biol* **50**, 77-85 (2017).
166. Kleinstiver, B.P. et al. High-fidelity CRISPR-Cas9 nucleases with no detectable genome-wide off-target effects. *Nature* **529**, 490-495 (2016).
167. Tsai, S.Q. et al. GUIDE-seq enables genome-wide profiling of off-target cleavage by CRISPR-Cas nucleases. *Nat Biotechnol* **33**, 187-197 (2015).
168. Armache, J.P. et al. Cryo-EM structure and rRNA model of a translating eukaryotic 80S ribosome at 5.5-A resolution. *Proc Natl Acad Sci U S A* **107**, 19748-19753 (2010).
169. Tong, H. et al. High-fidelity Cas13 variants for targeted RNA degradation with minimal collateral effects. *Nat Biotechnol* (2022).
170. Tang, X.E., Tan, S.X., Hoon, S. & Yeo, G.W. Pre-existing adaptive immunity to the RNA-editing enzyme Cas13d in humans. *Nat Med* **28**, 1372-1376 (2022).
171. Duncan, G.A., Jung, J., Hanes, J. & Suk, J.S. The Mucus Barrier to Inhaled Gene Therapy. *Mol Ther* **24**, 2043-2053 (2016).
172. Tenchov, R., Bird, R., Curtze, A.E. & Zhou, Q. Lipid Nanoparticles horizontal line From Liposomes to mRNA Vaccine Delivery, a Landscape of Research Diversity and Advancement. *ACS Nano* **15**, 16982-17015 (2021).
173. Banskota, S. et al. Engineered virus-like particles for efficient in vivo delivery of therapeutic proteins. *Cell* **185**, 250-265 e216 (2022).
174. Segel, M. et al. Mammalian retrovirus-like protein PEG10 packages its own mRNA and can be pseudotyped for mRNA delivery. *Science* **373**, 882-889 (2021).
175. Dobrowolski, C. et al. Nanoparticle single-cell multiomic readouts reveal that cell heterogeneity influences lipid nanoparticle-mediated messenger RNA delivery. *Nat Nanotechnol* **17**, 871-879 (2022).
176. Hou, X., Zaks, T., Langer, R. & Dong, Y. Lipid nanoparticles for mRNA delivery. *Nat Rev Mater* **6**, 1078-1094 (2021).

177. Schoenmaker, L. et al. mRNA-lipid nanoparticle COVID-19 vaccines: Structure and stability. *Int J Pharm* **601**, 120586 (2021).
178. Ozcan, A. et al. Programmable RNA targeting with the single-protein CRISPR effector Cas7-11. *Nature* **597**, 720-725 (2021).
179. Kato, K. et al. Structure and engineering of the type III-E CRISPR-Cas7-11 effector complex. *Cell* **185**, 2324-2337 e2316 (2022).
180. Konermann, S. et al. Genome-scale transcriptional activation by an engineered CRISPR-Cas9 complex. *Nature* **517**, 583-588 (2015).
181. Schmiderer, L., Yudovich, D., Oburoglu, L., Hjort, M. & Larsson, J. Site-specific CRISPR-based mitochondrial DNA manipulation is limited by gRNA import. *Sci Rep* **12**, 18687 (2022).
182. Anzalone, A.V. et al. Search-and-replace genome editing without double-strand breaks or donor DNA. *Nature* **576**, 149-157 (2019).
183. Komor, A.C., Kim, Y.B., Packer, M.S., Zuris, J.A. & Liu, D.R. Programmable editing of a target base in genomic DNA without double-stranded DNA cleavage. *Nature* **533**, 420-424 (2016).
184. Muik, A. et al. Neutralization of SARS-CoV-2 Omicron by BNT162b2 mRNA vaccine-elicited human sera. *Science* **375**, 678-680 (2022).
185. Krienke, C. et al. A noninflammatory mRNA vaccine for treatment of experimental autoimmune encephalomyelitis. *Science* **371**, 145-153 (2021).
186. Cao, J. et al. High-throughput 5' UTR engineering for enhanced protein production in non-viral gene therapies. *Nat Commun* **12**, 4138 (2021).
187. Chen, R. et al. Engineering circular RNA for enhanced protein production. *Nat Biotechnol* (2022).
188. Neri, U. et al. Expansion of the global RNA virome reveals diverse clades of bacteriophages. *Cell* **185**, 4023-4037 e4018 (2022).

Danksagungen

Zunächst möchte ich mich bei Prof. Wolfgang Wurst bedanken. Wolfgang, ich bin dir zutiefst dankbar für das riesige Vertrauen, das du in mich investiert hast. Du hast mir die Freiheit gegeben, meiner Begeisterung und meinen Interessen zu folgen und dabei nicht gezweifelt, dass ich damit erfolgreich sein werde. Du hast immer das richtige Maß an Unterstützung und Freiheit für mich gefunden. Du bist eine Inspiration für mich, was man erreichen kann, wenn man seine Arbeit liebt.

Des Weiteren möchte ich mich bei Dr. Florian Giesert bedanken. Florian, vielen Dank, dass du immer ein offenes Ohr für jede verrückte Idee hast und meine Begeisterung dafür teilen kannst. Eine meiner größten Freuden ist es, mit dir alles, von molekularen Details bis hin zu großen Ideen, zu diskutieren. Danke, dass du immer bereit bist zu helfen, an meiner Meinung interessiert bist und einfach ein unkomplizierter Mensch bist. Danke, dass du immer den richtigen Ton triffst und jedem – ob Praktikant oder Professor – mit Respekt begegnest.

Bedanken möchte ich mich auch bei vielen Studenten, die mir während dieser Arbeit geholfen haben. Hervorheben möchte ich die HiWis Lea Krautner, Ann-Caroline Heiler, Marina Luchner und Friederike Reinhardt. Danke, dass ihr so begeistert von eurem Fach seid, wie ich, wodurch ich es geliebt habe, mit euch zusammen zu arbeiten. Es macht mich stolz zu sehen, wie ihr euch entwickelt habt und dass ich dazu beitragen konnte.

Danke an alle Mitglieder des IDG, dass ihr so kollegial seid, dass ihr alle zur perfekten Organisation des Instituts beitragt und danke, dass jeder bereit ist, dem anderen zu helfen. Danke vor allem an Dr. Jessica Giehrl-Schwab, dass du mir in der Anfangszeit geholfen hast, mich im Institut zurechtzufinden und später eine wunderbare Kollegin warst. Bedanken möchte ich mich auch bei Annerose Kurz-Drexler. Danke, dass du dich wortwörtlich um alles kümmerst. Es gibt nichts, wo du nicht weiterhelfen könntest und kein Problem, worum du dich nicht kümmern würdest. Jemand wie du ist das größte Geschenk für eine Arbeitsgruppe. Vielen Dank an Dr. Daniela Vogt-Weisenhorn und Dr. Karin Ganea. Danke, für eure Hilfe bei unzähligen Praktikantenverträge, die großartige Unterstützung beim Einwerben von Finanzierung und bei jedem organisatorischen Problem. Danke, dass man sich immer auf euch verlassen kann.

Danke an Dr. Jeffery Truong für den Austausch von Gedanken und Ideen. Danke, dass du so ein brillanter Wissenschaftler bist und trotzdem bereit bist, immer zu helfen. Danke, dass ich von dir nahezu alles gelernt habe, worauf ich diese Arbeit aufbauen konnte.

Danke an alle Wissenschaftler und Kollaborationspartner, die mir bei dieser Arbeit geholfen haben, für eure großzügige Hilfe, euren Gedanken und Ideen. Danke dafür vor allem an euch, Prof. Gil Westmeyer, Prof. Stefan Stricker, Valter Bergant und Richard Koll.

Danke, an meine Eltern Sabine und Meinhard Gruber, dass ihr mich immer dazu angetrieben habt, noch eine Stufe höher anzustreben und dabei daran geglaubt habt, dass ich das schaffen kann. Danke, dass ihr nie ungeduldig geworden seid und mich auch bei Wegen abseits eines geradlinigen Abschlusses finanziell und moralisch unterstützt habt.

Zuletzt möchte ich der wichtigsten Person danken: Meiner Frau Jennifer Gruber. Du hast mir das Selbstbewusstsein und die Freiheit gegeben, diese Arbeit nach meiner Vorstellung zu gestalten. Es wäre unmöglich gewesen, so viel Zeit und Herzblut hineinzustecken, ohne deine Hilfe. Ich weiß, wieviel du zurückstecken musstest, um mich zu unterstützen und dafür werde ich dir immer dankbar sein.

Abschließend noch einige Wort an meinen Sohn Emil. Emil, wenn du diesen Text in ein paar Jahren liest, hoffe ich, dass du mir verzeihen kannst, dass ich oft so viel gearbeitet habe. Diese Doktorarbeit war mehr Selbstverwirklichung als Arbeit für mich und ich hoffe, du stimmst mir zu – es hat sich gelohnt.